

EFFECT OF NOTCHES ON LOW-CYCLE FATIGUE

A Literature Survey

Prepared for the

METALS PROPERTIES COUNCIL

by B. M. Wundt

STP 490



AMERICAN SOCIETY FOR TESTING AND MATERIALS

EFFECT OF NOTCHES ON LOW-CYCLE FATIGUE

A Literature Survey

Prepared for the

METALS PROPERTIES COUNCIL

by B. M. Wundt

ASTM SPECIAL TECHNICAL PUBLICATION 490

List price \$3.00

04-490000-30



AMERICAN SOCIETY FOR TESTING AND MATERIALS
1916 Race Street, Philadelphia, Pa. 19103

© BY AMERICAN SOCIETY FOR TESTING AND MATERIALS 1972
Library of Congress Catalog Number: 75-152133

NOTE

The Society is not responsible, as a body,
for the statements and opinions
advanced in this publication.

Printed in Alpha, N. J.
May 1972

TABLE OF CONTENTS

SECTION A.	INTRODUCTION AND SUMMARY	1
SECTION B.	NOMENCLATURE	3
SECTION C.	CYCLIC STRESS-STRAIN DIAGRAM	5
	Discused Ref. 3, 4, 11, 24, 30	
	Other Ref. 33, 45, 56	
SECTION D.	NEUBER'S RELATIONSHIP BETWEEN STRESS AND STRAIN CONCENTRATION FACTORS AND APPLICATION TO LOW-CYCLE FATIGUE	11
	Discussed Ref. 38, 39, 49, 54	
	Other Ref. 7, 30	
SECTION E.	STOWELL-HARDRATH-OHMAN EQUATION AND ITS APPLICATION TO LOW-CYCLE FATIGUE	15
	Discussed Ref. 4, 6, 7, 8, 12, 14, 16, 33, 44, 46, 56, 57	
	Other Ref. 3, 6, 20, 21, 22, 23, 35, 40, 42	
SECTION F.	FATIGUE STRENGTH-REDUCTION FACTORS ON STRAIN BASIS	29
	Discussed Ref. 19, 23, 26, 27, 28, 29, 45	
SECTION G.	FATIGUE STRENGTH REDUCTION FACTORS ON STRESS BASIS	45
	Discussed Ref. 2, 20, 37, 53	
	Other Ref. 52	
SECTION H.	FATIGUE STRENGTH REDUCTION FACTORS IN BENDING	53
	Discussed Ref. 1, 5, 17	
SECTION I.	MISCELLANEOUS STUDIES ON EFFECT OF NOTCHES IN LOW-CYCLE FATIGUE	61
	Discussed Ref. 9, 26, 40, 41, 42	
SECTION J.	PROPOSED FUTURE WORK	65
	Discussed Ref. 31	
SECTION K.	REFERENCES	67

SECTION A. INTRODUCTION AND SUMMARY

A.1. — This literature review was prepared for Subcommittee 3 of the Metal Properties Council. At present there are not available comprehensive reviews of literature pertaining to the effect of notches and discontinuities on life in low-cycle fatigue. Note that in Section 1 of R.55 there are listed reviews and annotations pertaining to low-cycle fatigue, some of which touched upon the above subject.

A.2. — This review consists of eleven sections, A to K. It contains selected figures from papers reviewed. The Sections are listed in the Table of Contents. Note that the discussed references are listed in each Section.

A.3. — Practically all of the 59 references listed in Section K were taken from Section 4 of R.55, which was prepared by the reviewer for the Metal Properties Council. All papers reviewed were published between 1955 and early 1969, either in the United States or in the United Kingdom, except for one published in Japan and two in Germany. In some instances the prepared reviews were more comprehensive than in others, depending on the content and the clarity of the paper. Also, in most cases a number of the original figures were reproduced.

A.4. — The reviewer has found it advisable to develop a consistent nomenclature of his own and to use it throughout the literature survey. For details of nomenclature and abbreviations used, see Section B.

A.5. — The cyclic stress-strain diagrams which lately have assumed considerable importance in low-cycle fatigue analysis are discussed in a separate Section C.

The total imposed strain range in the apex of a notch is of particular importance in cyclic life of notched specimens. Its approximate determination, as proposed in a number of references, is discussed in Section D (Neuber's relation) and in Section E (Stowell-Hardrath-Ohman equation).

A.6. — The experimental fatigue strength reduction factor k_f which is the ratio of endurance strength of an unnotched specimen to the nominal endurance strength of a specimen with a notch, is well known. However, when an attempt is made to extend the concept to a limited cyclic life rather than to fatigue endurance, complications arise because depending on the particular test procedure used, a number of definitions are possible. The main reason for it is the non-linear relationship between the imposed stress range and the resulting strain range in the low-cycle fatigue region.

As a rule, in tension-compression or zero-tension low-cycle fatigue tests, *notched* specimens are controlled by a nominal stress range, referred to the net section. On the other hand, cycling loading of *unnotched* specimens may be controlled either by a stress range or by a strain range.

The fatigue strength reduction factor "FS-thRF" is larger than one and is usually defined as the ratio of the controlling stress or strain range for the *unnotched* specimen to the respective, controlling stress or strain range for the *notched* specimen, corresponding to the same cyclic life.

If a properly constructed cyclic stress-strain diagram is available, it may be used to derive a nominal strain range which corresponds to a given controlling nominal stress range and which may be used in calculating a "FS-thRF".

A.7. — "FS-thRF" which are calculated with the help of *strain controlled, unnotched* specimens will be identified as Q_C (for cracking) or Q_f (for fracture) and will be identified as derived on a "*strain basis*". The references which discuss experimentally obtained factors Q_C and Q_f are reviewed in Section F.

"FS-thRF" which are calculated with the help of *stress controlled, unnotched* specimens will be identified as K_C (for cracking) or K_f (for fracture) and will be identified as derived on a "*stress basis*". The references which discuss experimentally obtained factors K_C and K_f are reviewed in Section G.

In addition to this division of the "FS-thRF", derived for zero-tension and for tension-compression tests, additional subdivisions are discussed in Section F. This separation of the experimentally determined factors in accordance with their derivation helps to clarify the reasons for their differences in magnitude.

A.8.— In Section H are discussed three references pertaining to "LCF" tests in bending. In one of the references the "FS-thRF" in bending was defined as the ratio of strain range measured on the surface of an unnotched cantilever beam divided by the strain range measured on the smooth surface of another beam whose other surface was notched. The strain ranges were measured for the same cyclic life. These "FS-thRF" in bending were designated Q_{bc} and Q_{bf} .

A.9. — A few interesting references pertaining to the effect of notches in "LCF" were reviewed shortly in Section I. These references did not fit into Sections F, G or H.

A.10. — The reviewer has found only one paper devoted exclusively to proposed future work on the effect of notches on low-cycle fatigue life. This paper, R. 31 is reviewed in Section J.

A.11. — It must be pointed out that this review is a detailed literature survey and not an interpretive report. It will be of value mainly to those doing experimental work and research in this area. It is intended to supplement this review with an interpretive report at a later date.

A.12 – Since the 59 references were originally compiled and reviewed in 1970, 15 additional, more recent references were published. These new references 60 to 76 were added to the list of references but were not reviewed in this literature survey.

SECTION B. NOMENCLATURE

B.1. — The reviewer has found it advisable to evolve his own nomenclature because the papers reviewed differed considerably in nomenclature. Note that except for Δ , Greek characters are not used in this nomenclature. This is contrary to the nomenclature employed by many others, e.g. Fig. 1-1-11.

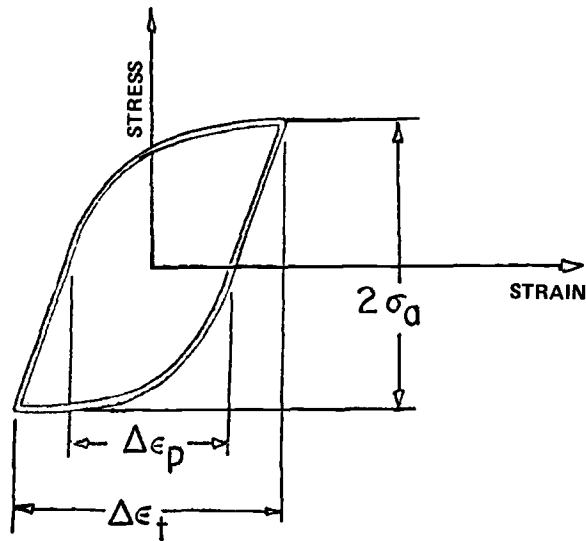


FIG. 1-1-11 — Schematic of mechanical hysteresis loop with characterizing parameters.

For convenience, the reviewer introduced also multiple letter abbreviations for often used expressions and definitions, e.g. “FSRF” for fatigue strength reduction factor, “ESCF” for elastic, theoretical stress or strain concentration factor, etc.

The titles of reproduced figures were not changed and therefore contain the original nomenclature used by the authors. The figures are numbered as follows: e. g., Fig. 125-26-40 indicates that its consecutive figure number is 125 and that it is Fig. 26 in reference 40.

Note that the elasto-plastic stress concentration factor “PS-sCF” is designated k_p and that the elasto-plastic strain concentration factor “PS-nCF” is designated q_p . These symbols are simpler than the usual.

Correspondingly, the fatigue strength reduction factors to cracking or to fracture, on stress basis and on strain basis are designated K_c or K_f and Q_c or Q_f , respectively. This separation of symbols is convenient in analysis of experimental data.

B.2. — ABBREVIATIONS

- “LCF” — Low-Cycle Fatigue
- “SHO” — Stowell-Hardrath-Ohman Method
- “ESCF” — Theoretical elastic stress or strain concentration factor, k_t

- “PS-sCF” — Elasto-plastic stress concentration factor, k_p
- “PS-nCF” — Elasto-plastic strain concentration factor, q_p
- “FS-thRFC” — Fatigue strength reduction factor to cracking on stress basis, K_c on strain basis, Q_c
- “FS-thRFF” — Fatigue strength reduction factor to fracture, on stress basis, K_f on strain basis, Q_f
- R. 39 — Indicates reference 39

B.3. — SYMBOLS

- R — Load or stress ratio during cycling loading
- $R = 0$ — Repeated or pulsating loading
- $R = -1$ — Reversed constant amplitude loading
- r — Notch root radius
- N_c — Number of cycles to cracking
- N_f — Number of cycles to fracture
- S_t — Tensile strength
- S_y — Yield strength
- S_{pl} — Proportional limit
- S_{max} — Maximum cyclic, local stress at a stress concentration, usually at the apex of a notch
- S_{min} — Minimum cyclic, local stress at a stress concentration, usually at the apex of a notch
- ΔS — Range of local cyclic, stress at the apex of a notch = $S_{max} - S_{min}$
- \bar{S}_{max} — Cyclic maximum *nominal* stress based on net cross-section of specimen
- \bar{S}_{min} — Cyclic minimum *nominal* stress based on net cross-section of specimen
- $\overline{\Delta S}$ — Range of cyclic *nominal* stress during one reversal = $\bar{S}_{max} - \bar{S}_{min}$
- \bar{S}_m — Mean cyclic *nominal* stress = $\frac{\bar{S}_{max} + \bar{S}_{min}}{2}$
- \bar{S} — *Nominal* stress based on net cross-section
- E — Modulus of elasticity
- E_s — Secant modulus corresponding to the maximum local stress S_{max}
- E_{sn} — Secant modulus corresponding to \bar{S} , nominal stress based on net section
- E_{sy} — Secant modulus corresponding to yield stress S_y
- e_y — Elastic strain at yield stress S_y
- $e_y = \frac{S_y}{E}$

- e_{yt} – Total strain at yield stress S_y

$$e_{yt} = \frac{S_y}{E_{sy}}$$
- k_p – Elasto-plastic stress concentration factor
 abbrev. “PS-sCF”. $k_p = \frac{\Delta S}{\Delta \bar{S}} = \frac{S_{max}}{\bar{S}_{max}}$
- k_t – Theoretical elastic stress or strain concentration factor.
 Abrev. “ESCF”, $k_t = \frac{S_{max}}{\bar{S}}$
- k_f – Fatigue strength reduction factor abbrev. “FS-thRF”. Experimentally derived from high-cycle fatigue tests on smooth and notched bars. Ratio of endurance limit of unnotched bars to the endurance limit of notched bars.
 $k_f \leq k_t$
- K_C – Fatigue strength reduction factor, on *stress* basis, to macrocracking.
 Abbrev. “FS-thRFC”
- K_f – Fatigue strength reduction factor, on *stress* basis, to fracture.
 Abbrev. “FS-thRF”
- K_{fm} – Fatigue strength reduction factor, on *stress* basis, to fracture, for the same mean cyclic nominal stress \bar{S}_m
- e_{max} – Maximum cyclic, local, total strain at a stress concentration, usually at the apex of a notch
- e_{min} – Minimum cyclic, local, total strain at a stress concentration, usually at the apex of a notch
- Δe – Range of local, cyclic, total strain at the apex of a notch = $e_{max} - e_{min}$
- \bar{e}_{max} – Cyclic maximum *nominal*, total strain based on net cross-section of specimen
- \bar{e}_{min} – Cyclic minimum *nominal*, total strain based on net cross-section of specimen
- \bar{e}_m – Mean cyclic *nominal*, total strain

$$\bar{e}_m = \frac{\bar{e}_{max} + \bar{e}_{min}}{2}$$
- $\overline{\Delta e}$ – Range of cyclic *nominal*, total strain during one reversal = $\bar{e}_{max} - \bar{e}_{min}$
- \bar{e} – *Nominal* total strain which corresponds to the nominal stress \bar{S} , across the net section.

$$\bar{e} = \frac{\bar{S}}{E_{sn}}$$
- q_p – Elasto-plastic strain concentration factor

$$= \frac{\Delta e}{\Delta \bar{e}} = \frac{e_{max}}{\bar{e}_{max}}$$
 Abbrev. “PS-nCF”
- Q_C – Fatigue strength reduction factor, on *strain* basis, to macrocracking
 Abbrev. “FS-thRFC”
- Q_f – Fatigue strength reduction factor, on *strain* basis, to fracture
 Abbrev. “FS-thRFF”
- Q_{bc} and Q_{bf} – The same as above, in bending.

SECTION C

CYCLIC STRESS-STRAIN DIAGRAM

C.1.— Under the conditions of continuously increased loading, the relationship between stress and strain is represented by the well-known monotonic stress-strain diagram. However, under conditions of cycling loading, e. g., in the case of completely reversed total strain, a more or less defined, so-called “cyclic” stress-strain diagram or curve may be derived which may or may not coincide with the monotonic stress-strain diagram. It seems that a properly determined cyclic stress-strain diagram offers a more satisfactory method of studying material behavior in notches in the presence of cyclic plastic deformation. It was observed that after a number of fatigue cycles the varying relationship between stress range and total strain range becomes “stabilized” for practical purposes. It appears that both Manson in R35 and Peterson in R40 (Fig. 48-39-40) proposed the use of “stabilized” cyclic stress-strain curves in analyzing the behavior of material in notches subjected to low-cycle fatigue. See C.3 for definition of cyclic stress-strain curves.

At present, engineers are becoming more and more aware of the necessity of using such “stabilized” cyclic stress-strain diagrams in place of monotonic diagrams. See R30.

Changes in the stress response occur rapidly in the early portion of the life but reach a reasonably stable response or steady state condition after about 10 to 20% of the life. Plots of the stress required to enforce the strain limit as a function of cycles are called cyclic strain hardening or softening curves. See Fig. 2-2C-11. An example of cyclic softening of a low carbon martensitic

steel is shown by the hysteresis loops in Fig. 3-3-11. After the transient stage, a steady state is attained during which the hysteresis loops maintain an essentially constant shape until just prior to complete fracture.

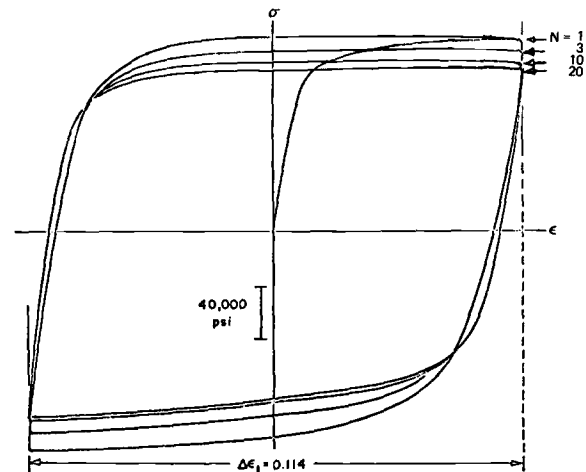


FIG. 3-3-11 — Stress-strain response of a low carbon martensite steel during completely reversed strain cycling. This material exhibits cyclic softening.

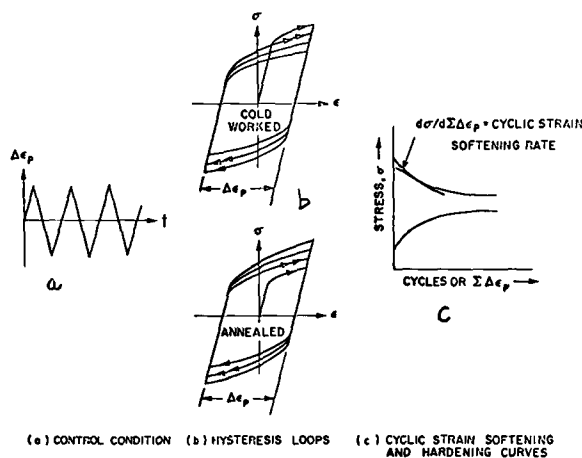


FIG. 2-2-11 — Schematic representation of material response to reversed strain cycling.

C.2. — Feltner, et al, in R11 discuss the behavior of materials undergoing low-cycle fatigue. Their exposition is very clear and the reviewer quotes verbatim. The authors state, “During cycling straining materials may harden or soften, depending upon their thermomechanical history. For example, annealed materials will undergo a cyclic hardening process which is indicated by an increase in the stress required to enforce the strain limit on successive cycles. On the other hand, cold worked materials generally soften and the stress required to enforce the strain limit on successive cycles decreases. See Fig. 2-2B-11.

The curve drawn through the tips of these stabilized hysteresis loops obtained from specimens tested at different amplitudes is called the “cyclic stress-strain curve”. See Fig. 4-4A-11. It provides a convenient description of the steady state cyclic stress-strain response of a material. Monotonic and cyclic stress-strain curves may thus be displayed on the same diagram.” See Fig. 4-4B-11.

The authors point out that Manson has proposed a rule by which it is possible to predict from monotonic stress-strain properties alone, whether or not a material will cyclically harden or soften. This rule states, “if the ratio of the tensile strength to 0.2% offset yield strength is larger than 1.4, hardening will occur and if this ratio is less than 1.2, softening will occur. For ratios between

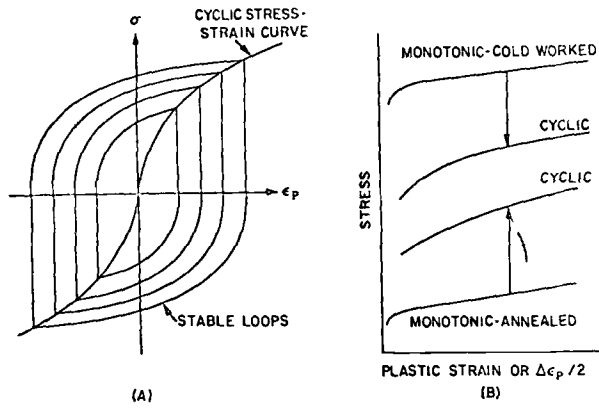


FIG. 4-4AB-11 – (A) Cyclic stress-strain curve as determined from tips of stabilized hysteresis loops. (B) Comparison of monotonic and cyclic stress-strain curves for two initial conditions of a material.

1.2 and 1.4 a prediction can not be made, but the material should be relatively stable”.

C.3. – Landgraf, et al, in R30 discuss experimental methods for the determination of cyclic stress-strain diagrams. The authors point out that a survey of literature indicates that there is no agreement as to the exact definition of the cyclic stress-strain diagram nor on testing procedures for determining it. They state that a definition of the cyclic stress-strain curve which has gained some measure of acceptance is the locus of tips of the stable hysteresis loops from several companion tests at different, completely reversed constant strain amplitudes. Such a curve can be compared directly with the monotonic stress-strain curve. If the cyclic stress-strain curve is above

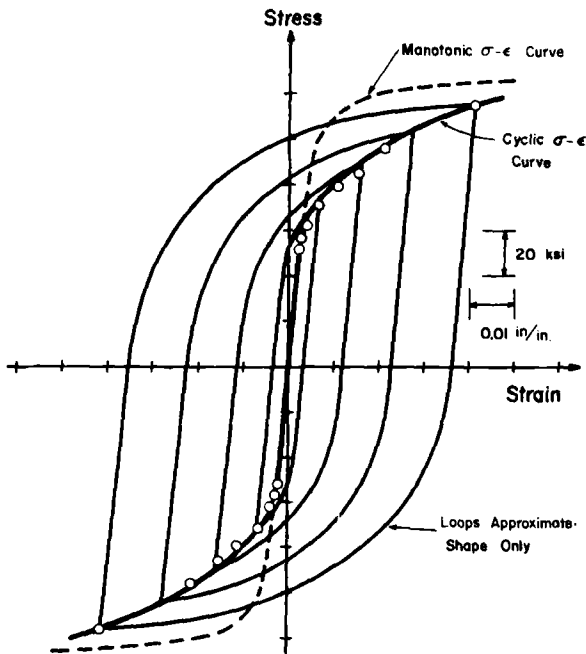


FIG. 5-1-30 – Monotonic and cyclic stress-strain curves for SAE 4340 steel. Points are tips of stable loops from companion specimens.

the monotonic curve, the metal cyclically hardens; if the cyclic curve is below the monotonic, the metal cyclically softens. Fig. 5-1-30 is an example of a cyclic stress-strain diagram obtained as described above. This method requires a number of identical specimens and considerable testing time. Therefore, the authors propose four alternative procedures for obtaining this information with preferably one specimen. Only one of the proposed procedures will be described here. For the others, consult the original paper. This “multiple step test procedure” is explained by the authors as follows: “It is known that the hysteresis loop rapidly adjusts to a stable steady state following sudden changes in cyclic strain amplitude. This makes it possible to obtain several points on the cyclic stress-strain curve from a single specimen by cycling at different strain amplitudes. This is shown in Fig. 6-2a-30.

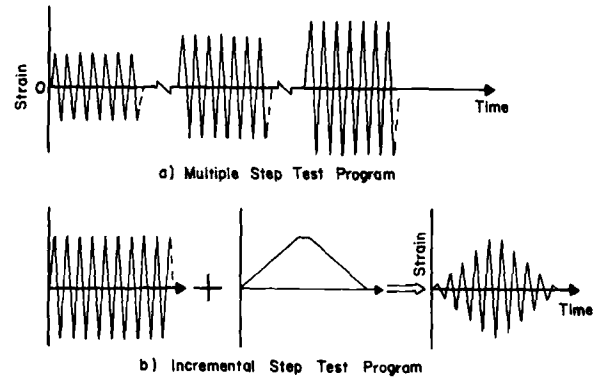


FIG. 6-2-30 – Strain control programs for obtaining an approximate cyclic stress-strain curve from one specimen.

Each strain amplitude step and the corresponding stable stress amplitude provide one point on the cyclic stress-strain curve.” Monotonic and cyclic stress-strain curves for several materials are shown in Fig. 7-7-30 and Fig. 8-8-30.

The authors point out that the relation between cyclic

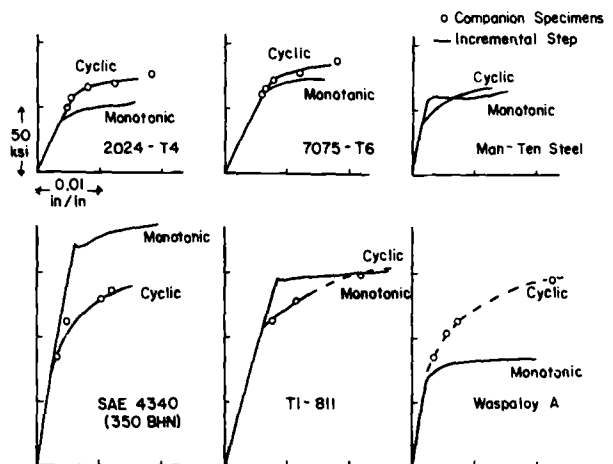


FIG. 7-7-30 – Monotonic and cyclic stress-strain curves for several materials.

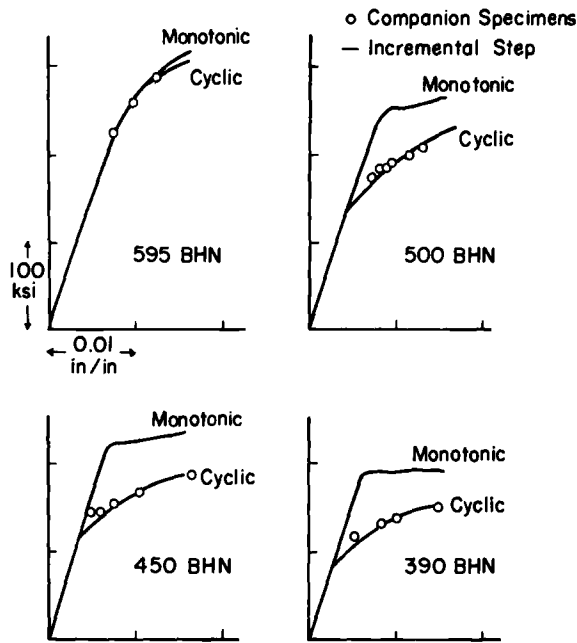


FIG. 8-8-30 – Monotonic and cyclic stress-strain curves for four hardnesses of quenched and tempered SAE 1045 steel.

stable stress amplitude and the stable plastic strain amplitude may be described by a power function as shown by the equation

$$S = k \left(\frac{\Delta \epsilon_p}{2} \right)^{n_c}$$

n_c is the cycling strain hardening exponent. It is interesting that according to the authors the value of n_c is found to be between 0.10 and 0.20 and usually close to 0.15 for most metals regardless of their initial conditions. They conclude that metals with a high monotonic strain

hardening exponent would be expected to cyclically harden while those with a low initial value would be expected to cyclically soften. An interesting comparison of monotonic and cyclic properties of several metals is shown in Fig. 9-Table 1-30.

C.4. – Blatherwick, et al, in R4 include cyclic stress-strain diagrams for SAE 1018 steel. See Fig. 10-5-4. In

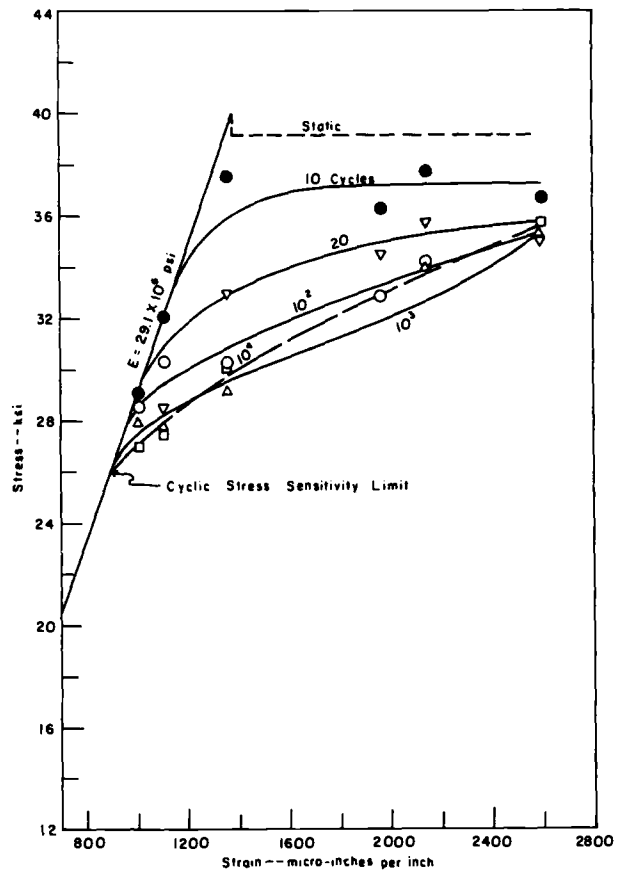


FIG. 10-5-4 – Cyclic stress-strain curves for SAE 1018 steel at various numbers of cycles.

TABLE 1—Material and properties.

Material	Condition	0.2% Yield Strength, monotonic σ_y /cyclic σ_u , ksi	Strain Hardening Exponent, n (monotonic)/ n' (cyclic)	Cyclic Behavior
OFHC copper [9].....	annealed	3/20	0.40/0.15	hardens
	partial annealed	37/29	0.13/0.16	stable
	cold worked	50/34	0.10/0.12	softens
2024 aluminum alloy [18]....	T4	44/65	0.20/0.11	hardens
7075 aluminum alloy [18]....	T6	68/75	0.11/0.11	hardens
Man-Ten steel.....	as-received	55/50	0.15/0.16	softens and hardens
SAE 4340 steel [18].....	quenched and tempered, 350 BHN	170/110	0.066/0.14	softens
Ti-8Al-1Mo-1V [18].....	duplex annealed	145/115	0.078/0.14	softens and hardens
Waspaloy.....	Ref 11	79/102	0.11/0.17	hardens
SAE 1045 steel.....	quenched and tempered, 595 BHN	270/250	0.071/0.14	stable
	quenched and tempered, 500 BHN	245/185	0.047/0.12	softens
	quenched and tempered, 450 BHN	220/140	0.041/0.15	softens
	quenched and tempered, 390 BHN	185/110	0.044/0.17	softens
SAE 4142 steel.....	as-quenched, 670 BHN	235/...	0.14/...	hardens
	quenched and tempered, 560 BHN	245/250	0.092/0.13	stable
	quenched and tempered, 475 BHN	250/195	0.048/0.12	softens
	quenched and tempered, 450 BHN	230/155	0.040/0.17	softens
	quenched and tempered, 380 BHN	200/120	0.051/0.18	softens

FIG. 9-T.1-30

addition to the monotonic diagram, cyclic diagrams are shown for 10, 20, 10², 10³, and 10⁴ cycles. Cyclic softening effect is evident in the curves.

C.5. — Berling, et al, in R3 discuss the cyclic stress-strain curves for three stainless steels at three tempera-

tures. The curves are shown in Fig. 11-14-3 for AISI-304, in Fig. 12-15-3 for AISI-316, and in Fig. 13-16-3 for AISI-348. Each of the diagrams contains two curves, distinguished by open and closed circles. The open circles represent the stabilized values of stress and strain obtained

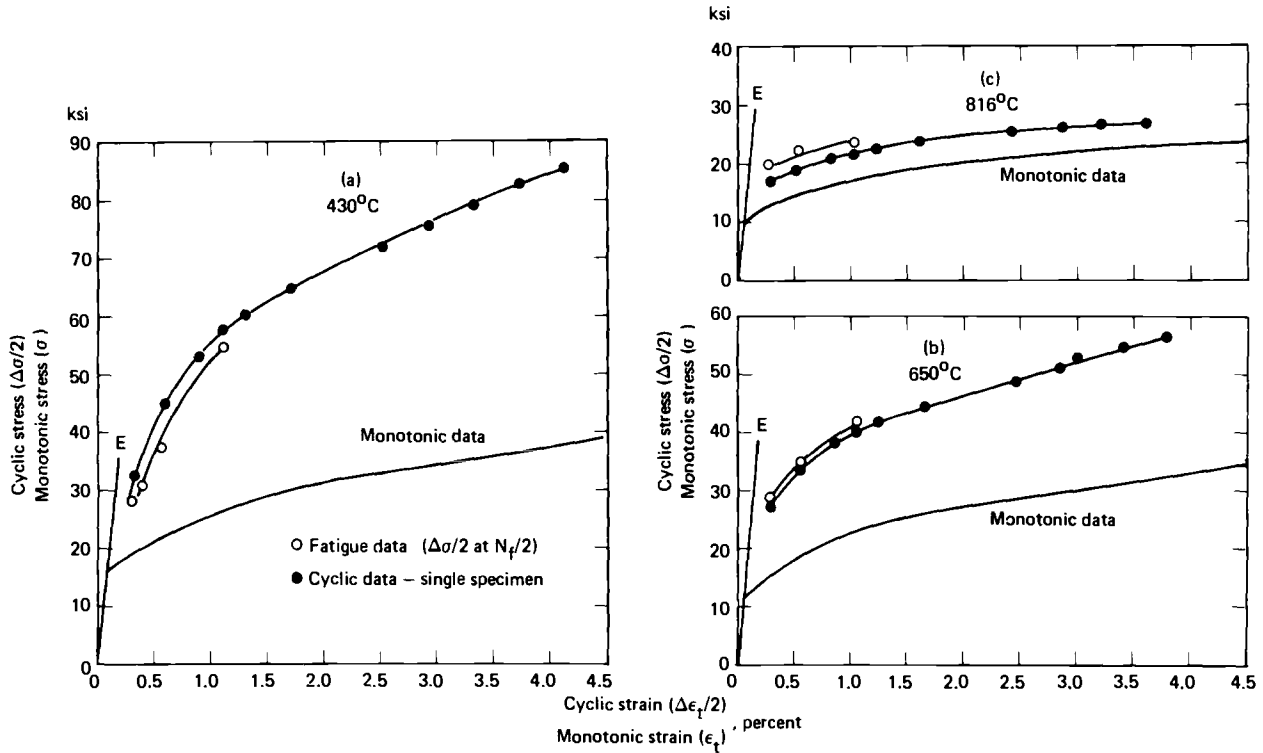


FIG. 11-14-3 — Cyclic and monotonic stress-strain diagrams for AISI 304 stainless steel at 430°, 650°, and 816°C (axial strain rate $4 \times 10^{-3} \text{ sec}^{-1}$).

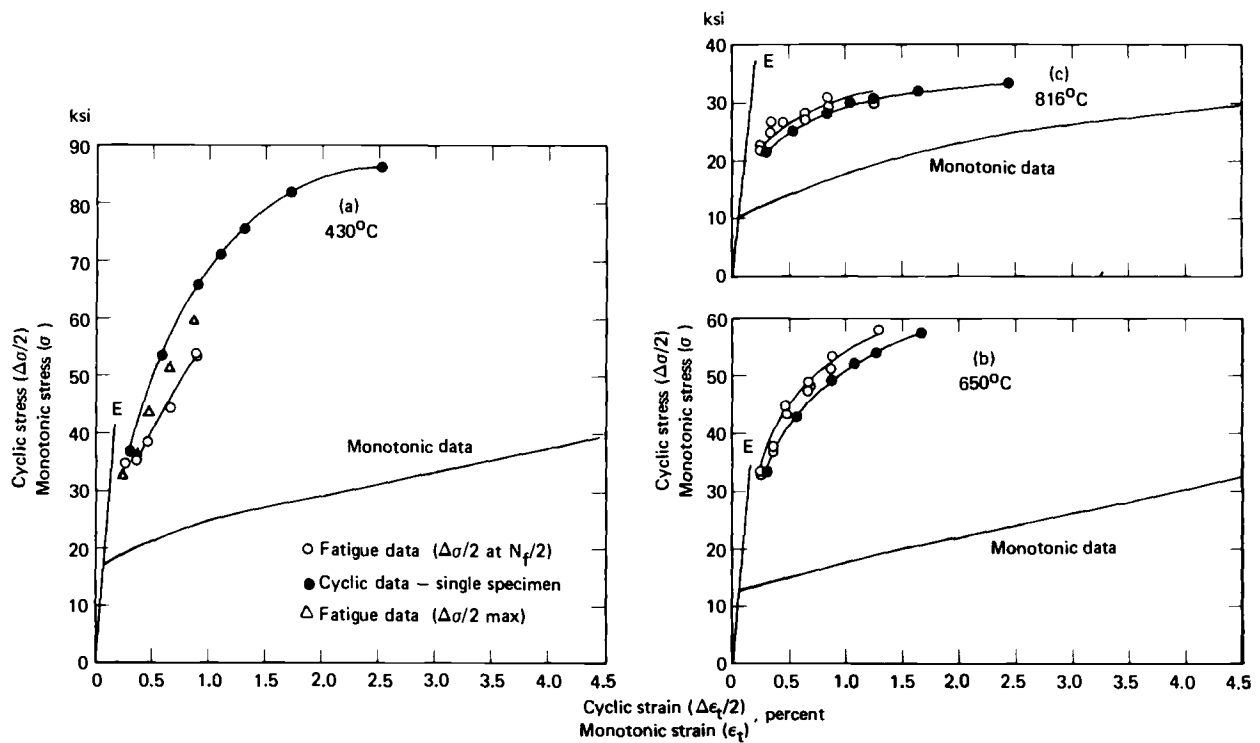


FIG. 12-15-3 — Cyclic and monotonic stress-strain diagrams for AISI 316 stainless steel at 430°, 650°, and 816°C (axial strain rate $4 \times 10^{-3} \text{ sec}^{-1}$).

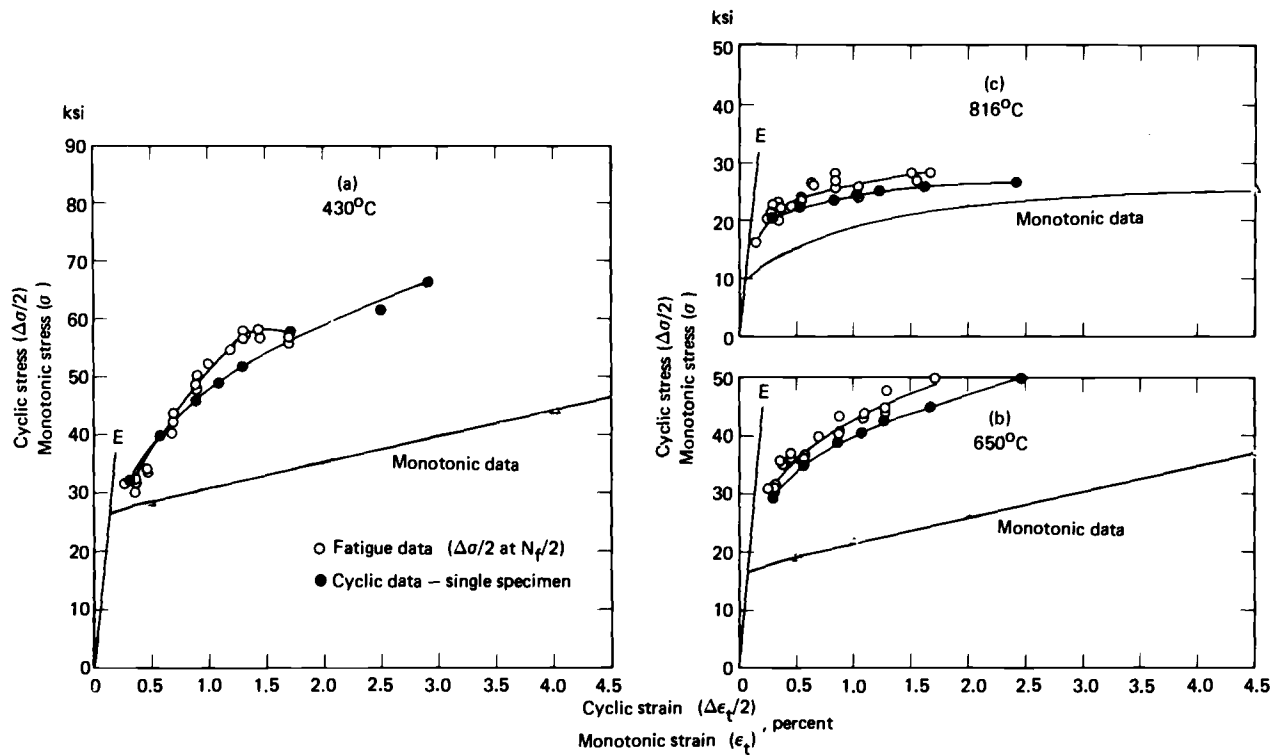


FIG. 13-16-3 – Cyclic and monotonic stress-strain diagrams for AISI 348 stainless steel at 430°, 650°, and 816°C (axial strain rate $4 \times 10^{-3} \text{ sec}^{-1}$).

with the help of a number of individual fatigue tests. The closed circles represent test results obtained with a single specimen which was cyclically loaded for 50 to 100 cycles at each of several successively higher strain levels. This method, defined as “multiple step tests” was described previously in D.3. It appears that the data obtained with a single specimen are a good approximation of the curve representing many specimens. For comparison, the monotonic true stress-strain data obtained in tension tests are also shown. Considerable strain hardening is evident in all cases.

C.6. – Krempl in R24 presents a comparison between monotonic and cyclic stress-strain diagrams for three steels at room temperature. Fig. 14-B7-24 is for low-carbon steel, Fig. 15-B8-24 is for 2 1/4 Cr - 1 Mo steel, and Fig. 16-B9-24 is for type 304 stainless steel. In the three cases definite strain hardening was observed. The curve marked “cyclic” was derived from stabilized hysteresis loops obtained as a result of fatigue testing to failure of many specimens.

C.7. – Younger in R56 discusses the difference between the cyclic stress-strain curve and the so-called “envelope curve”. He points out that the envelope curve is the envelope of several *stable* hysteresis loops which have been shifted to a common point at the peak compression stress. See Fig. 17-2-56. On pages 12-15 the author points out that other investigators have shown that the envelope of the outer traces of hysteresis loops and the cyclic stress-strain curve differ by a factor of 2 in the region between 10^2 and 10^4 cycles. Therefore,

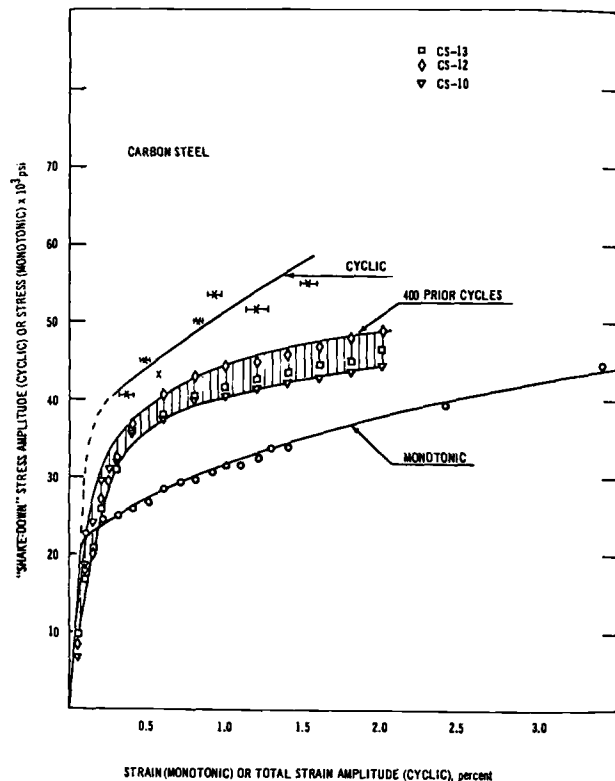


FIG. 14-B7-24 – Monotonic and cyclic stress-strain curves for carbon steel.

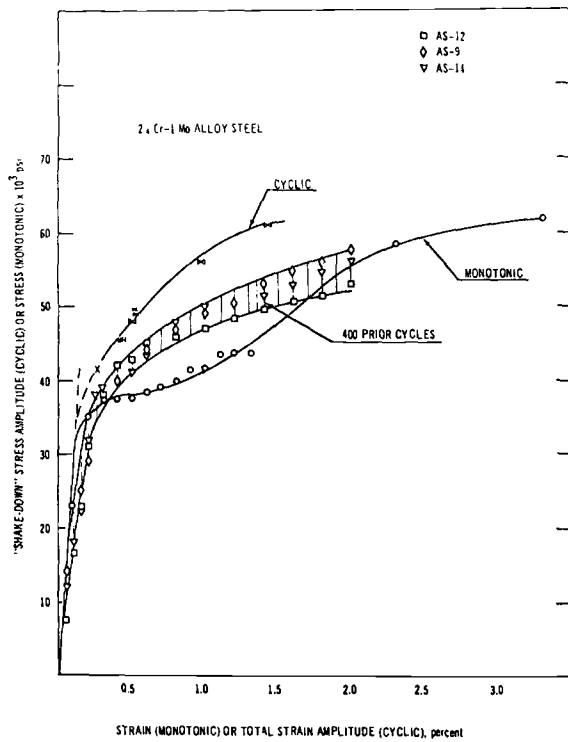


FIG. 15-B8-24 - Monotonic and cyclic stress-strain curves for 2 1/4 Cr-1 Mo alloy steel.

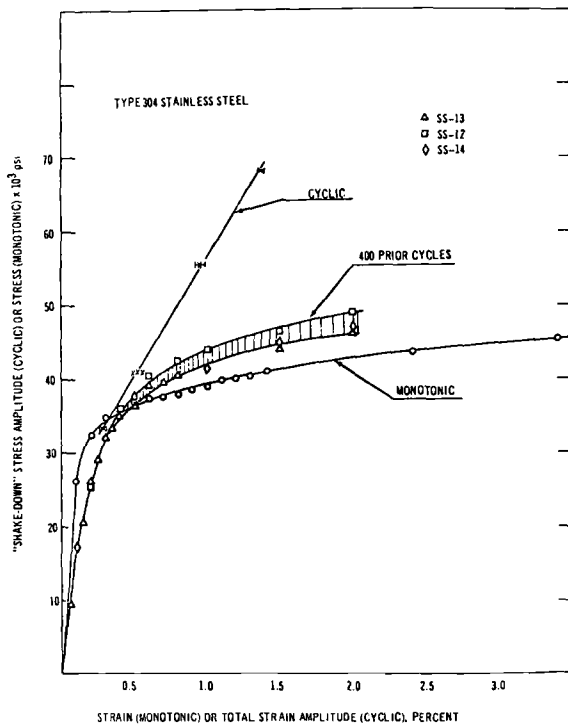


FIG. 16-B9-24 - Monotonic and cyclic stress-strain curves for type 304 stainless steel.

the stresses and strains connected with the envelope curve are double amplitude values, while the stresses and strains in the case of the cyclic stress-strain curve are single amplitude values. See Fig. 18-4-56.

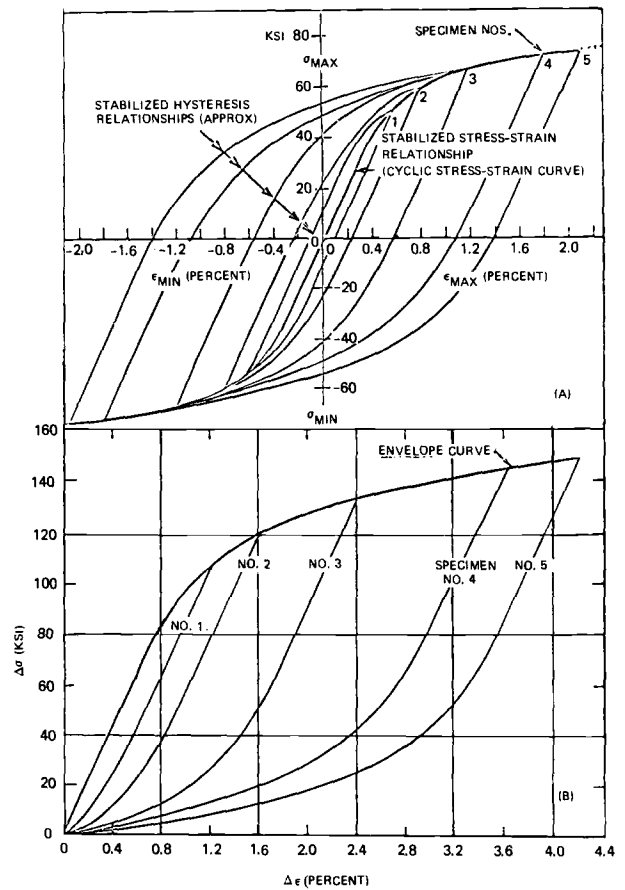


FIG. 17-2-56 - The relationship between the envelope curve and the cyclic stress-strain curve (2024-T351 aluminum alloy).

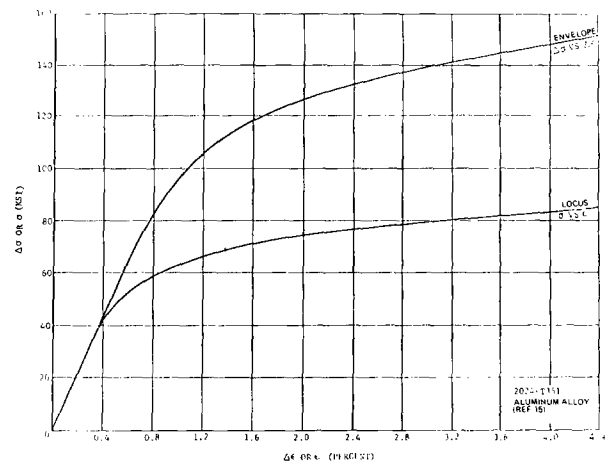


FIG. 18-4-56 - Cyclic stress-strain envelope and locus curves.

C.8. - Snow et al in R.45 present two cyclic stress-strain diagrams obtained at room temperature. Their Fig. 1 shows the diagram for Ni-Cr-Fe Alloy 600(Inconel). Fig. 4 shows the diagram for low-alloy steel A302B.

C.9. - Manson, et al, in R. 33 (Fig. 6) shows cyclic stress-strain diagrams for 7075-T6 aluminum alloy and annealed AISI 4340 steel.

SECTION D
NEUBER'S RELATIONSHIP BETWEEN STRESS AND STRAIN
CONCENTRATION FACTORS AND APPLICATION TO
LOW-CYCLE FATIGUE

D.1. — According to Neuber there exists an approximate relationship between the theoretical elastic stress concentration factor, abbr. "ESCF" k_t and elasto-plastic stress concentration factor, abbr. "PS-sCF" k_p and elasto-plastic strain concentration factor "PS-nCF" q_p in the form

$$k_t^2 = k_p \cdot q_p \quad (1)$$

This relationship was developed by Neuber in R38, page 550 and in R39. Neuber states that although Eq. (1) was derived for two-dimensional shear only, it could be generalized with good approximation to arbitrary two or three-dimensional states of stress. Obviously Eq. (1) applies strictly when the local stresses and strains are within the proportional limit, because then $k_t = k_p$. In some limited region beyond the proportional limit Eq. (1) appears plausible, because it is known from other considerations that with increasing average stress on the net section, k_p begins to decrease and q_p increases, so that the product may remain approximately constant.

However, the evidence indicates that the product does not remain constant beyond a limited small region and that it gradually decreases with increasing nominal stress. This can be seen from Figs. 3, 5 and 7 in R50, by multiplying the corresponding values of k_p and q_p shown in the figures.

It must be understood that the stress and strain concentration factors may be either referred to the nominal stress and strain based on the net section or to the stress and strain based on the gross section. For instance, see Fig. 5 in R39.

Note that because the nominal strain e_n rapidly increases when the nominal stress increases past the yield strength S_y , the "PS-nCF" q_p , defined as the ratio of e_{max} to e_n , reaches a maximum and then begins to decrease. For instance, see Fig. 24 in R30.

In spite of the above, Neuber's approximate relationship was used by a number of investigators to estimate the cyclic life of notched specimens.

D.2. — Topper, et al, in R49 use Neuber's relationship between k_p and q_p for the determination of fatigue life of notched specimens. The authors replace the "ESCF" k_t by k_f the fatigue strength reduction factor "FS-thRF" k_f , which is almost always smaller than k_t . See original paper for definition of k_f .

Neuber's relationship becomes

$$k_p \cdot q_p = k_f^2 \quad (2)$$

k_p is the "PS-sCF" and q_p is the "PS-nCF".

In the following we confine ourselves to the totally

reversed tension-compression loading of notched specimens, $R = -1$.

If $\overline{\Delta S}$ is the range of *nominal* stress based on net cross-section and ΔS is the corresponding range of *local* stress at the apex of the notch, then by definition

$$k_p = \frac{\Delta S}{\overline{\Delta S}} \quad (3)$$

Similarly, if $\overline{\Delta e}$ is the range of *nominal* strain, based on net cross-section and Δe is the corresponding range of *local* strain at the apex of the notch, then by definition

$$q_p = \frac{\Delta e}{\overline{\Delta e}} \quad (4)$$

Therefore, Eq. (2) becomes

$$k_f^2 = \frac{\Delta S}{\overline{\Delta S}} \cdot \frac{\Delta e}{\overline{\Delta e}}$$

multiplying by modulus of elasticity E

$$k_f^2 \cdot \overline{\Delta S} \cdot \overline{\Delta e} \cdot E = \Delta S \cdot \Delta e \cdot E \quad (5)$$

The physical meaning of Eq. (5) is pointed out by the authors as follows. $\overline{\Delta S}$ and $\overline{\Delta e}$ are the *nominal* stress and strain ranges at the notch apex. If the notch apex remains elastic during cycling, then

$$\Delta S = \Delta e \cdot E \text{ and } \overline{\Delta S} = \overline{\Delta e} \cdot E$$

Eq. (5) becomes

$$k_f \cdot \overline{\Delta S} = \Delta S$$

This is the familiar form which relates local stress with the product of nominal stress and k_f .

However, if only the nominal stress and the corresponding strain are limited to the elastic region, which often occurs, then only $\overline{\Delta S} = \overline{\Delta e} \cdot E$ and Eq. (5) becomes

$$(k_f \cdot \overline{\Delta S})^2 = \Delta S \cdot \Delta e \cdot E \quad (6)$$

Note that Eq (5) applies to all values of nominal stress, while Eq. (6) applies for nominal stresses less than the yield stress.

Equations (5) and (6) relate the nominal stress and strain behavior at the net section of a notched specimen with stress and strain behavior at the apex of the notch.

It can also be interpreted as furnishing indices of equal damage in notched and unnotched specimens of the same material. In completely reversed constant amplitude tests, a notched specimen and a smooth specimen will form macrocracks at the same fatigue life provided $k_f^2 \cdot \overline{\Delta S} \cdot \overline{\Delta \epsilon} \cdot E$ for the notched specimen is equal to $\Delta S \cdot \Delta \epsilon \cdot E$ for the smooth specimen. This means that smooth specimen results can be used to produce master life plots for estimating the fatigue life of notched members.

When a strain range controlled fatigue test is performed on an unnotched specimen, the strain range $\Delta \epsilon$ is known for a particular cyclic life. Stress range ΔS is then obtainable with the help of the cyclic stress-strain diagram which pertains to the used material. (For the discussion of cyclic stress-strain diagrams see Section C). Such a master plot is shown in Fig. 19-1a-49 for two aluminum alloys, 2024-T4 and 7075-T6.

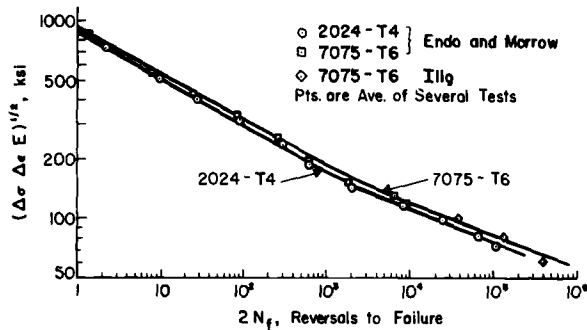


FIG. 19-1a-49 — Smooth specimen fatigue data in a form suitable for predicting lives of notched members.

For a notched specimen of the same material the imposed nominal stress range $\overline{\Delta S}$ is known. The corresponding nominal strain range $\overline{\Delta \epsilon}$ is again obtainable from the previously mentioned cyclic stress-strain diagram. The “FS-th RF” k_f or the “ESCF” are also known. The product $k_f^2 \cdot \overline{\Delta S} \cdot \overline{\Delta \epsilon} \cdot E$ is calculated and the predicted life of the notched specimen is obtained from the master plot described above.

For comparison with experimental results the authors used cyclic life data from R.20 pertaining to completely reversed tests on notched plates with $k_t = 2.0$ and 4.0 . The data points were plotted on the master plot shown in Fig. 19-1a-49 and the results of comparison are shown in Fig. 20-1b-49 and 21-1c-49 for the two aluminum alloys. Agreement between actual life data and predictions is seen to be good.

The authors conclude that for completely reversed amplitude loading, $R = -1$, which does not introduce significant mean stresses at notch roots, the master plot curve derived from cyclic life data of unnotched specimens may be used to estimate the cyclic fatigue life of notched specimens made from the same material.

Note that this method is limited to predicting crack initiation or final failure when the crack propagation stage is negligible.

D.3 — Wetzell in R. 54 proposes a method which utilizes

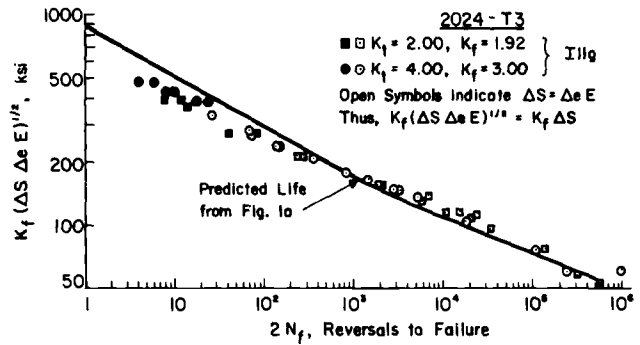


FIG. 20-1b-49 — Notched fatigue data compared to the life curve predicted from smooth specimen data.

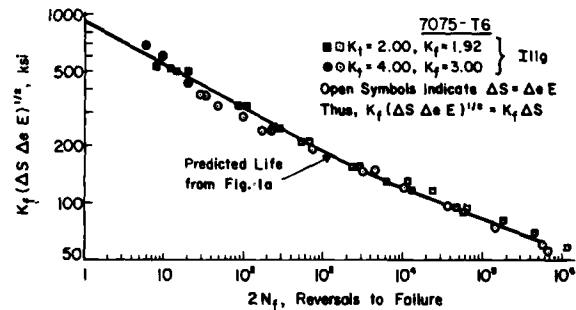


FIG. 21-1c-49 — Notched fatigue data compared to the life curve predicted from smooth specimen data.

Neuber’s equation to help to predict the behavior of material at the notch root during cyclic loading.

He describes twelve, specially controlled fatigue tests with zero to maximum load, $R = 0$, performed on unnotched specimens. The purpose of these tests was to investigate if such specially controlled tests with $R = 0$, performed on unnotched specimens will yield data which could be used to predict fatigue life of similarly loaded notched specimens.

The underlying assumption in these specially controlled tests was the contention that if the unnotched bar is forced to simulate the behavior of the metal at the apex of a notch in a cyclically zero to maximum loaded plate, then the bar will fail in the same number of cycles as the notched plate.

In setting up the tests it was assumed that the maximum nominal stress across the net section does not exceed the yield strength of the material and therefore, Eq. (6) applies. Eq. (6) is re-written

$$\frac{(k_f \overline{\Delta S})^2}{E} = \Delta S \cdot \Delta \epsilon \quad (6a)$$

For zero to maximum (pulsating) loading of notched plates $\overline{\Delta S}$ is the nominal stress range for each half-cycle. Therefore,

$$\frac{(k_f \overline{\Delta S})^2}{E}$$

is a constant and the product of local stress and strain

range $\Delta S \cdot \Delta e$ must be equal to the same constant during each half-cycle.

In other words, if the unnotched bar is controlled so that the product of the half-cycle change in stress and in strain is kept constant throughout the test, it ought to simulate the behavior of the metal at the notch root. It follows then that the product of maximum local stress S and the maximum local strain e is constant during each half-cycle.

Therefore, in a "S - e" coordinate system the peaks of hysteresis loops must locate themselves on hyperbolas with a different origin for each subsequent cycle. This is shown in Fig. 22-3-54. This figure indicates cycle dependent strain hardening and also a relaxation of mean stress.

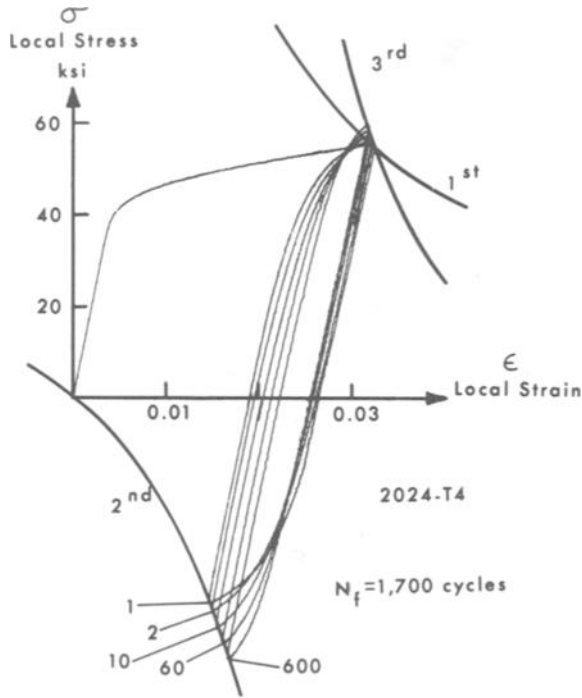


FIG. 22-3-54 –Recorded data from a smooth specimen simulation of the local stress-strain behavior of a notch.

Note that because $k_f \cdot \overline{\Delta S}$ is constant the test results obtained with one unnotched specimen may be used to simulate the behavior of a number of plates with notches of different geometry (k_f).

The 12 unnotched bars were fatigue tested, $R = 0$, and controlled as described above. For each of the bars the product $\Delta S \cdot \Delta e$ was constant; it varied from 2.47 to 0.15 and the corresponding number of cycles to failure varied from 800 to a few million cycles. Test data are tabulated in Fig. 23a-T1-54. The author chose three values of $k_f = 1.9, 2.3$ and 3.3 . The corresponding values of nominal stress range $\overline{\Delta S}$ which satisfy the control constants are tabulated.

Fig. 23-4-54 shows test results of fatigue tests with zero to maximum load on three aluminum alloy plates with "FS-th RF" $k_f = 1.9, 2.3$ and 3.3 . The three curves were available in the literature. The same figure contains points which represent test results obtained by the author with the twelve unnotched bars intended to simulate the behavior of notched plates with $k_f = 1.9, 2.3$ and 3.3 . The author states that the agreement between fatigue curves for the notched plates and the fatigue results obtained with the unnotched specimens is good.

For additional details and explanations see the original paper.

For a similar approach in using Neuber's equation and companion specimens to simulate behavior of notches during low-cycle fatigue, see Crews, R.7 and Section E.3.

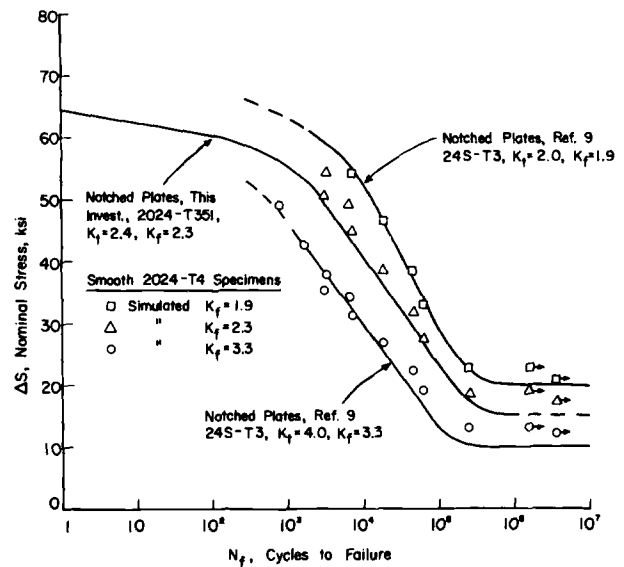


FIG. 23-4-54 – S-N curves for 0-max loaded notched plates compared with smooth specimen simulation data.

TABLE 1—Data from smooth 2024-T4 aluminum simulation specimens.

Constant = $(K_f \Delta S)^2/E$, ksi	N_f , cycles	Stabilized Values, ksi		Typical Simulated Values of ΔS , ksi		
		$\Delta \sigma$	σ_{max}	$K_f = 1.9$	$K_f = 2.3$	$K_f = 3.3$
2.47	800	123	0	85.1 ^a	70.2 ^a	49.0
1.85	1 700	119	0	73.6 ^a	60.9 ^a	42.4
1.47	3 300	116	0	65.7 ^a	54.3	37.8
1.27	3 100	112	0	61.1 ^a	50.5	35.2
1.22	6 700	109	0	59.7 ^a	49.4	34.4
0.98	7 300	100	0	54.2	44.8	31.2
0.72	19 000	88.6	5	46.3	38.3	26.7
0.49	46 000	70.6	5	38.5	31.8	22.1
0.38	62 000	61.9	13	33.0	27.2	19.0
0.18	1 700 000 ^b	43.5	21	22.9	19.0	13.2
0.17	250 000	42.9	21	22.6	18.6	13.0
0.15	4 700 000 ^b	40.2	20	21.2	17.5	12.2

^a Value is in error because it seriously exceeds the yield strength (see text: Limitations).

^b Did not fail, runout.

FIG. 23a-T1-54

SECTION E
STOWELL-HARDRATH-OHMAN EQUATION AND
ITS APPLICATION TO LOW-CYCLE FATIGUE

E.1. — Griffith in R. 12 (1948) and Stowell in R. 46 (1950) have initiated a successful attempt, both experimental and analytical, to simplify the calculation of elastic stresses in a circular hole in an infinite sheet subjected to uniform tension at a remote distance from the hole. They obtained a rather simple formula for k_p , the elasto-plastic stress concentration factor, abbreviated as “PS-sCF”

$$k_p = 1 + 2 \frac{E_s}{E} \quad (7)$$

In this formula E is modulus of elasticity at a point remote from the hole where the stress S is applied and where elastic behavior prevails. E_s is the secant modulus corresponding to the maximum local stress S_{max} . For definition of secant modulus see R. 12 and Fig. 42-5-56, 24-2-6 and 48-39-40. The “PS-s CF” is defined as

$$k_p = \frac{S_{max}}{S} \quad (8)$$

Note that the secant ratio $\frac{E_s}{E}$ is intended to account for local plasticity.

Hardrath and Ohman in R. 14 (1953) intuitively evolved a much more general equation which could be applied not only to wide sheets but also to commonly encountered geometric discontinuities. The equation is rather simple

$$k_p = 1 + (k_t - 1) \frac{E_s}{E_{sn}} \quad (9)$$

Here, k_t is the well known theoretical elastic stress or strain concentration factor, abbreviated as “ESCF”. Also, by definition the “PS-s CF” is

$$k_p = \frac{S_{max}}{\bar{S}} \quad (10)$$

where \bar{S} is the nominal stress based on the net cross-section of the specimen and which may exceed the proportional limit. E_{sn} is the secant modulus which corresponds to the nominal stress \bar{S} and replaces E in Eq. (7). As before, E_s is secant modulus which corresponds to the local stress S_{max} .

The elasto-plastic strain concentration factor, designated here as q_p and abbreviated “PS-nCF” is defined as

$$q_p = \frac{e_{max}}{\bar{e}} \quad (11)$$

e_{max} is the maximum strain usually in the apex of notch. \bar{e} is the nominal strain which corresponds to the nominal stress \bar{S} and which is based on the net cross-section of the specimen.

$$e_{max} = \frac{S_{max}}{E_s} \quad (12)$$

and

$$\bar{e} = \frac{\bar{S}}{E_{sn}} \quad (12a)$$

q_p , the “PS-nCF”, is obtained from the following simple relation

$$\frac{q_p}{k_p} = \frac{E_{sn}}{E_s} \quad (13)$$

and is always larger than “PS-sCF” k_p .

Eq. 9, which has to be solved by successive approximations, requires the determination of secant moduli E_s and E_{sn} . Under monotonic conditions of loading the secant moduli are determined from the well known stress-strain diagram. However, under cycling loading conditions it is logical to derive their values from a properly determined cyclic stress-strain diagram as suggested by Manson and Peterson. See Section C for additional discussion.

Eq. (9) and the procedure suggested by Stowell, Hardrath and Ohman for the approximate determination of “PS-sCF” k_p and “PS-nCF” q_p will be referred to as the “SHO” method. For additional discussion, including the successive approximation procedure, secant moduli, etc. see Manson R. 35 (p. 6-11) and Younger R. 56.

The “SHO” method as described above was intended to apply only to stress concentrations in thin sheets. However, the method was extended by Sarney, R 44 to cylindrical bars with circumferential notches in tension. A short description of Sarney’s extension of “SHO” method may be found in Zwicky, R. 57. See E. 4 and E. 8.

In the following references the “SHO” method was used by several investigators to approximate the behavior of material in stress concentrators (notches) during the first fatigue cycle or cycles.

For additional discussion of factor q_p and of the “SHO” method, see E. 4, Krempl R23 and F. 3, Manson

E. 10 and Peterson I.4, Fig. 128-6-41.

E.2. — Crews, et al, in R. 6 describe an interesting set of experiments with large, 12-in. wide edge-notched plate specimens from 2024-T3 aluminum alloy with “ESCF” $k_t = 2$, referred to the net section. They have subjected these specimens to repeated tension loading, load ratio $R = 0$ and to completely reversed constant amplitude loading, load ratio $R = -1$. Strain gauges were mounted in the notch roots and local strains were measured during cycling loading whose magnitude was defined by the nominal stress across the net section.

In order to determine the magnitude of stresses which correspond to the measured strains, unnotched companion specimens were provided. These specimens were subjected to the *same strain history as measured in the root of the notch* and the measured stresses were assumed to represent the stress history at the notch root because in this region a practically uniaxial state of stress exists. The nominal stresses were over the range from that corresponding to incipient yielding at the notch root to that approaching the yield stress of the aluminum alloy on the net section.

The authors describe as follows the behavior of material at the notch root. See also Fig. 24-2-6. For the first complete loading and unloading cycle of pulsating

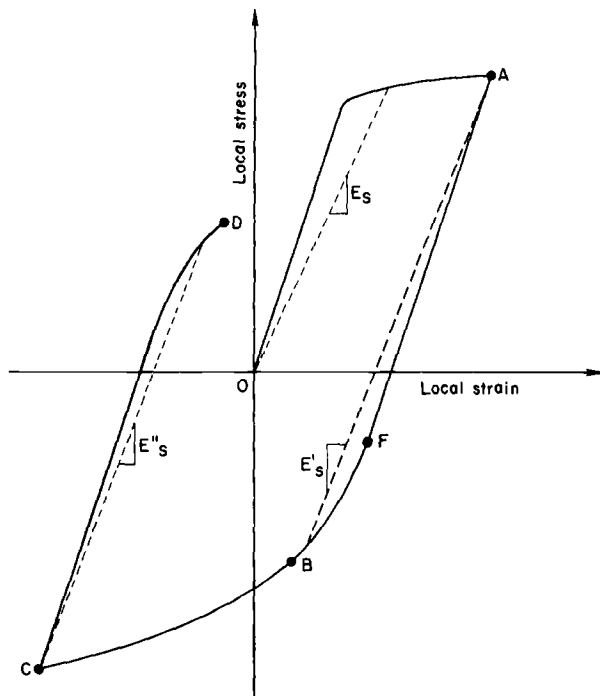


FIG. 24-2-6 – Local stress-strain curve for first cycle of loading.

load, $R = 0$, a typical behavior of local stress is described by the curve OAB; where A represents the maximum local stress and strain and B represents the compressive residual stress and strain occurring upon unloading to zero from the maximum load. For the first *complete* cycle of *completely reversed loading*, $R = -1$, a typical set of local stresses and strains is depicted by the curve OABCD. C represents the minimum local stress and strain when the load is at the minimum (compression) and D represents

the tensile residual stress and strain at the end of the full cycle of loading when again the load reaches zero.

Fig. 25-3-6 illustrates stress-strain relationship at the notch for the first complete cycle of pulsating loading, $R = 0$, for six different values of maximum nominal stress.

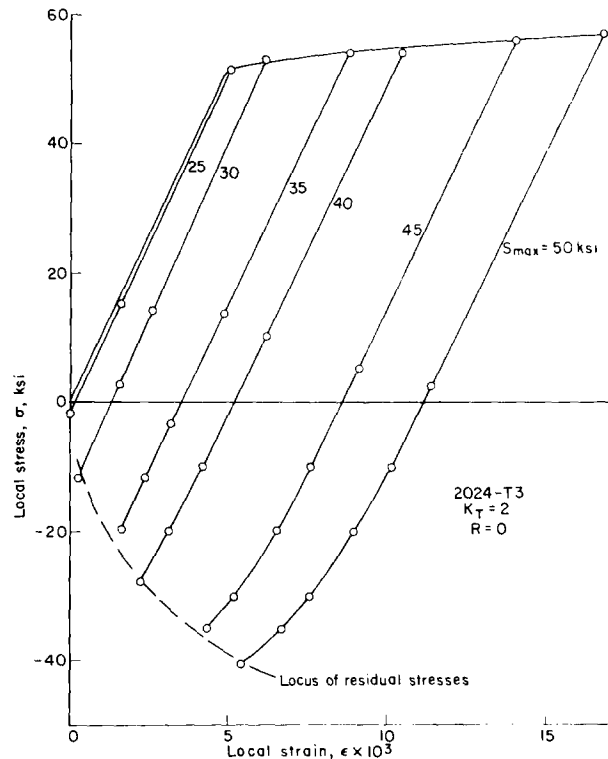


FIG. 25-3-6 – Local stress-strain curves for first cycle repeated loading ($R = 0$).

The unloading part of each load cycle produced a compressive local residual stress. In tests with high nominal stress yielding in the notch root occurred upon unloading. Beyond the tenth cycle local stresses returned essentially to the same value. During cycling the stress range remained virtually unchanged. It is seen that the mean value of *local* stress decreased considerably when the *nominal* stress increased from 25,000 to 50,000 psi.

Fig. 26-5-6 illustrates stress-strain relationship at the notch root for the first complete cycle of completely reversed loading, $R = -1$, for three values of maximum nominal stress; For these tests, four characteristic values of *local* stress are of interest: the maximum, the residual compressive stress after unloading when nominal stress is zero at the end of first half-cycle, the minimum compressive stress at the minimum load, and the residual, tension stress after completing the cycle when the nominal stress reaches again zero. It is seen that the magnitudes of residual stresses are influenced by the amplitude of nominal stresses.

The authors observed that, for the aluminum alloy, under constant amplitude load cycling for both $R = 0$ and $R = -1$, the stabilization of local stresses in the notch apex occurred in less than 30 cycles.

In addition to the above experimental analysis pertaining to the behavior of local stresses during cycling,

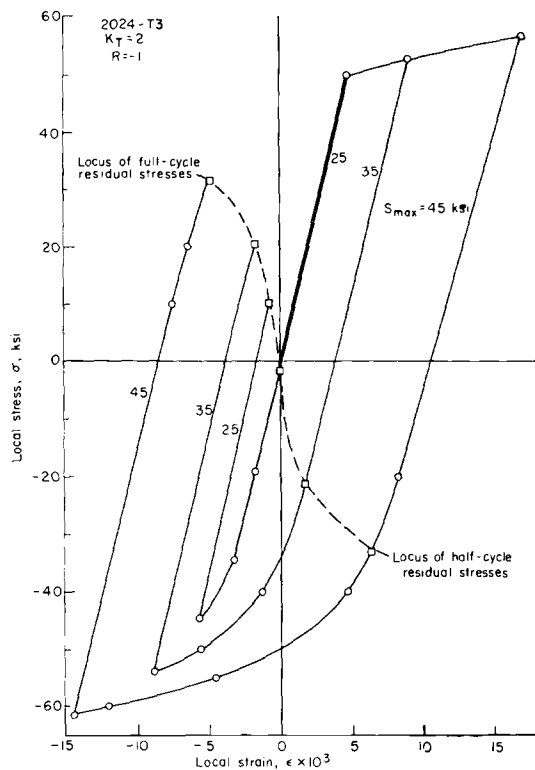


FIG. 26-5-6 —Local stress-strain curves for first cycle of reversed loading ($R = -1$).

the authors attempted to predict fatigue life of notched specimens similar to those used in this paper for the measurements of local strains. For this purpose they used fatigue life data generated by Illg, R. 20, on similar, but smaller, specimens with $k_t = 2$ for $R = 0$ and for $R = -1$. The authors state that they predicted fatigue lives on the assumption that fatigue failure would occur in notched specimens in the same number of cycles that produced failure in unnotched companion specimens subjected by them to repeated stresses equal to the local stabilized stresses observed in the tests described above. The estimates of life of the unnotched specimens were taken from a fatigue diagram (of alternating vs. mean stresses) for available fatigue tests performed on the same material by other investigators. The authors state that the estimates agree well with the data except at low nominal stresses. For more details, see original paper.

The above is encouraging because there is a possibility that the fatigue lives of notched parts could be estimated from behavior of companion, unnotched specimens. Unfortunately, the key information needed to accomplish this is the *relation between the applied nominal stresses and the stabilized stresses at the notch root* and this relationship is obtainable only by rather painstaking tests.

To help this situation the authors attempted to provide a method for *computing* the desired local stresses for the first cycle of loading only. For these purposes they made use of the "HSO" empirical relation, Eq. (9), which defines approximately the "PS-sCF" k_p . The authors develop a relation between S , the local stress during unloading from A and nominal stress \bar{S} , as follows

$$S = S_{max} k_p - (S_{max} - \bar{S}) k_p'$$

where k_p' is obtained using the secant modulus E_s' as shown in Fig. 24-2-6. For loading from C the local stress S is

$$S = S_{max} k_p - (S_{max} - S_{min}) k_p' - (S_{min} - \bar{S}) k_p''$$

where k_p'' is obtained using the secant modulus E_s'' as shown in Fig. 24-2-6.

It is obvious that these equations require trial and error solution and procedure becomes rather complicated. However, the authors have made a number of simplifications and were able to evaluate the *maximum local stress*, *minimum stress*, and the *half and full cycle residual stresses* for a number of nominal stresses and for load ratios $R = 0$ and $R = -1$. The results are plotted in Fig. 27-9-6 and Fig. 28-10-6.

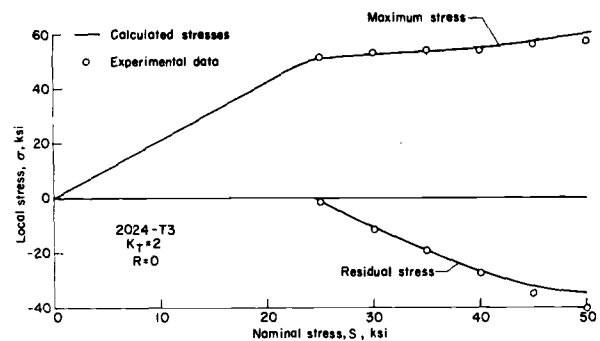


FIG. 27-9-6 —First-cycle stresses for repeated loading.

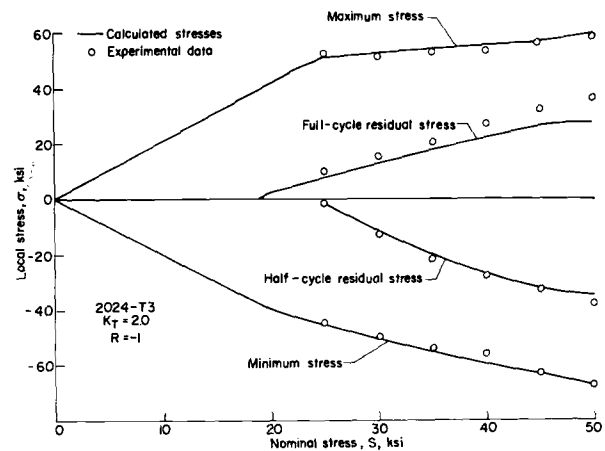


FIG. 28-10-6 — First-cycle stresses for completely reversed loading.

The authors hope that these preliminary calculations of first cycle stresses will ultimately lead to the calculation of stabilized stresses at the notch root. For more details see the original paper. For application of the above procedure see paper by Picket, et al, R. 42 (Appendix).

E.3. — Crews in R. 7 continues the experimental and analytical work described in R. 6, in E. 2. In addition to $k_t = 2$ he also considers $k_t = 4$ and 6 and in addition to

aluminum alloy 2024-T3 he also considers SAE4130 steel. Pairs of notched and companion specimen were cut from adjacent positions in the sheet stock as shown in Fig. 29-1-7. As before, the sequence of strain reading at the notch root was reproduced in strain gages on an unnotched companion specimen to determine the stress corresponding to each strain level. As before, the notched specimens were subjected to full cycles of completely reversed tensile and compressive loading, $R = -1$.

\bar{S}_{max} the cyclic, maximum nominal stress (based on netsection) was selected to give products of $k_t \bar{S}_{max} = 60000, 100000$ and 150000 psi.

A set of first-cycle stress-strain curves derived with the help of companion specimens is shown in Figs. 30-2-7 to 33-6-7. Each Fig. is for a different "ESCF" k_t and shows first cycle hysteresis curves for three values of \bar{S}_{max} . Each curve shows the stress-strain history at the root of the notch during a full cycle of completely reversed loading. See also Fig. 34-11-7.

The loci of half-cycle and full-cycle residual stresses and strain are shown in each Figure. The author states that the antisymmetry of the loci displayed in Fig. 30-2-7 is not generally characteristic of the residual stress-strain behavior for completely reversed loading. This can be seen from Fig. 31, 32, 33.

The following conclusions reached by the author for the edge-notched sheet specimens studied under reversed constant-amplitude loading are quoted from the paper.

For specimens which had elastic stress-concentration factors approximately 2, 4 and 6, the local stress-strain

behavior at the notch root was essentially the same for constant values of the product of maximum nominal stress \bar{S}_{max} and "ESCF" factor k_t .

Stabilization of local stresses appeared to occur in approximately 15 cycles of reversed loading for 2024-T3. The *local* stress range increased and the *local* strain range decreased during the stabilization phase. In a single test with 4130 steel the *local* stress range decreased slightly but did not stabilize in 30 cycles of reversed loading.

Crews devoted a major portion of his paper to the calculation of *local* stresses and strains caused by the cycling of completely reversed loading. For this purpose he used the "SHO" Eq. for "PSCF" k_p and also the Neuber relationship between k_p and q_p , described in Section D. He transformed the "SHO" equation to obtain a relationship between monotonic local stress excursion, monotonic local strain excursion and the monotonic variation of nominal stress which caused the local excursion, the "ESDF" k_t and modulus of elasticity E . See his Eq. (3) in the original paper.

He also suitably transformed the Neuber relationship to obtain an explicit expression for the product of *local* stress and strain excursions in terms of the monotonic *nominal* stress variation and k_t and E . See his Eq. (4) in the original paper.

The procedure for the analytical determination of *local* stresses during cycling is rather involved and will not be described here. Those interested are referred to the original paper.

Note that Crews' approach is similar to the approach

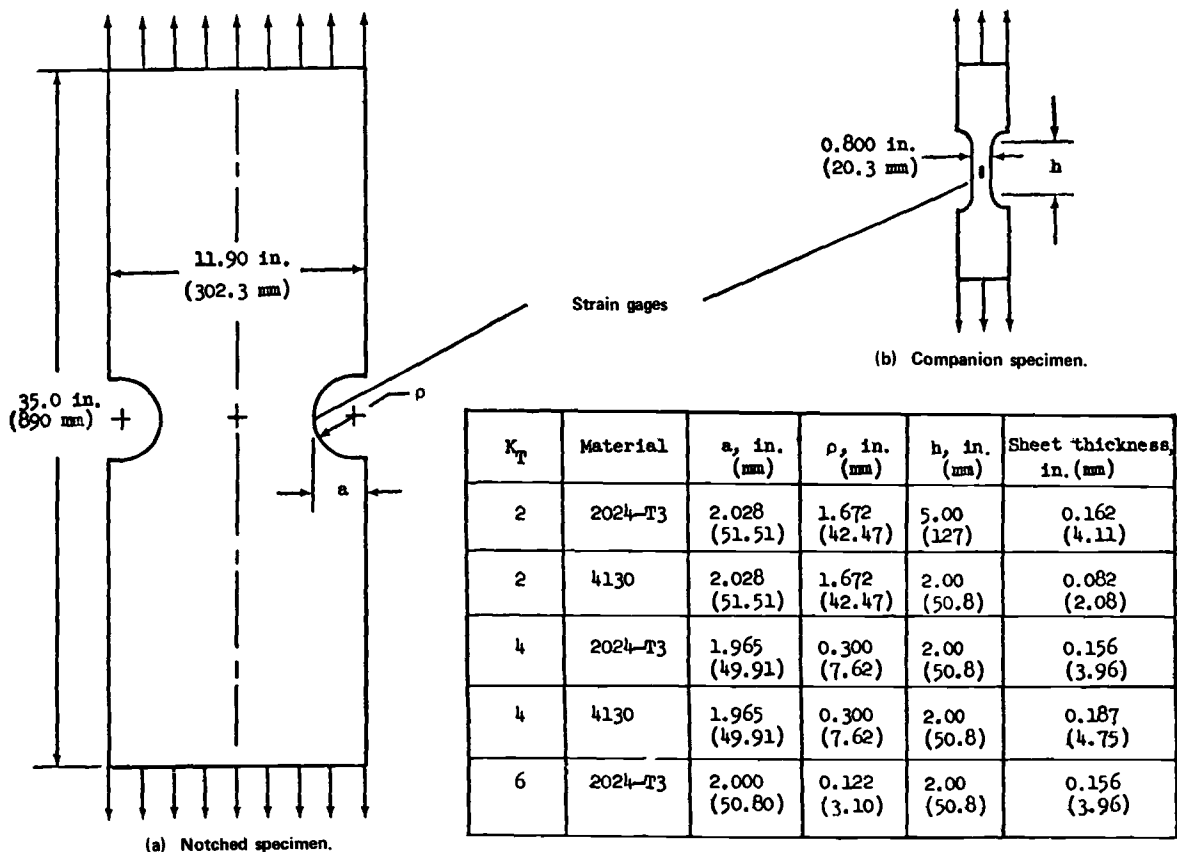


FIG. 29-1-7—Specimen dimensions and instrumentation.

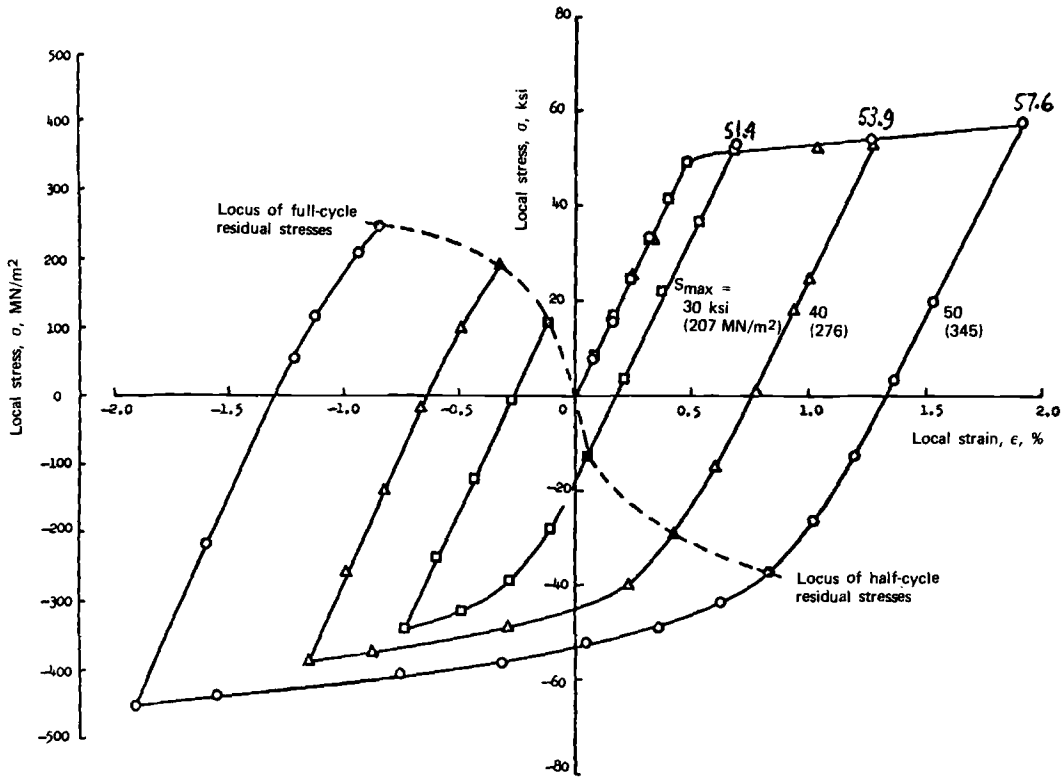


FIG. 30-2-7 – Local stress-strain curves for first cycle. $K_T = 2$: 2024-T3: $R = -1$.

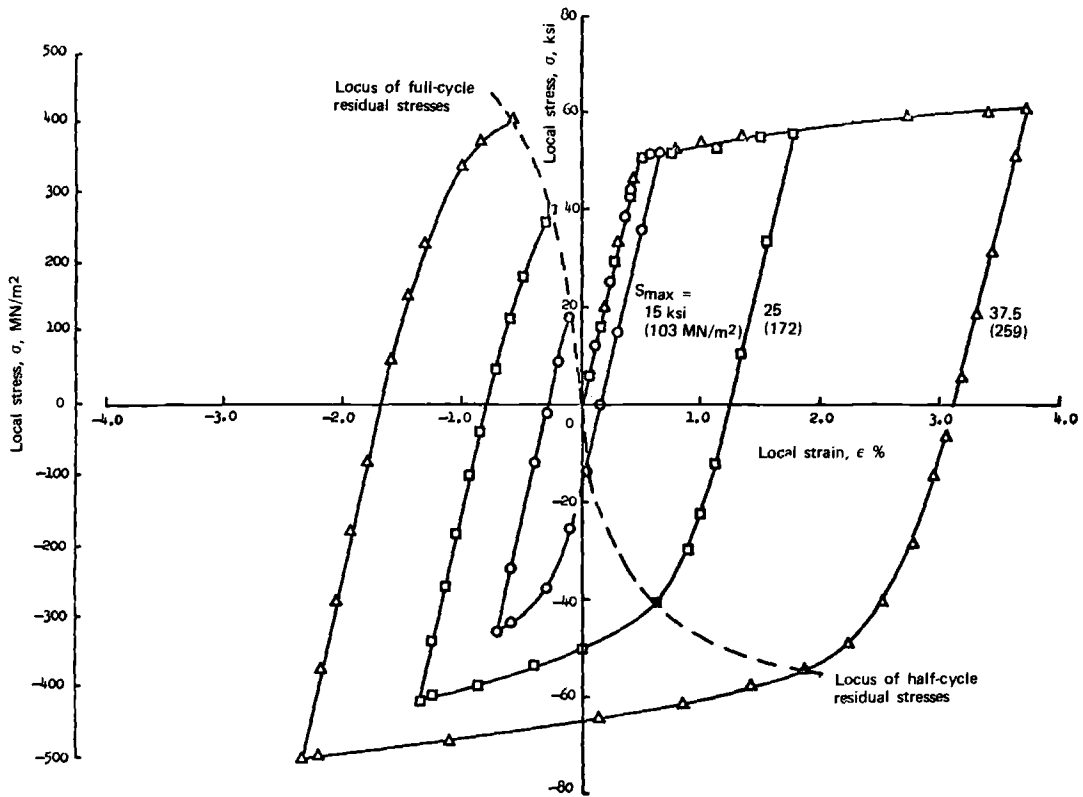


FIG. 31-3-7 – Local stress-strain curves for first cycle. $K_T = 4$: 2024-T3: $R = -1$.

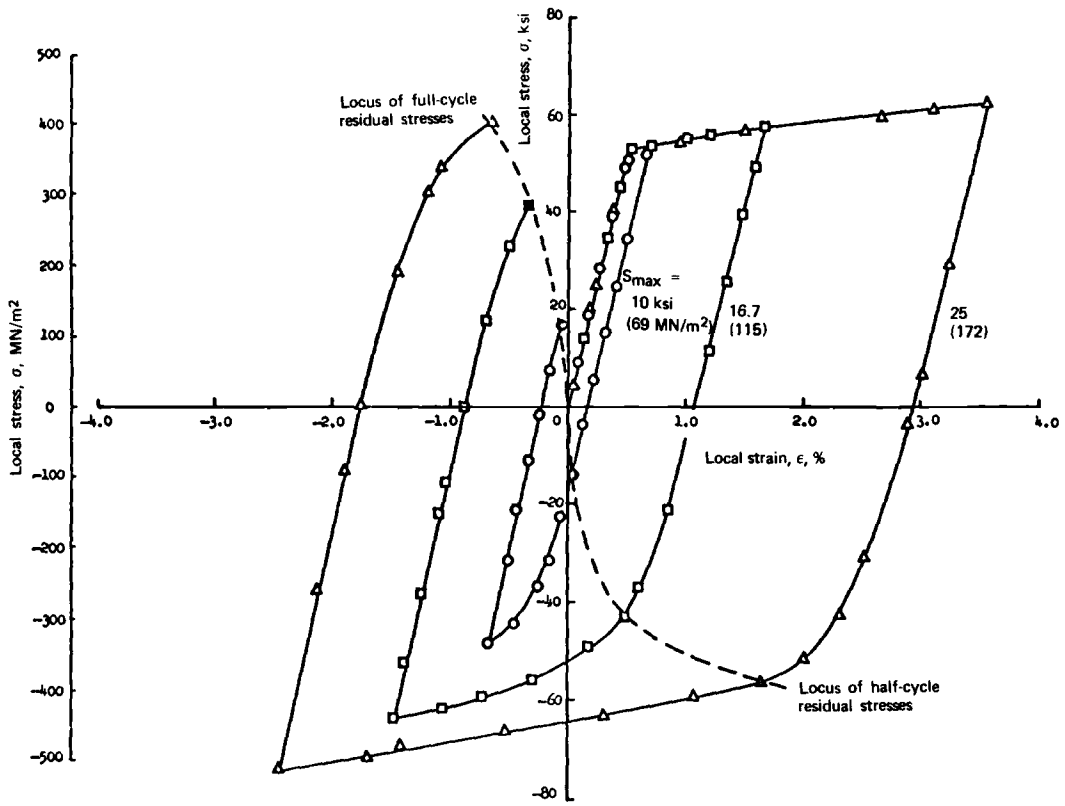


FIG. 32-4-7 – Local stress-strain curves for first cycle. $K_T = 6$; 2024-T3; $R = -1$.

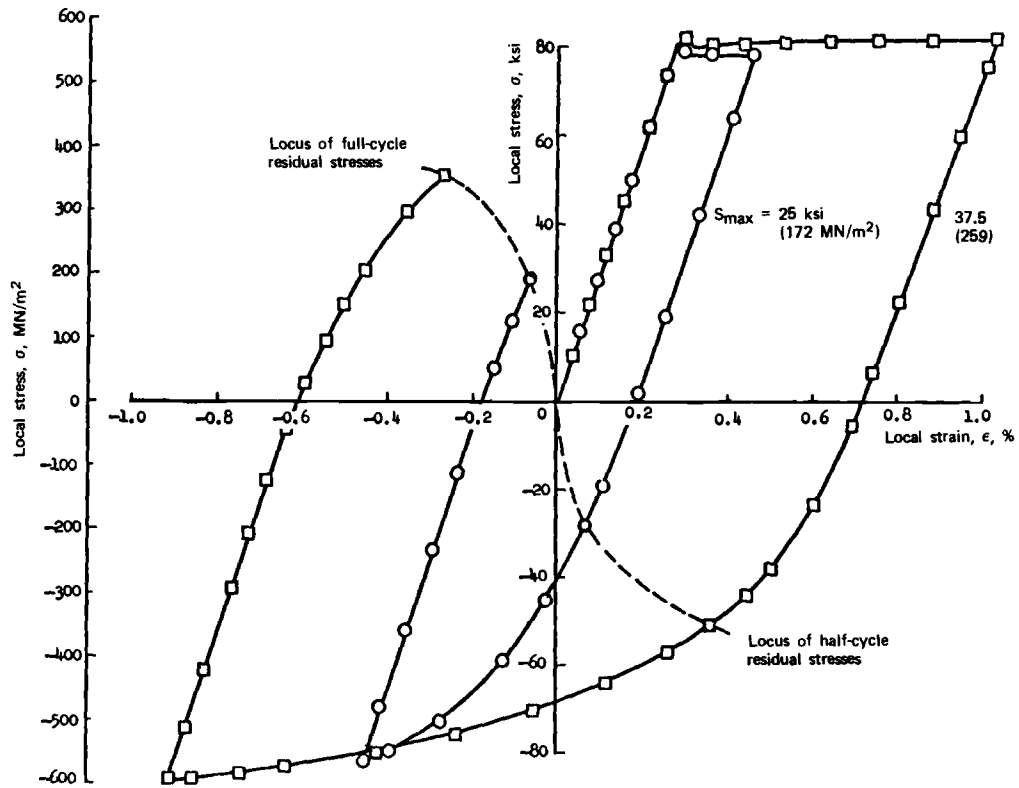
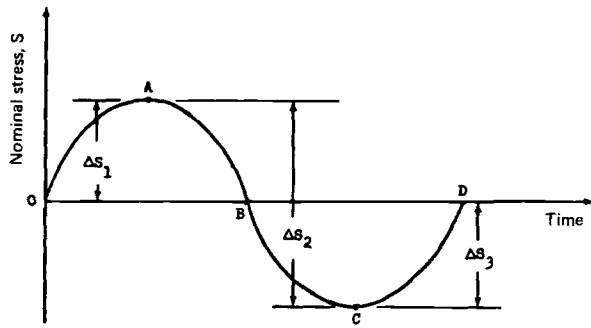
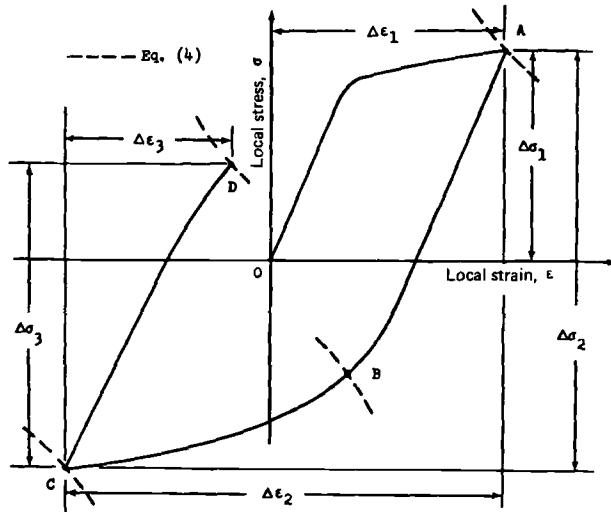


FIG. 33-6-7 – Local stress-strain curves for first cycle. $K_T = 4$; AISI 4130 (normalized); $R = -1$.



(a) Nominal stress cycle.



(b) Estimated local stress-strain curve.

FIG. 34-11-7 – Nominal loading and estimated local stress-strain curve for the first loading cycle.

used by Wetzel in R. 54 and described in Section D.

The author in his Fig. 12, (not reproduced) shows 12 graphs which depict the stress-strain relationship between the local stresses and strains during the first cycle, for $k_t = 2, 4$ and 6 , as obtained experimentally and by using “SHO” and Neuber’s equations.

He concludes that estimates of local stress and strain made by either using the modified “SHO” Equation or the Neuber Equation were good approximations to experimental results for the first cycle of reversed loading. Also estimates of local cyclic stress found for 2024-T3 by repeatedly applying the Neuber equation in a cycle-by-cycle manner correlated well with experimental results during the first 30 cycles of loading.

In this elaborate paper the author succeeds in the elucidation of behavior of local stresses and strains in an edge-notched 2024-T3 sheet during the first complete cycle imposed by totally reversed loading.

E.4 – Zwicky in R. 57 modifies the simple “SHO” relation in order to determine the total strain range Δe at the root of notch in terms of nominal stress range ΔS across the net section. Because the “SHO” relation is applicable only to monotonic loading the author uses a somewhat more complex relation which applies also to unloading and reloading during the first cycle, developed

by Crews, et al, in R. 6 and previously discussed in E.2 and E.3. He then proceeds to modify this expression in order to make it suitable for cycling loading by assuming that the hysteresis loop shown in Fig. 35-4-57 is symmetrical and stabilized. If the nominal stress is cycled

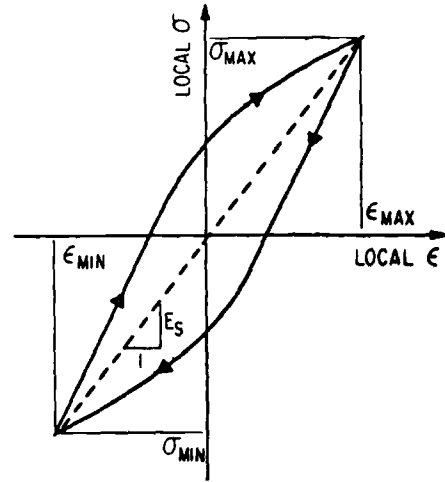


FIG. 35-4-57 – Typical cyclic stress-strain relation

with a stress range $\Delta \bar{S}$ between \bar{S}_{max} and \bar{S}_{min} , and the corresponding local stress cycles between S_{max} and S_{min} the equations in R. 6 assume the form

$$S_{min} = S_{max} - (\bar{S}_{max} - \bar{S}_{min}) [1 + (k_t - 1)] \frac{E_s}{E} \quad (14)$$

$$\text{By definition secant modulus } E_s = \frac{S_{max} - S_{min}}{e_{max} - e_{min}} = \frac{\Delta S}{\Delta e} \quad (15)$$

where $S_{max} - S_{min}$ is the local stress range Δs and $e_{max} - e_{min}$ is the local strain range Δe .

$$S_{max} - S_{min} = \Delta S \quad (16)$$

$$e_{max} - e_{min} = \Delta e \quad (17)$$

In order to simplify the problem and to obtain explicit expression for Δe the author assumes that the local stress range ΔS is equal to twice the yield stress S_y

$$\Delta S = 2 S_y.$$

It is debatable to what extent the ensuing simplification is justified by this assumption.

Defining the nominal stress range $\Delta \bar{S}$

$$\bar{S}_{max} - \bar{S}_{min} = \Delta \bar{S} \quad (18)$$

and e_y , the elastic strain at yield stress S_y

$$e_y = \frac{S_y}{E}$$

the author obtains, after some transformations

$$\frac{\Delta e}{2e_y} = (K_t - 1) \frac{\left(\frac{\overline{\Delta S}}{2S_y}\right)}{1 - \left(\frac{\overline{\Delta S}}{2S_y}\right)} \quad (19)$$

This expression is convenient to use in low-cycle fatigue problems since it defines the total *local* strain range Δe in terms of nominal stress range $\overline{\Delta S}$, yield strain e_y , yield strength S_y and modulus of elasticity E .

Ratio $\frac{\Delta e}{2e_y}$ in expression (19) is shown in Fig. 36-8-57

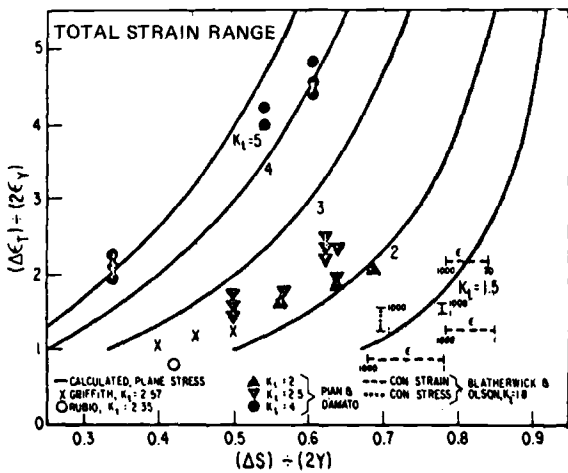


FIG. 36-8-57 – Comparison of measured and calculated strain ranges for various geometries and materials. The σ and ϵ on the Blatherwick and Olson tests refer to constant load or constant strain tests; the numbers refer to the cycle number at which the data were taken.

as a function of

$$\frac{\overline{\Delta S}}{2S_y} \quad \text{for } K_t = 1.5, 2, 3, 4 \text{ and } 5.$$

The elasto-plastic strain concentration factor is defined as

$$q_p = \frac{\Delta e}{\Delta e}$$

the ratio of total *local* strain range to total *nominal* strain range.

Assuming that $\overline{\Delta S}$ does not exceed the yield stress range, then

$$\overline{\Delta e} = \frac{\overline{\Delta S}}{E}$$

and

$$q_p = \frac{\Delta e}{\overline{\Delta S}} \cdot E$$

Substituting $\frac{\Delta e}{\overline{\Delta S}}$ from Eq. (19) we obtain

$$q_p = \frac{K_t - 1}{1 - \frac{\overline{\Delta S}}{2S_y}} \quad (20)$$

This is an explicit expression for “PS-nCF” q_p in terms of “ESCF” K_t , nominal stress range $\overline{\Delta S}$ and yield stress S_y .

Fig. 37-5-57 shows q_p as a function of ratio $\frac{\overline{\Delta S}}{2S_y}$ for different K_t varying from 1.5 to 5.

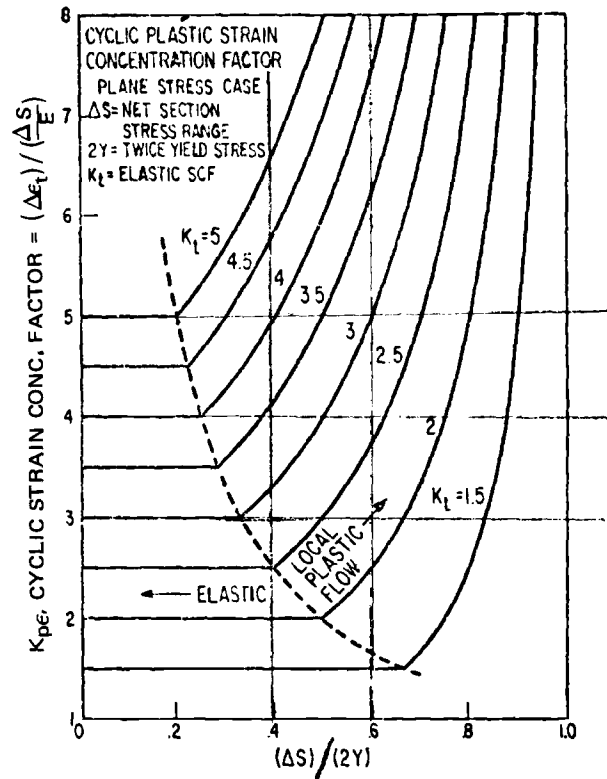


FIG. 37-5-57 – Cyclic strain concentration factors during local yielding under plane stress conditions.

The above discussion applies only to notches in a thin plate subject to plane stress conditions.

The author extended the above analysis for a notched plate to plane strain conditions, e.g. to a cylinder longitudinally stressed with a circumferential notch. He based this on work by Sarney, R. 44, who extended the original plane stress “SHO” relationship to plane strain conditions under monotonic loading. Combining Sarney’s approach with cycling, Zwicky developed new relations for the cycled notched cylinder which are more complicated than Eq. (19) and (20). These expressions are not explicit and must be solved by successive approximations.

The author has calculated and plotted the total local strain range $\frac{\Delta e'}{2e_y}$ in Fig. 38-6-57 which is similar to pre-

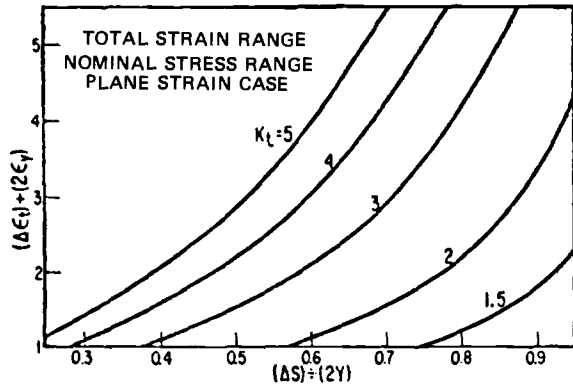


FIG. 38-6-57 – Total strain range for plane strain conditions including effects of local yielding.

viously discussed Fig. 36-8-57. He also plotted the plane strain, elasto-plastic strain concentration factor

$$q_p' = \frac{\Delta e'}{\Delta s}$$

to Fig. 37-5-57.

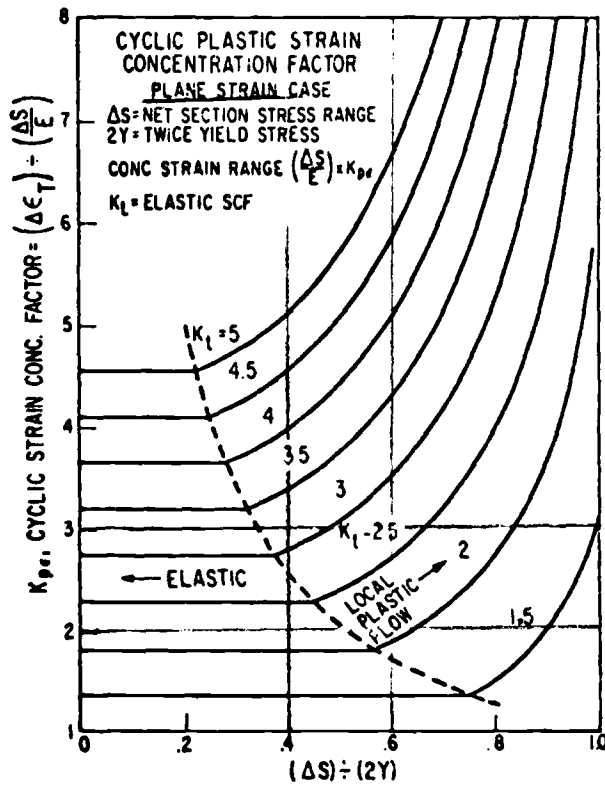


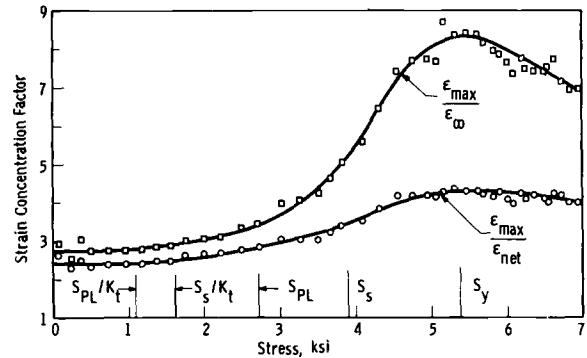
FIG. 39-7-57 – Cyclic strain concentration factors during local yielding under plane strain conditions.

Note that the new q_p' is less than q_p for the plane stress case. It is even lower than the plane strain factor in the elastic regime which is $(1 - \nu^2)$ times the plane stress factor.

The "PS-nCF" q_p in Fig. 37-5-57 and 39-7-57 is con-

tinuously increasing with ratio $\frac{\Delta S}{2S_y}$. It must be remembered that it was assumed that the *nominal* stress range ΔS is within the *yield* range of the material and that therefore, the ratio $\frac{\Delta S}{2S_y}$ is less than 1.

However, it is known from other investigations that when the ratio $\frac{\Delta S}{2S_y}$ approaches 0.9 to 0.95, q_p reaches a maximum and then decreases with further increase of this ratio. For instance, see Figs. 40-24-40 and 47-40-40,



Hole diam = $\frac{1}{4}$ plate width; PL denotes proportional limit; S denotes secant limit corresponding to tangency to a slope of 0.7 E.

FIG. 40-24-40 – Experimental strain concentration factors at a hole in an axially stressed aluminum alloy plate.

Peterson R. 40. Also Figs. 74-8-23, 75-9-23 and 76-10-23 and discussion in F3.

In the reviewer's opinion the occurrence of such a maximum will considerably decrease the large values of q_p for ratios $\frac{\Delta S}{2S_y}$ near 1.0. See also discussion in E5.

The author's formulae permit the calculation of total *local* strain range Δe in terms of known *nominal* stress range ΔS and yield strength S_y . He points out that the yield strength should be obtained preferably from a cyclic stress-strain diagram rather than from a monotonic.

In order to compare his calculations with actually measured local strain ranges due to cyclic loading, the author plotted in Fig. 36-8-57 the results of several experiments published in the literature.

He reviewed the tests by Griffith, R. 12, Blatherwick, et al, R. 4, Kooistra, et al, R. 22, Isberg, et al, R. 21 and others.

In general, good correlations were obtained between the experimental and his calculated values. In most cases the yield strength S_y was obtained from monotonic stress-strain diagrams in absence of cyclic data. For the results of comparison and for discussion see the original paper.

Zwicky suggests that the total calculated local strain range Δe may be used to determine the crack initiation in notched specimens. However, he warns that Δe is not necessarily the best guide for these purposes.

Dawson in R. 8 (See E. 7) calculates the total strain

range for a circumferential groove on the inside surface of a turbine shell.

E.5. – Haydl in R. 16 modifies Zwicky’s expression for the ratio of $\frac{\Delta \epsilon_p}{2\epsilon_y}$. See E. 4 Eq. (19) and R. 57.

He does it by combining the “SHO” expression with Neuber’s approximate relationship between k_p , q_p and k_t . See section D. He points out that k_p is always larger than 1 and lower than k_t . According to his equations, although q_p is increasing and approaches k_t^2 it does not increase to infinity as it would follow from “SHO” expression. This is shown in Fig. 41-8-16 where he compares his results with Zwicky’s Eq. (19).

Haydl summarizes his paper as follows. A new formulation for calculating stress and strain concentration factors in plastic range was suggested and applied to low cycle fatigue study. The formulae presented in this paper are more general than those in Zwicky’s and show good agreement with existing experimental data. It is demonstrated that the present theory can also be applied when the material away from discontinuity enters the inelastic or plastic range.

The reviewer points out that the paper is not too clearly written and it is difficult to follow the author’s reasoning.

E.6. – Younger in R. 56 uses the “SHO” expression to calculate the fatigue life of externally notched 2024-T3 aluminum alloy plates loaded in a fully reversed manner,

$R = -1$. The “SHO” Eq. (9) is rewritten

$$k_p = \frac{S_{max}}{\bar{S}} = 1 + (k_t - 1) \frac{E_s}{E_{sn}} \quad (21)$$

In this equation the “ESCF” k_t is replaced by k_f , fatigue strength reduction factor “FS-th RF” as suggested by Petersen, R. 40. k_f is always less than k_t and introduces the effect of geometric size or notch sensitivity.

It may be derived from high-cycle fatigue tests on smooth and notched bars as the ratio of endurance limit of unnotched specimens to the endurance limit of notched specimens.

The “PS-sCF” k_p is replaced by K_F which is a fatigue stress reduction factor, abbreviated “FS-sRF” for a given notch (k_t) and whose value changes with fatigue life. Eq. (21) becomes

$$K_F = \frac{S_{max}}{\bar{S}} = 1 + (k_f - 1) \frac{E_s}{E_{sn}} \quad (22)$$

which corresponds to Younger’s Eq. (17).

The secant moduli E_s and E_{sn} are to be derived from an available cyclic stress-strain diagram, e. g. see Fig. 42-5-56.

For each assumed value of nominal stress \bar{S} , the maximum local stress S_{max} may be found using an iterative

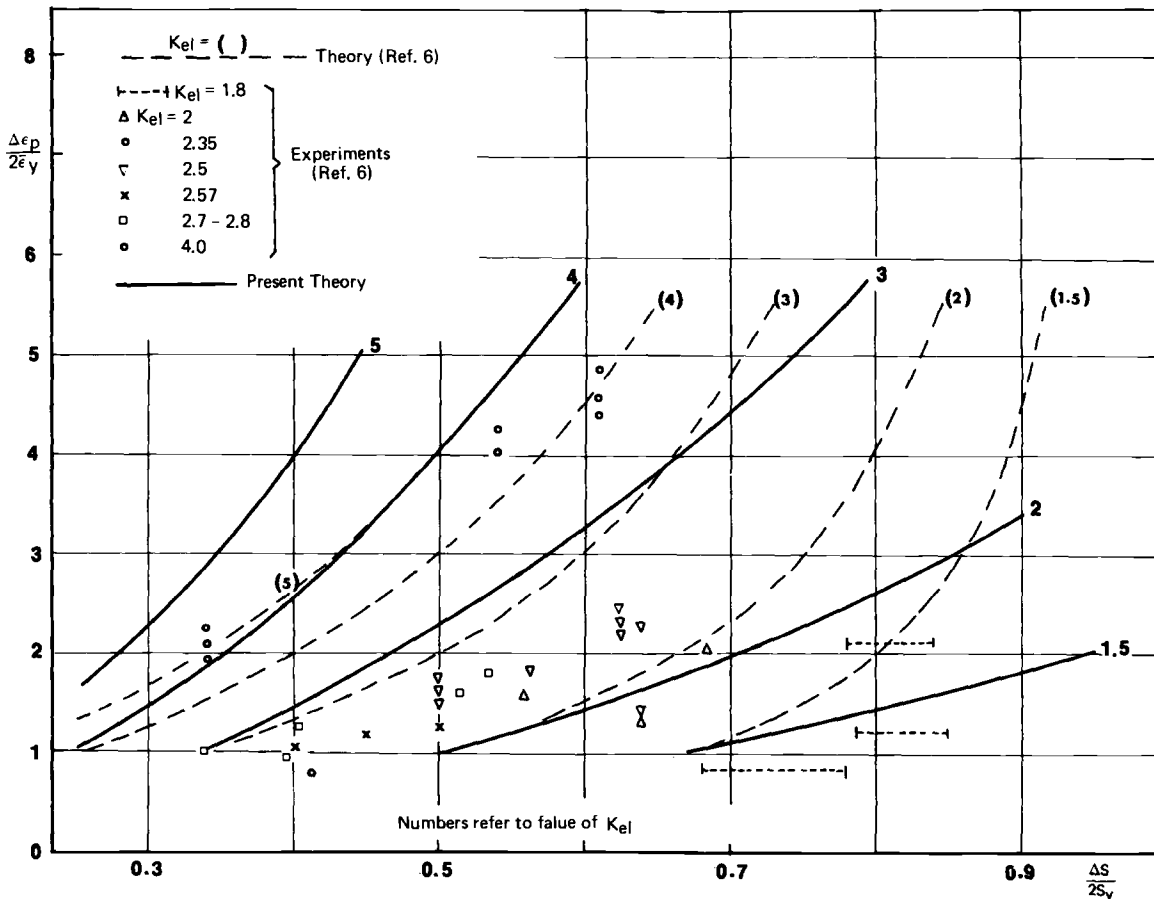


FIG. 41-8-16 – Total strain vs. applied stress.

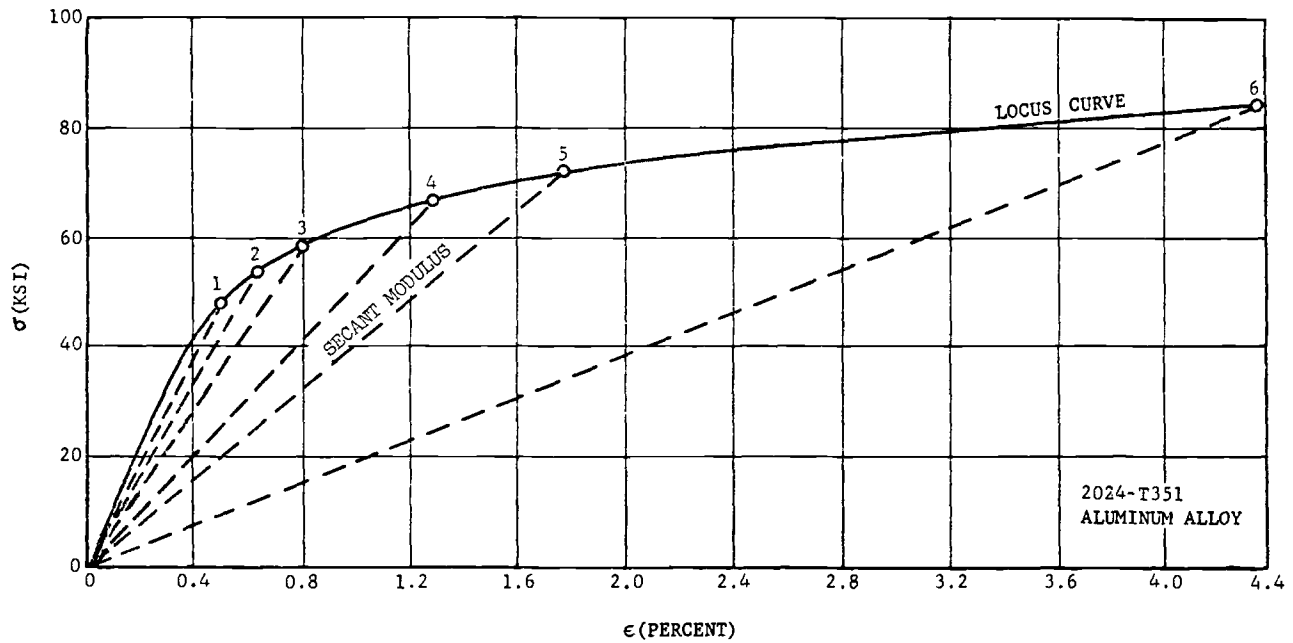


FIG. 42-5-56 – Secant moduli employed in the determination of fatigue stress – concentration factors.

method. Convergence is rapid and only a few trials are required to find solutions.

Younger describes the calculation of K_F as follows. Once combinations of pairs of S_{max} and \bar{S} are found, the point corresponding to each S_{max} value is located on the fatigue life curve for *unnotched* specimens and the corresponding value of \bar{S} is plotted directly below, at the same fatigue life. Finally, the resulting curve passing through the several plotted values of \bar{S} constitutes the desired notch-fatigue curve for a particular k_f .

The “FS-sRF” K_F is calculated as a ratio $\frac{S_{max}}{\bar{S}}$.

Fig. 43-6-56 shows the variation of K_F as a function of \bar{S} for three different “FS-thRF” $k_f = 2.8, 2.0$ and 1.8 . It is seen the K_F is equal to k_f for small values of \bar{S} and rapidly decreases to only slightly more than one for high values of \bar{S} where cyclic plasticity becomes important.

Younger describes his approach as follows. The *unnotched* fatigue-life curve becomes the curve that relates fatigue-life with the stabilized maximum local stresses at the root of the notch. The notched fatigue-life curves, on the other hand, relate fatigue-life with the nominal stresses. For additional details the reader is referred to the original paper.

E.7. – Dawson in R. 8 makes use of “SHO” expression to derive thermal strains at an internal circumferential groove in an internally heated cylinder. Because biaxial conditions exist on the internal surface Dawson determines the required secant moduli using the equivalent (Mises) stress and strain concept. Also the cyclic stress-strain diagram is used for this purpose.

After making a number of simplifying assumptions the author obtains an expression for the equivalent strain in the groove. This is not an explicit expression and an iterative method of solution is necessary.

Dawson has calculated the equivalent strain in the

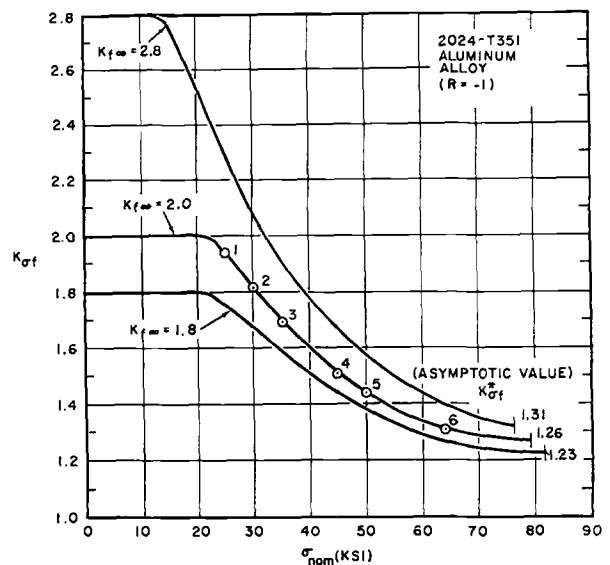


FIG. 43-6-56 – Stress concentration factors during stabilized cyclic plasticity.

notch for type 316 stainless steel at 600°C for $k_t = 1.5$ and 3.0 and plotted it as a function of total axial strain away from the groove. His Fig. 4 (not reproduced) indicates that the equivalent strain in the groove is much larger than the elastically computed strain. Because of its relative complexity the details of the analysis were not described here and those interested are referred to the original paper. See also R. 44 and E. 8.

E.8. – Sarney in R. 44 extends the “SHO” relations which apply to monotonic loading under uniaxial conditions to monotonic loading but under plane strain conditions. Sarney assumed that the “SHO” equation applied also under plane strain conditions provided that

the secant moduli were defined in terms of the effective stress and strain at the notch. He also introduced a pseudo-Poisson's ratio which varies between 0.3 and 0.5, depending on the ratio of secant moduli. In addition, in the particular case of a circumferentially grooved cylinder he assumed that the tangential strain in the groove is zero. Zwicky in R. 57 has concisely described Sarney's approach. For more detailed analysis see the original paper.

E.9. — Blatherwick, et al, in R. 4 describe fatigue tests on a low carbon C1018 steel, 0.0875 inches thick, 2 inches wide, edge-notched plate with "ESCF" $k_t = 1.8$.

Unnotched, companion specimens were used to determine the cyclic stress-strain curves. See Fig. 10-5-4. These curves were used to determine the stress distributions corresponding to the strain distributions observed in the tests on notched specimens. Only the tension half of the stress-strain curves is shown, the compression half was identical. It is evident that considerable cyclic softening occurs in this steel.

The first series of fatigue tests were controlled by the strain amplitude at the apex of the circular notch. This amplitude was varied between equal positive and negative limits. Fig. 44-6-4 shows typical results of strain measurements across the net section after 1, 20 and 1000 cycles.

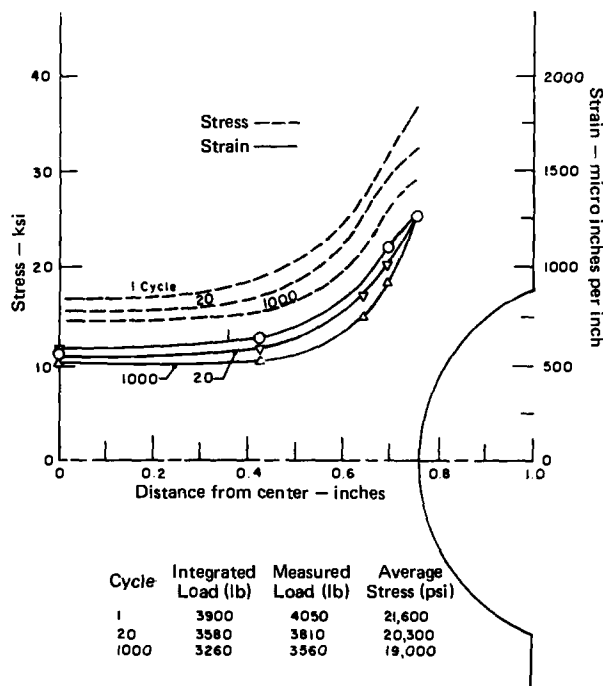


FIG. 44-6-4 — Stress and strain distributions in notched specimen under controlled strain amplitude.

The stresses derived from cyclic stress-strain curves obtained from tests performed on companion specimens are also shown. It is seen that the strain amplitude was kept at constant magnitude at the notch root but that it decreases across the net section with increasing number of cycles. Note that the stress amplitude decreases across the net section with increasing number of cycles and therefore, the stress concentration factor at the apex of notch decreases.

The second series of fatigue tests were controlled by a load across the net section which varied between fixed positive and negative magnitudes, $R = -1$. The results of strain and stress measurements are shown in Fig. 45-7-4.

The measured strain amplitude at the notch root increases with number of cycles resulting in increasing

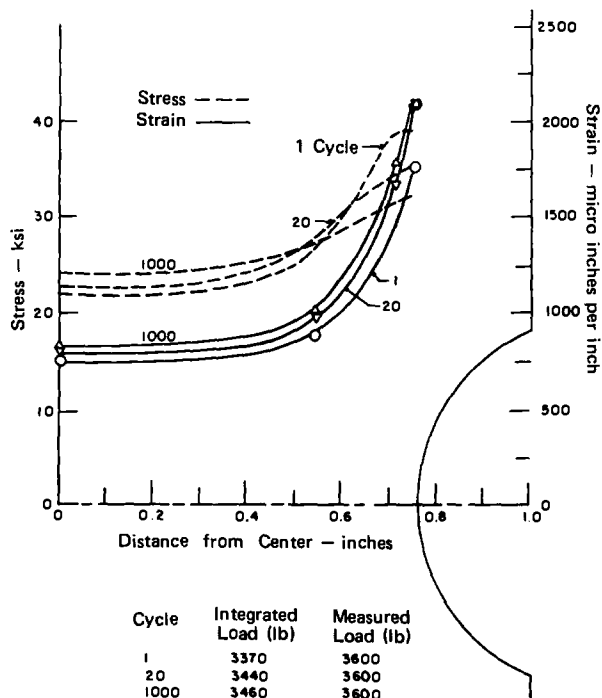


Fig. 45-7-4 — Stress and strain distributions in notched specimen under controlled force amplitude.

strain concentration factor. However, the stress at the notch root decreases but not as much as in the controlled notch-strain tests. Note that in the center portion of the specimen the stress increases, this in order to balance the reduction near the notch since the maximum total force is held constant during cycling. It appears that the stress distribution becomes more uniform with cycling.

The variation of stress concentration factor is depicted in Fig. 46-8-4. As expected, it decreases with increasing average stress across the net section and decreases with increasing cycling. The authors state that "tests under both controlled strain and controlled load conditions gave nearly identical results in Fig. 46-8-4." They concluded that the stress history effects (constant notch-strain or nominal stress) are not relatively important and that the effect of the number of cycles of stress is much more important.

In this investigation under controlled load amplitude, $R = -1$, the maximum stress at the notch decreases while the maximum strain increases. This was observed for a cyclic-softening material. The authors expect that cyclic hardening materials would exhibit the opposite effect.

The authors state that there is increasing evidence that strain is the governing parameter in low-cycle fatigue and therefore, the cyclic-softening materials would be more notch sensitive than those which cyclically harden.

E.10 – Manson, et al, in R. 33 describe the application of both the “SHO” procedure and of Neuber’s relation in conjunction with cyclic stress-strain diagrams to the determination of local strains in notches during cycling. See also Section I.2.

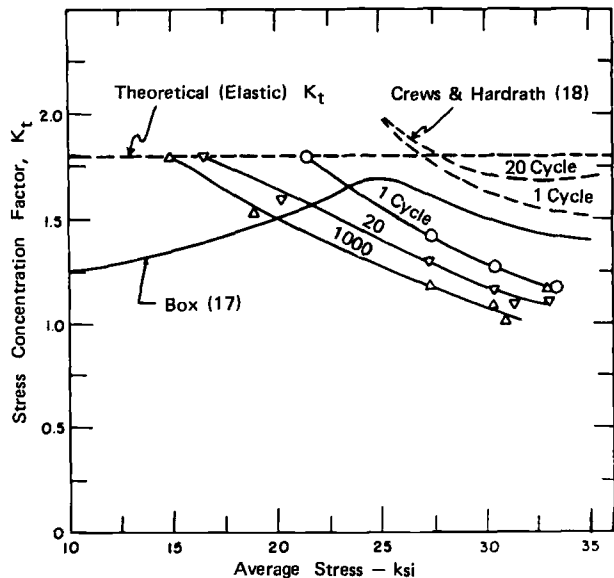


FIG. 46-8-4 – Stress concentration at notch root versus average stress for various numbers of cycles.

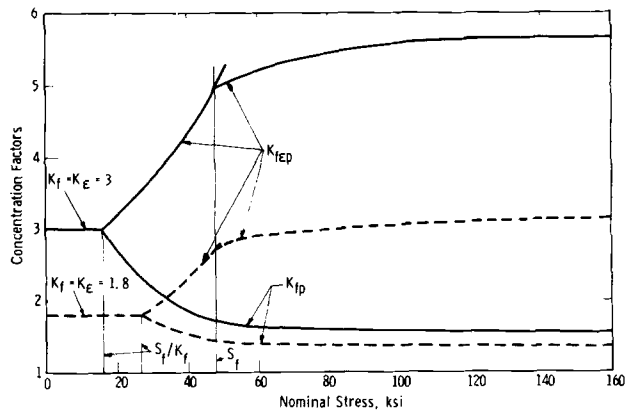


FIG. 47-40-40 – Stress and strain concentration factors obtained from analysis applied to notched members.

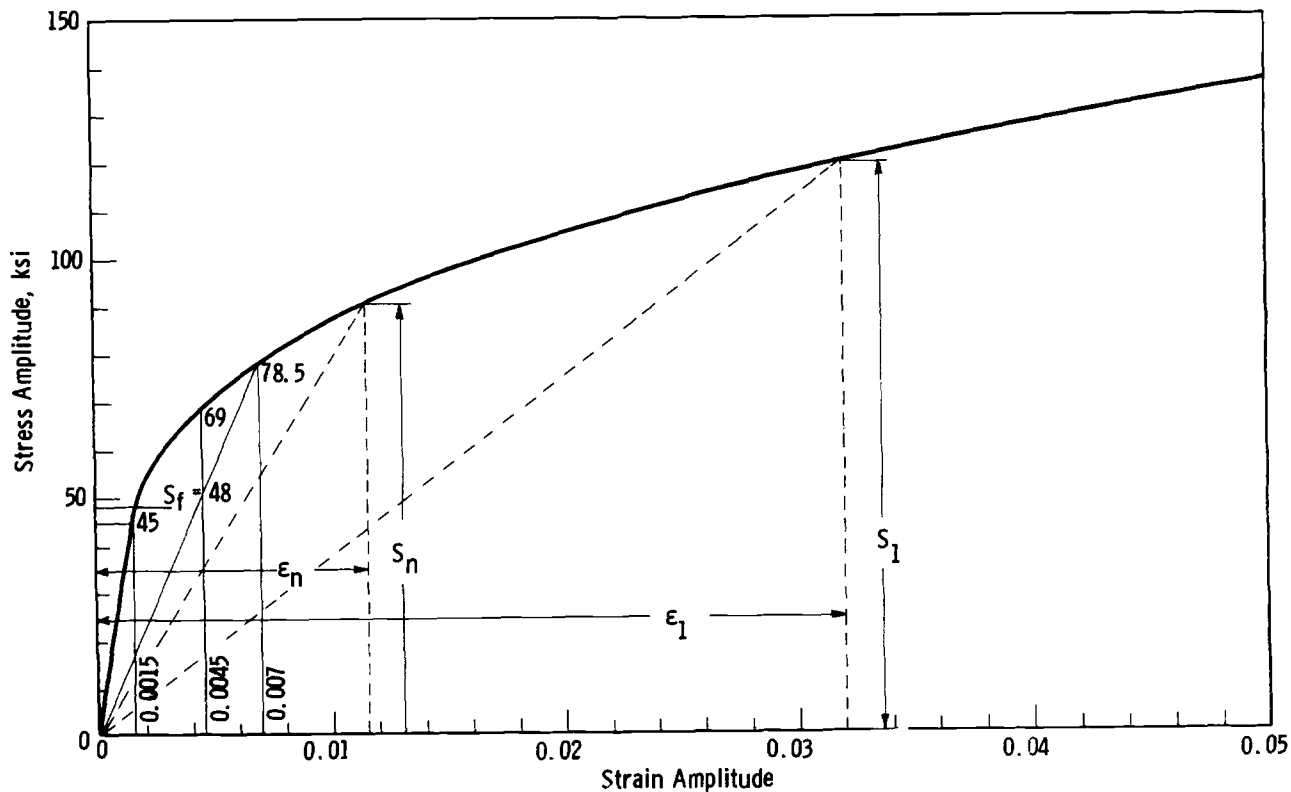


FIG. 48-39-40 – Cyclic stress-strain curve used for analysis (SAE 4130 normalized steel).

SECTION F
FATIGUE STRENGTH REDUCTION FACTORS ON
STRAIN BASIS RESULTS OF L.C.F. TESTS

F.1. — Krempl in R27 describes “LCF” tests performed at room temperature on large notched cylinders 2 in. dia., 12 in. long, with a circumferential notch of a semi-circular shape, 0.1 in. dia. and 0.155 in. deep with “ESCF” $k_t = 3.3$, see Fig. 49-1-27. The cylinders were tested under completely reversed load, $R = -1$, controlled by the nominal stress in the net section. Three annealed steels commonly used in structural nuclear application were tested;

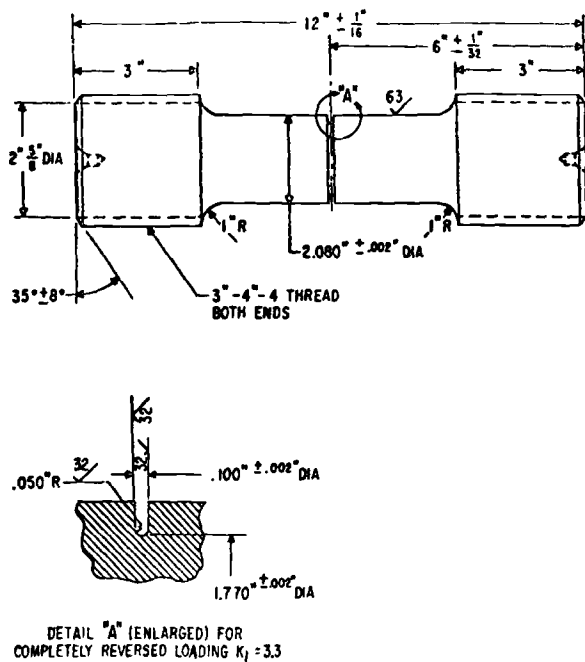


FIG. 49-1-27

low-carbon steel, 2-1/4 Cr – 1 Mo steel, and Type 304 stainless steel.

In addition, unnotched cylindrical bars were fatigue tested under completely reversed tension-compression $R = -1$, and controlled by maintaining a constant imposed strain range. Also, in addition to cyclic fatigue life, “cyclic stress-strain diagrams” were obtained, see Figs. 14-B7-24, 15-B8-24 and 16-B9-24.

Note that the cycles-to-cracking for the *unnotched* bars were obtained from the load record. A precipitous drop of the maximum tensile load was taken as cycles to crack. Near-separation constituted failure. Using these definitions N_c and N_f were very close.

The change in crosshead displacement was continuously monitored. Very little change in displacement range occurs throughout the life of the specimens. Yielding takes place only in the net section area, therefore in these tests load

control was practically equivalent to displacement control for most of the fatigue life.

For the notched bars, Krempl observed cycles to cracking N_c and cycles to fracture N_f . Periodic examination with red dye was used to determine crack initiation. The appearance of a 0.005 to 0.015 in. long crack in the root of the notch was taken as cycles to crack initiation. It was observed that for these notched bars N_c could be less than 20% of N_f .

Tables III, IV and V reproduced in Fig. 50-T-27 tabulate cycles to crack initiation N_c and cycles to fracture N_f for the notched cylinders as a function of nominal stress amplitude. Crack propagation consumes 70% of total life for

TEST RESULTS GROOVED CYLINDER SPECIMENS,
 COMPLETELY REVERSED LOAD CONTROLLED
 LOADING AT ROOM TEMPERATURE

Spec. #	Nominal Stress Amplitude, 10^3 psi	Cycles-to-Crack	Cycles-to-Failure	R	σ_c 10^3 psi
---------	--------------------------------------	-----------------	-------------------	---	-----------------------

TABLE III

Material: Carbon Steel

CG-4A	40.7	75	1664	0.46	87
CG-5A	35.0	300	6346	0.41	84
CG-1A	28.8	950	17237	0.39	73
CG-3A	25.0	4000 to 8000	38346	0.39	64
CG-2A	21.0	6200	52526	0.36	59

TABLE IV

Material: 2 1/4 Cr – 1 Mo Alloy Steel

AG-6A	40.7	150	3641	0.55	73
AG-8A	36.0	565	9504	0.43	84
AG-1A	30.9	850	20478	0.36	86
AG-7A	27.0	4850	23354	0.46	58
AG-5A	26.8	2786	43954	0.31	86
AG-2A	22.5	9206	98088	0.28	79

TABLE V

Material: Type 304 Stainless Steel

SG-5A	40.7	447	1643	0.29	138
SG-2A	35.0	1132*	6438	0.22	158
SG-3A	30.5	3900**	9043	0.23	130
SG-4A	27.0	4000	18822	0.19	141
SG-1A	23.2	8889	49519	0.16	145

* Cracked all around
 ** Large crack

$$R = \frac{\text{Final tensile fracture area}}{\text{Net section area}}$$

$$\sigma_c = \frac{\sigma_a}{R}, \text{ true stress at fracture}$$

$$\sigma_a = \frac{\text{Load amplitude}}{\text{Net section area}}$$

FIG. 50-T-27

the Type 304 stainless steel and about 90% for the other two steels. Results of the above fatigue tests are shown in Figs. 59-5-26, 60-6-26, and 61-7-26.

Krempl presents an informative discussion of fatigue strength reduction factors which relate low-cycle fatigue life of notched specimens with fatigue life of unnotched specimens.

Such “FS-th RF” are defined by dividing the stress or

strain obtained with *unnotched* specimens by the *nominal* stress or strain obtained with *notched* specimens which have the same life as the unnotched specimens. Of the two possible approaches, on the basis of stress control and on the basis of total strain control of unnotched specimens, the author chose the strain approach because it is favored in pressure vessel design.

Therefore, in order to derive "FS-th RF" on controlled strain basis it is necessary to have available completely reversed, $R = -1$, strain controlled cyclic life data for unnotched specimens and completely reversed, controlled by *nominal* stress cyclic life data for notched specimens.

To determine the "FS-th RF" on strain basis the author proposes three approaches, defined as methods 1a, 1b and 2. These methods are interpreted graphically by the author in Fig. 52-5-27.

Method 1b requires that a *cyclic* diagram, obtained with the help of unnotched specimens and connecting stress range ΔS_C and strain range Δe_C be available. For given cycles to cracking N_C the imposed total strain range Δe is obtained with the help of the unnotched cyclic life diagram which defines Δe in terms of N_C . Then with the help of available cyclic stress-range strain range diagram the stress range ΔS_C corresponding to Δe is obtained. Again from the available notched life data the *nominal* stress range $\overline{\Delta S}_N$ is obtained for the same N_C . The fatigue strength reduction factor on strain basis, to macrocracking "FS-th RFC" Q_C^{1b} is

$$Q_C^{1b} = \frac{\Delta S_C \text{ (from cyclic stress-strain diag.)}}{\overline{\Delta S}_N \text{ (from notched cyclic life)}} \quad (23)$$

For a particular "ESCF" k_t this factor Q_C^{1b} varies with cycles to cracking N_C or with the nominal stress range $\overline{\Delta S}_N$ across the net section. Fig. 53-6-27 shows for the 2-1/4 Cr - 1 Mo steel the variation of factor Q_C^{1b} with nominal stress amplitude for $k_t = 3.3$. It is seen that the factor is less than k_t and that it gradually decreases with increasing nominal stress amplitude or with decreasing cycles to cracking.

Method 1a like method 1b requires that a cyclic diagram for unnotched specimens be available. Fig. 52-5-27 defines the "FS-th RFC" Q_C^{1a} as follows

$$Q_C^{1a} = \frac{\Delta e}{\Delta e_C} \quad (24)$$

Δe is the imposed total strain range from the strain controlled, unnotched cyclic life data for a particular N_C .

Δe_C is the strain range, derived from the cyclic stress-strain. This strain range corresponds to cyclic stress range ΔS_C equal to the nominal stress range $\overline{\Delta S}$ obtained from the available notched life diagram for the same cycles to cracking N_C as above.

This factor Q_C^{1a} is plotted in Fig. 53-6-27 for the same $k_t = 3.3$. It is larger than k_t and it increases to a maximum of about 11 and then decreases with increasing nominal stress amplitude. The author points out that it is possible to multiply each strain range in Eq. (24) by the modulus of elasticity if one prefers working with fictitious stress ranges.

Method 2 as described by Krempl does not require a cyclic stress-strain diagram as the other two methods. Fig. 52-5-27 defines the "FS-th RFC" on strain basis as follows

$$Q_C^2 = \frac{\Delta e \cdot E}{\overline{\Delta S}_N} \quad (25)$$

For a particular N_C the strain range Δe is derived from the available cycle life diagram for *unnotched* specimens. As before, $\overline{\Delta S}_N$ is the nominal stress range derived from the available cycle life diagram for *notched* specimens for the same cyclic life N_C . Note that a fictitious smooth bar stress range is evolved in Eq. (25) by multiplying Δe by the modulus of elasticity E .

Factor Q_C^2 is plotted in Fig. 53-6-27. It is seen that at first it coincides with factor Q_C^{1a} but continues to increase with increasing nominal stress amplitude while Q_C^{1a} breaks away and even decreases.

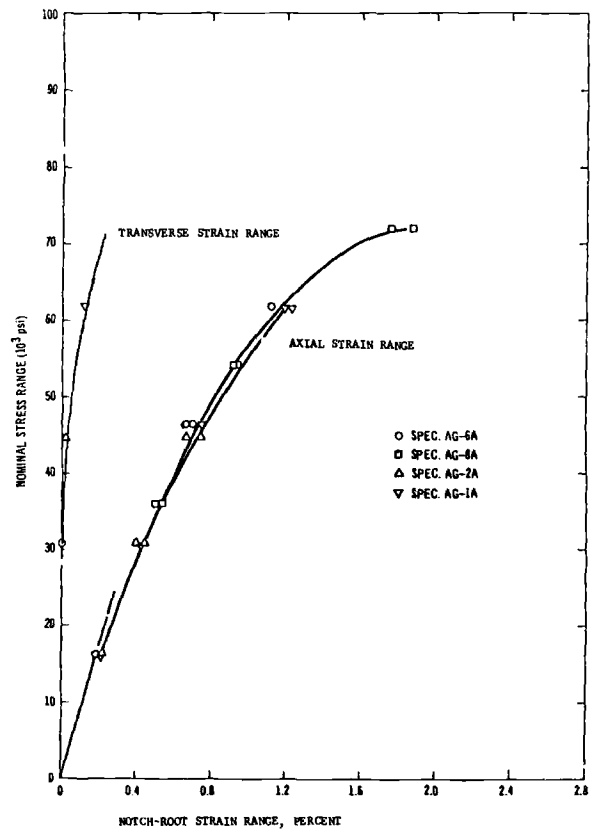


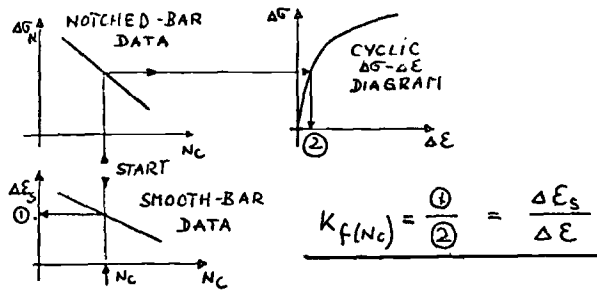
FIG. 51-2-27

Krempl states the factor Q_C^{1a} was initially proposed by him in R. 23 and that factor Q_C^2 was used by Snow, et al in R. 45.

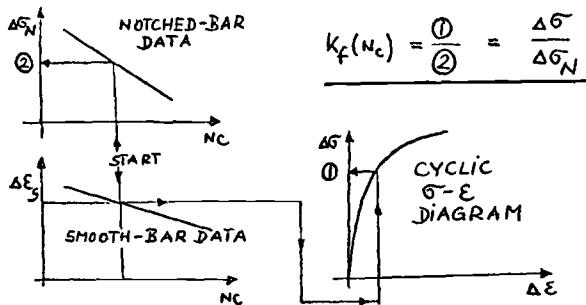
The factors for the other two materials exhibit the same trend as for the 2-1/4 Cr - 1 Mo steel shown in Fig. 53-6-27. The factor Q_C^2 is steadily increasing, the factor Q_C^{1a} shows a maximum and the factor Q_C^{1b} is always less than the "ESCF" k_t . Also, in each case the factor depends on the applied nominal stress range $\overline{\Delta S}$.

Krempl states that it follows from Fig. 53-6-27 that de-

METHOD Ia



METHOD Ib



METHOD II

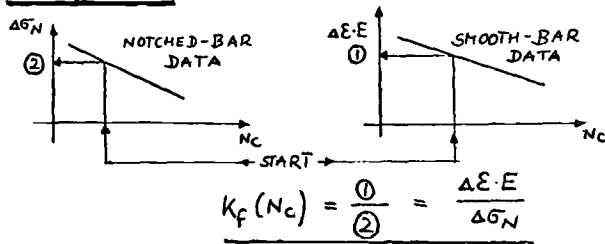


FIG. 52-5-27

pending on the definition, considerably different values of "FS-th RFC" can be obtained. If in addition, crack initiation is defined differently, even greater variations in the "FS-th RFC" can be expected. See, for instance, R 45, R 19 and R 17. Therefore, it is important that for design purposes a suitable definition of "FS-th RF" must be made. See R 48. Factors Q_C^{1a} , Q_C^{1b} , and Q_C^2 are *strain based* because they are defined with the help of total strain controlled cycling fatigue of unnotched specimens. Factors derived with the help of stress controlled cycling fatigue of unnotched specimens are defined as *stress based* and will be discussed later in Section G.

The geometry of notched specimens was such that it permitted the measurements of strains at the notch root and an important feature of tests with notched specimens were the measurements of both axial and circumferential (transverse) strains at the root of the notch during cycling using high elongation 1/64 in. foil strain gages. It is interesting that the measured transverse strain range is more than ten times smaller than the axial strain range. The strain measurements in the root of the notch were terminated by strain gage failures which occurred *before* the first cracks in the notch were visible. A sample of the strain data obtained during the loading-up of the 2-1/4 Cr - 1 Mo steel specimens with $k_t = 3.3$ is shown in Fig. 51-2-27. At

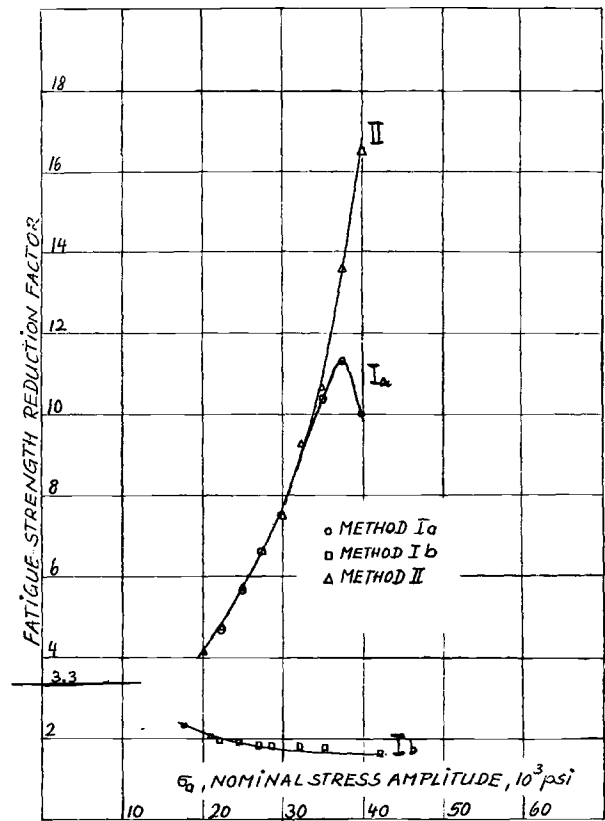


FIG. 53-6-27

the start of each test the applied load was raised in discrete steps. At each load level the hysteresis loop connecting load with strain at the root of the notch was obtained. After that the load was raised to the next step. When the final cycling load was reached the load-notch-strain hysteresis loop was taken at selected cycling intervals until the gage has failed. The curve shown in Fig. 51-2-27 is, therefore, only the *initial* curve and not the final stabilized curve.

For the 2-1/4 Cr - 1 Mo steel the author plotted, in Fig. 54-7-27, the total imposed strain range vs. cycles to cracking for the unnotched specimens. He also plotted in

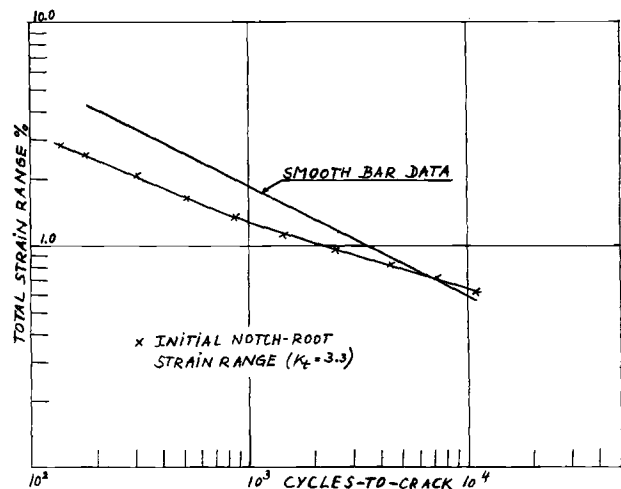


FIG. 54-7-27

the same figure, with the help of Fig. 51-2-27 and Table 4 in Fig. 50-T-27, the *measured* total strain range vs. cycles to cracking for the notched specimens with $k_t = 3.3$. Krempl states that it is often assumed that the imposed total strain range is the controlling factor in low cycle fatigue life. That is, if the total strain range is known at the critical location then the cyclic life could be predicted from the unnotched strain controlled cyclic life data. For instance, see D. 2.

The above contention is not substantiated by Fig. 54-7-27 which is based on the author's test results. For the same imposed total strain range the notched specimens crack before the unnotched. In addition, the author determined equivalent strains from the axial and circumferential strain measurements and used them to plot the cyclic life test results in Fig. 55-8-27. It seems that the correlation was not substantially improved. It should be

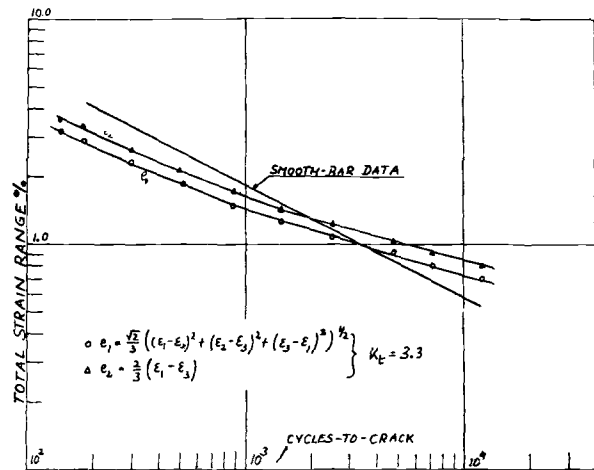


FIG. 55-8-27

pointed out that in the tests with unnotched bars the drop-off in the load was designated as cycles to cracking, while in the notched cylinders the occurrence of an 0.005 to 0.015 in. long crack in the root of the notch was used for this purpose. This difference may influence the degree of correlation.

F.2. — Krempl in R 26 reports “LCF” tests performed at room temperature on the same cylindrical specimens and materials described in R 27, see F.1. For chemical composition and physical properties see Fig. 62-T-26. In addition to completely reversed loading, $R = -1$, he reports also on results of tests with repeated tension, $R = 0$. See Fig. 56-1-26 for notch geometry used in reversed loading and in repeated tension tests. Fig. 57-2-26 and 58-3-26 show the interesting relationship between the nominal stress range ΔS and the local strain range $\Delta \epsilon$ at the notch root for monotonic, completely reversed and repeated tension loading for the 2-1/4 Cr - 1 Mo steel. It can be seen that in the case of the repeated tension loading a relatively small strain range is superposed on a high mean strain.

Note that Fig. 58-3-26 indicates that the strain range at the notch root for a given nominal stress range is less for the repeated tension case than for the completely reversed

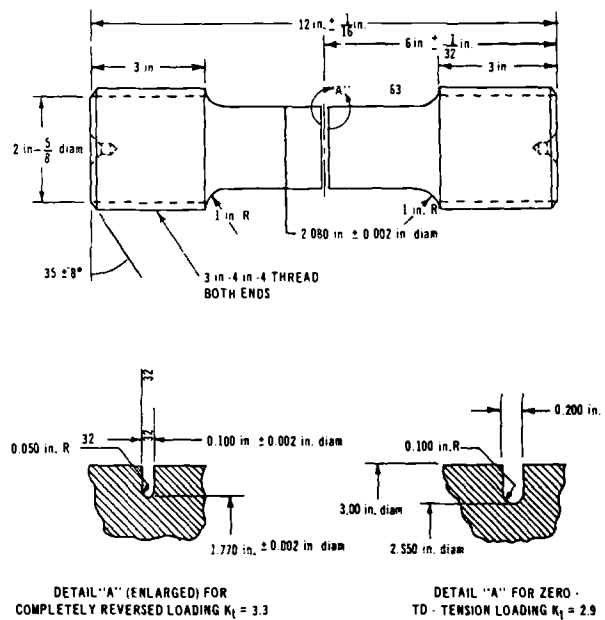


FIG. 56-1-26 – Test specimen for completely reversed and zero-to-tension load controlled tests.

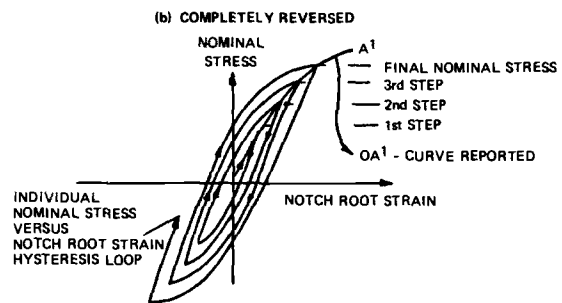
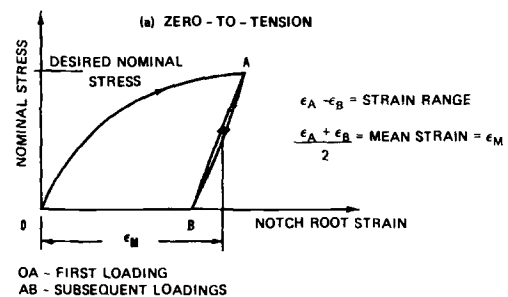


FIG. 57-2-26 – Schematic indicating nominal stress-notch root strain relationship for zero-to-tension and completely reversed loading.

condition. Also, the measured transverse strain range is considerably lower than the axial strain range. For additional discussion the reader is referred to the original paper.

Cycles to cracking N_C and cycles to fracture N_f are shown in Figs. 59-5-26, 60-6-26 and 61-7-26 for the three steels, respectively. These figures include also test results obtained for repeated loading, $R = 0$, of notched cylinders and for externally notched flat plates with “ESCF” $k_t = 3$ previously reported in R 23 and discussed in F.3. A com-

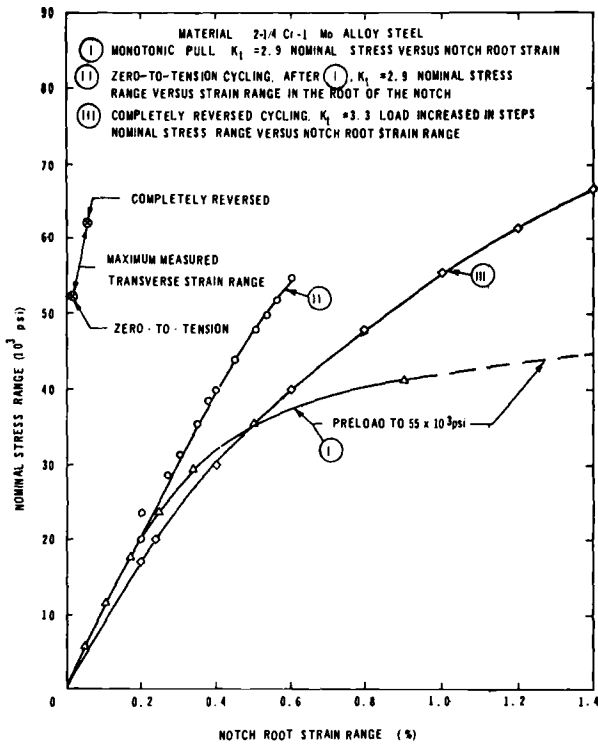


FIG. 58-3-26 – Comparison of measured nominal stress-notch root strain range curves for zero-to-tension and completely reversed loading material: 2-1/4 Cr - 1 Mo alloy steel.

parison of test results for the two loading conditions indicates that for the same imposed stress range cracking occurs first in the case of completely reversed loading, $R = -1$, but final fracture occurs first for the repeated loading, $R = 0$. For a given imposed nominal stress range low-carbon steel has the shortest life to crack initiation followed by 2-1/4 Cr - 1 Mo steel and by the Type 304 stainless steel. For a given imposed nominal stress range stainless steel has the shortest life to complete fracture followed by the low-carbon steel and the 2-1/4 Cr - 1 Mo steel.

The author introduces a fatigue strength reduction

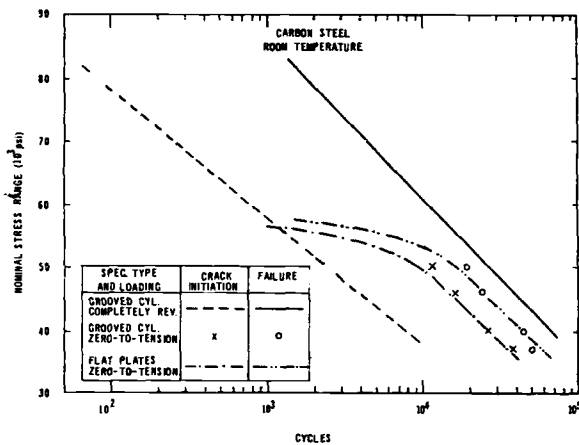


FIG. 59-5-26 – Cycles-to-crack and cycles-to-failure versus nominal applied stress range for zero-to-tension and completely reversed loading. Material: Carbon steel.

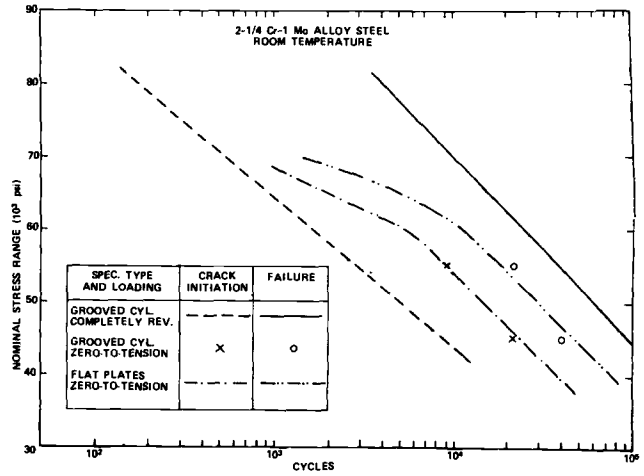


FIG. 60-6-26 – Cycles-to-crack and cycles-to-failure versus nominal applied stress range for zero-to-tension and completely reversed loading. Material: 2-1/4 Cr-1 Mo alloy steel.

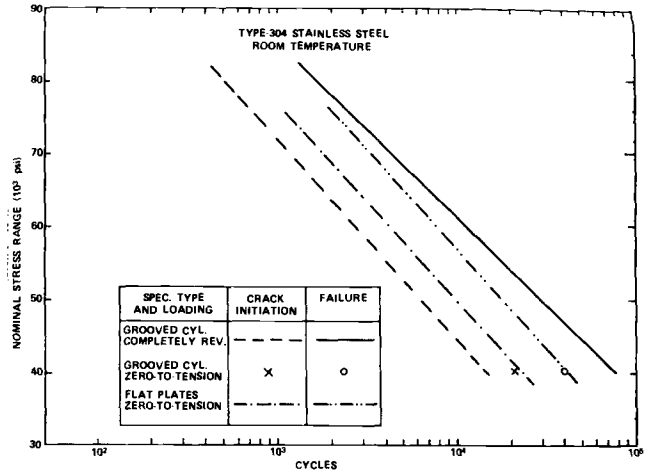


FIG. 61-7-26 – Cycles-to-crack and cycles-to-failure versus nominal applied stress range for zero-to-tension and completely reversed loading. Material: type-304 stainless steel.

factor to cracking “FS-th RFC”, Q_C^2 discussed previously in F.1. Figs. 63-11a-26, 64-11b-26 and 65-11c-26 show the plot of factor Q_C^2 vs. nominal stress amplitude for the three steels. It is seen that the factor is less for repeated loading, $R = 0$, than for the completely reversed loading, $R = -1$. The factor is much larger than the estimated high-cycle fatigue strength reduction factor k_f and approaches it only for very small nominal stresses.

Krempel points out that the number of cycles to cracking N_C is important in design against low cycle fatigue. Therefore, a designer would calculate the nominal applied stress amplitude at a discontinuity characterized by an elastic stress concentration factor k_t . The “FS-th RFC” Q_C^2 would be obtained from Figs. 63-11a-26, 64-11b-26, or 65-11c-26 for $R = 0$ and $R = -1$. The cyclic life for a given k_f would then be obtained from Fig. 66-12a-26, 67-12b-26, or 68-12c-26. If the obtained life is less than the desired

TABLE 1

CHEMICAL COMPOSITION (MILL ANALYSIS) OF MATERIALS TESTED

Material	Chemical Analysis (Mill Test)							
	C	Mn	P	S	Si	Ni	Cr	Mo
Carbon Steel	0.16	0.85	0.008	0.032	0.22			
304 Stainless Steel	0.07	1.45	0.021	0.028	0.53	8.77	19.00	
2-1/4 Cr-1 Mo Alloy Steel	0.12	0.54	0.010	0.015	0.31		2.39	1.00

TABLE 2

AVERAGE MECHANICAL PROPERTIES

Material	Proportional Limit (10 ³ psi)	0.2% Yield Strength (10 ³ psi)	Ultimate Stress (10 ³ psi)	Elongation Based on 2 in. Gage Length (%)	Reduction in Area (%)
Carbon Steel Direction of Rolling	21.0	29.4	62.4	35.0	55.8
Carbon Steel Transverse	21.7	29.0	61.1	32.5	51.0
Type-304 Stainless Steel	26.9	38.8	85.0	66.8	76.1
2-1/4 Cr-1 Mo Alloy Steel	28.6	36.7	74.6	31.5	67.5

FIG. 62-T-26

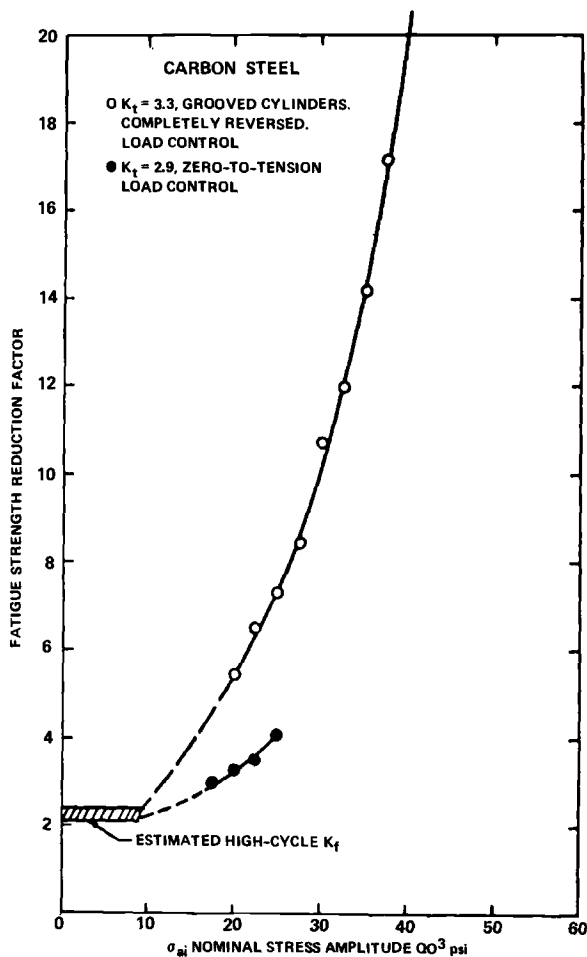


FIG. 63-11a-26 – Fatigue strength reduction factor versus nominal applied stress amplitude for zero-tension and completely reversed loading.

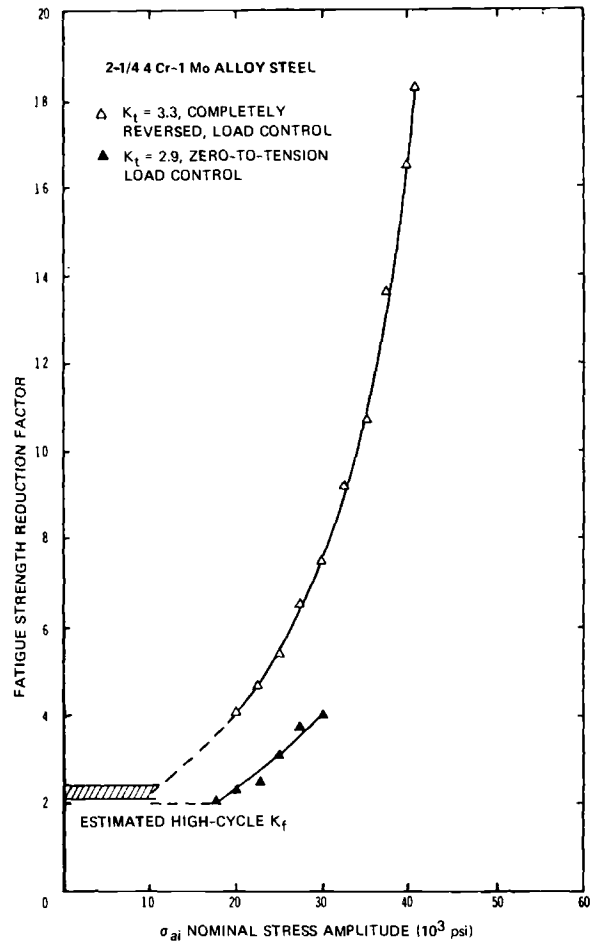


FIG. 64-11b-26 – Fatigue strength reduction factor versus nominal applied stress amplitude for zero-tension and completely reversed loading.

life the applied nominal stress amplitude will have to be reduced and procedure repeated.

It follows that the design against crack initiation should be based on rigorously defined “FS-th RFC” and on definition of “crack initiation”. In this investigation the magnitude of the factor Q_C^2 depends on the imposed nominal stress amplitude. In all cases the factor was higher than the “ESCF” k_f . The author determined the average crack growth rate for the three steels as a function of nominal stress amplitude. This is shown in Fig. 69-14-26. It is seen that the average crack propagation rate for a given nominal stress amplitude was higher for pulsating loading, $R = 0$, than for completely reversed loading, $R = -1$. Also, the highest crack propagation rate is shown by the Type 304 stainless steel followed by carbon steel and 2-1/4 Cr-1 Mo steel.

F.3. – Krempl in R 23 describes the “LCF” behavior of symmetrically edge-notched plates, 0.10 in. thick, tested at room temperature and made from annealed low-carbon steel, 2-1/4 Cr-1 Mo steel and Type 304 stainless steel. The plates with “ESCF” $k_t = 3$ were subjected to repeated tension loading, $R = 0$. The geometry of the plate specimens is shown in Fig. 70-3-23.

The results of the load controlled “LCF” tests (6 cycles/min.) are shown in Figs. 71-4-23, 72-5-23 and 73-6-23 for

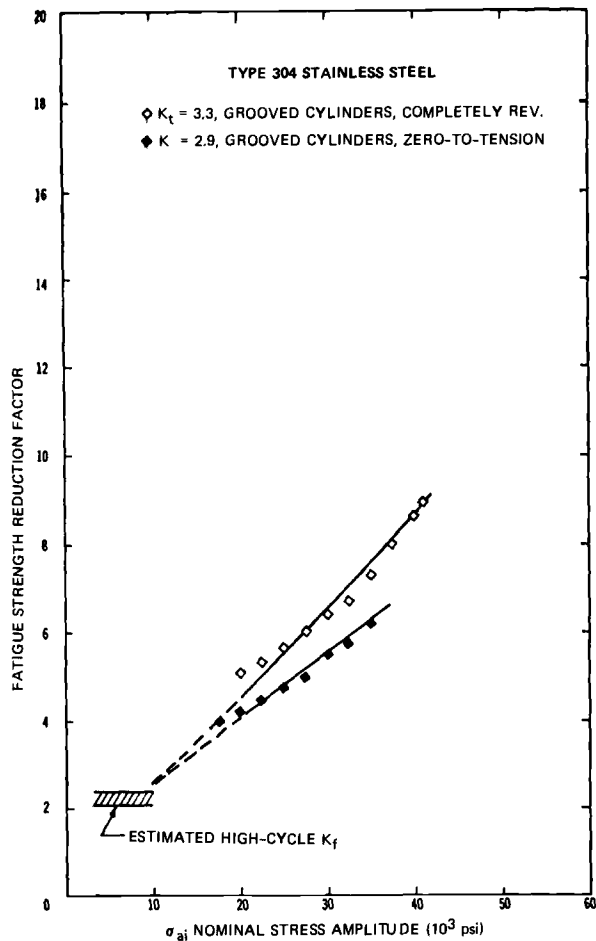


FIG. 65-11c-26 — Fatigue strength reduction factor versus nominal applied stress amplitude for zero-to-tension and completely reversed loading.

the three steels. In these figures the imposed maximum nominal stresses (on the net section) which controlled the tests are plotted against cycles to cracking N_c and cycles to fracture N_f . Note the significant difference between N_c and N_f . Crack growth consumes 50% and more of the total fatigue life in these notched tests. A visible crack 0.003 to 0.006 in. in the root of the notch determined cycles to cracking.

Unnotched specimens 0.505 in. diameter were used to determine the completely reversed, total strain-controlled “LCF” tests. Cycles to crack were defined by the appearance of a visible crack of 0.003 to 0.006 in. long. However, the difference between N_c and N_f was very small for these unnotched tests and was disregarded in plots. The fatigue diagrams depicting imposed total strain range vs. cycles to fracture are shown in Figs. 78-5-25, 79-6-25, 80-7-25 taken from Krempl R 25.

On the basis of his experimental data, Krempl calculated fatigue strength reduction factors on strain basis for cycles to cracking N_c . This “FS-th RFC” was designated as Q_C^{la} and calculated by the method la discussed previously in F.1. Fig. 77-11-23 shows Q_C^{la} vs. imposed maximum nominal stress for the edge-notched plates with $k_t = 3$ for repeated loading, $R = 0$. Factor Q_C^{la} increases with increasing maximum nominal stress and finally exceeds considerably the value of elastic stress concentration factor k_t . For more detailed discussion the reader is referred to the original paper.

Krempl performed strain measurements in the apex of the notch during monotonic loading of the 0.1 in. thick edge-notched plates. These strain measurements together with the available stress-strain diagrams permitted the calculation of elasto-plastic stress and strain concentration factors k_p and q_p . These “Experimentally” obtained concentration factors were compared with factors calculated using the “SHO” analytical method, discussed in E.1.

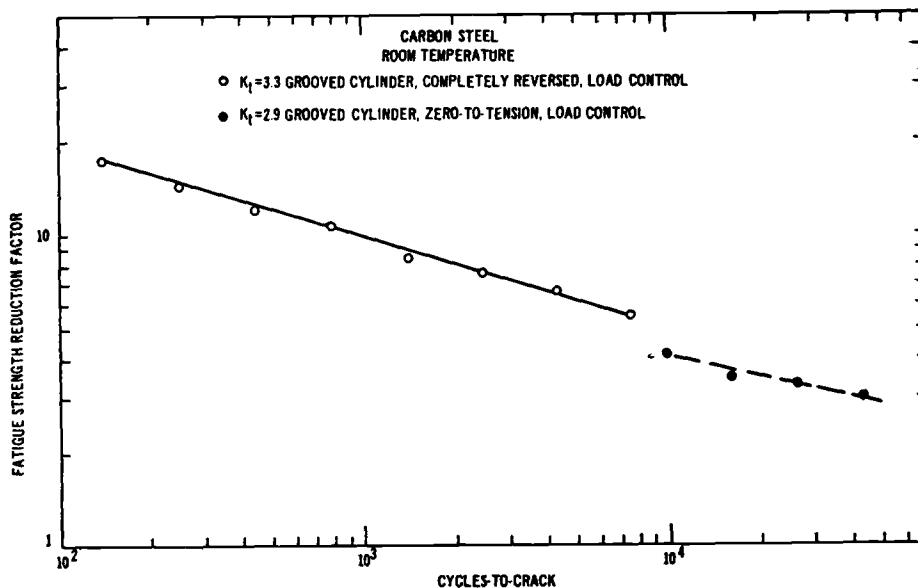


FIG. 66-12a-26 — Fatigue strength reduction factor based on crack initiation versus cycles-to-crack for zero-to-tension and completely reversed loading.

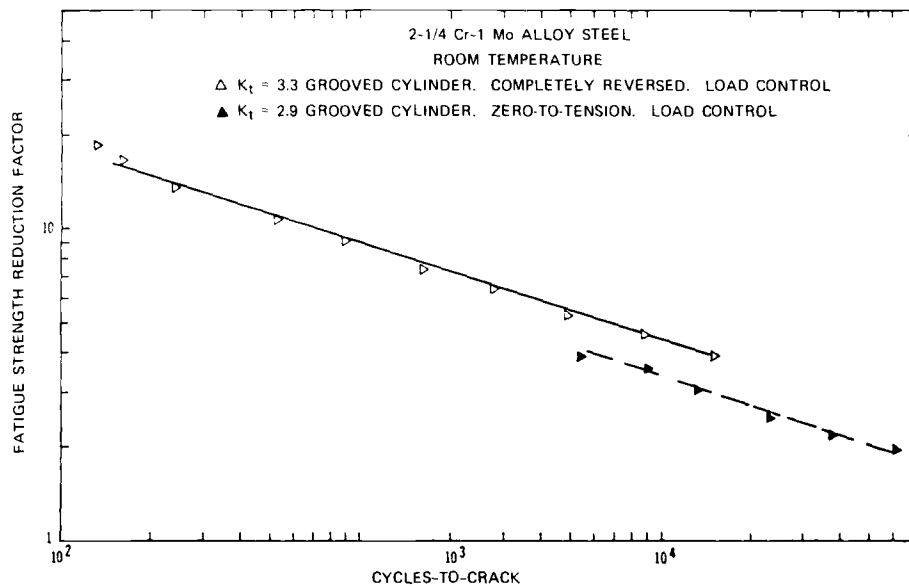


FIG. 67-12b-26 – Fatigue strength reduction factor based on crack initiation versus cycles-to-crack for zero-to-tension and completely reversed loading.

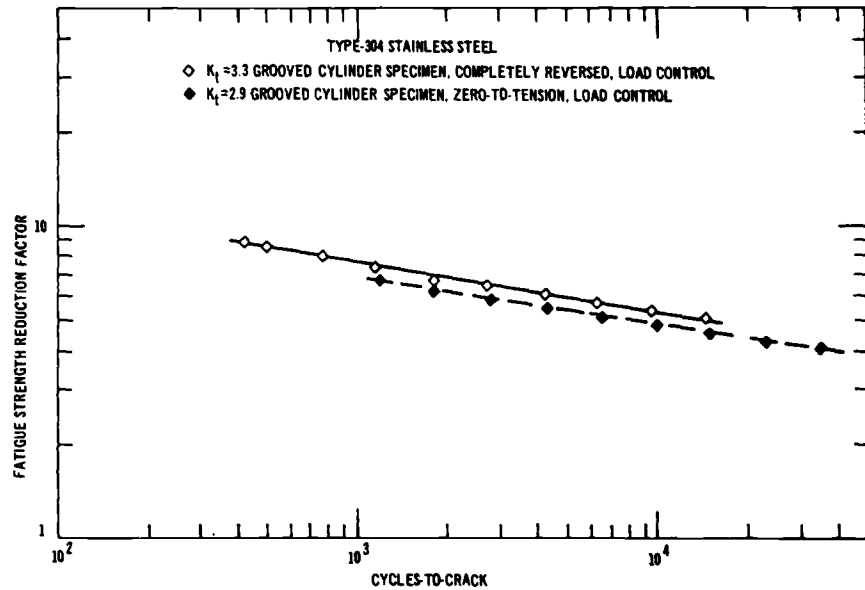


FIG. 68-12c-26 – Fatigue strength reduction factor based on crack initiation versus cycles-to-crack for zero-to-tension and completely reversed loading.

Figs. 74-8-23, 75-9-23 and 76-10-23 show the “experimental” and “SHO” concentration factors vs. nominal applied stress for the three steels. For nominal stresses up to the proportional limit the elasto-plastic stress and strain concentration factors k_p and q_p showed good agreement. At higher nominal stresses the differences were attributed to inaccuracies in strain measurements and to the approximations inherent in the “SHO” method.

Note that the “PS-nCF” q_p is higher than the “PS-sCF” k_p in the whole elasto-plastic range and that the factor k_p is decreasing with increasing nominal stress and approaches a value slightly larger than one for large values of nominal stress. However, the “PS-nCF” q_p is increasing up to a maximum, approximately where the nominal stress reaches

proportional limit, and decreases with further increase of the nominal stress.

Krempel measured crack growth rate for the repeated loading, $R = 0$. He states that the crack growth rates in the edge-notched plates correlated surprisingly well with the stress-intensity factor. For details see the original paper.

F.4. — Iida in R 19 presents the results of completely reversed, strain controlled, room temperature LCF tests on unnotched and notched cylindrical specimens. Three low-alloy steels with 115000 psi tensile strength and different chemical composition were involved. The configuration of specimens is shown in Fig. 81-1-19. The unnotched specimens have a 14 mm radius and $k_t = 1.11$. The notched specimens have circumferential notches with

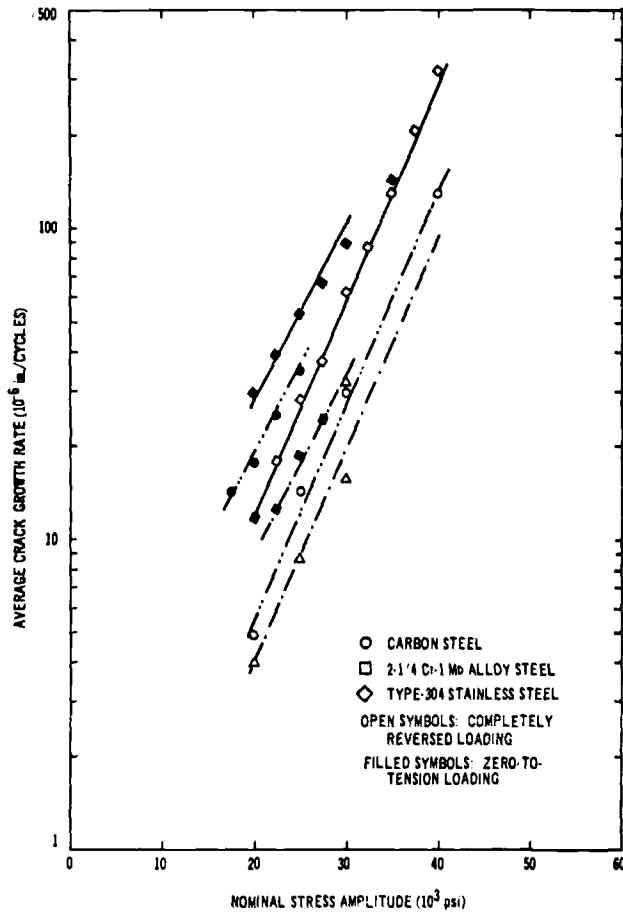


FIG. 69-14-26 – Average crack growth rate versus applied nominal stress amplitude for zero-to-tension and completely reversed loading.

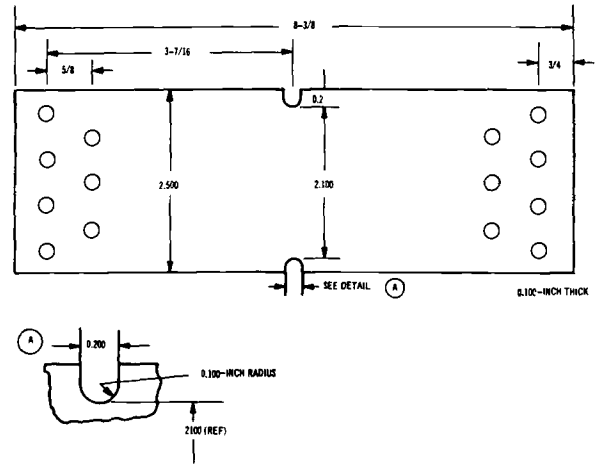


FIG. 70-3-23 – Edge-notched flat-plate.

radii 2.4 and 0.6 mm and “ESCF” $k_t = 1.57, 2.35, 2.48$ and 3.48. All fatigue tests were controlled by completely reversed, $R = -1$, diametrically measured, true strains for both unnotched and notched specimens. The true strains were calculated as

$$\ln \frac{d_o}{d_t} \text{ and } \ln \frac{d_c}{d_o},$$

where d_o , d_t and d_c are diameters of the minimum section in initial, stretched and compressed conditions.

The author presents in his Figs. 5 to 12, the relationship between the true total, plastic and elastic strain amplitudes and the number of cycles to crack initiation N_c and to fracture N_f . Note that the N_f did not exceed 3×10^3

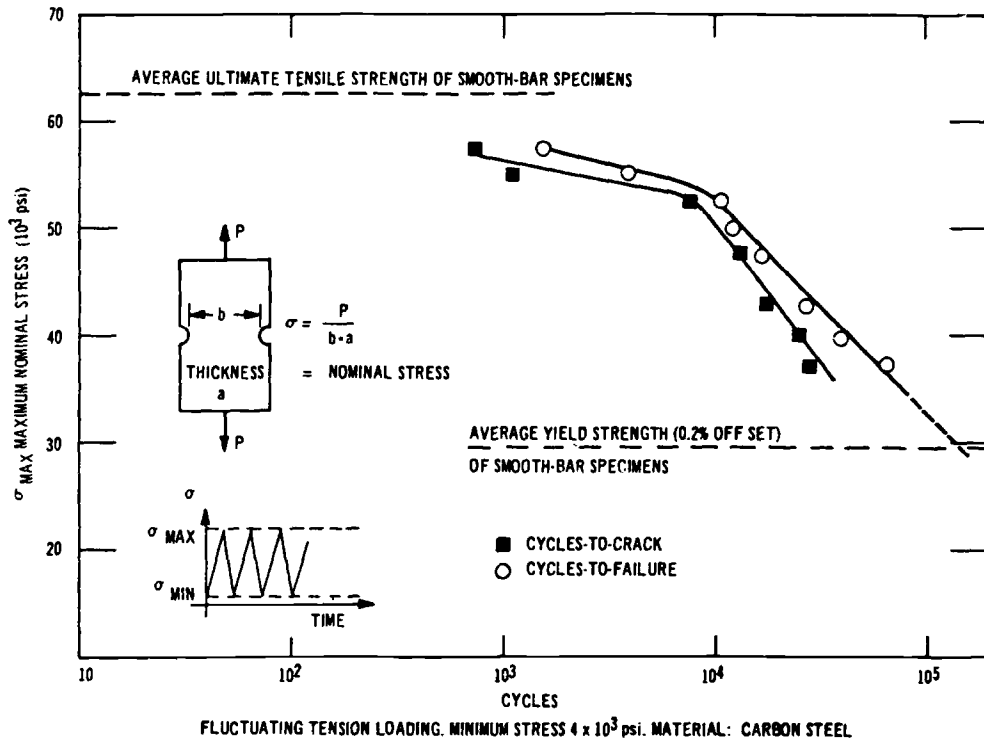
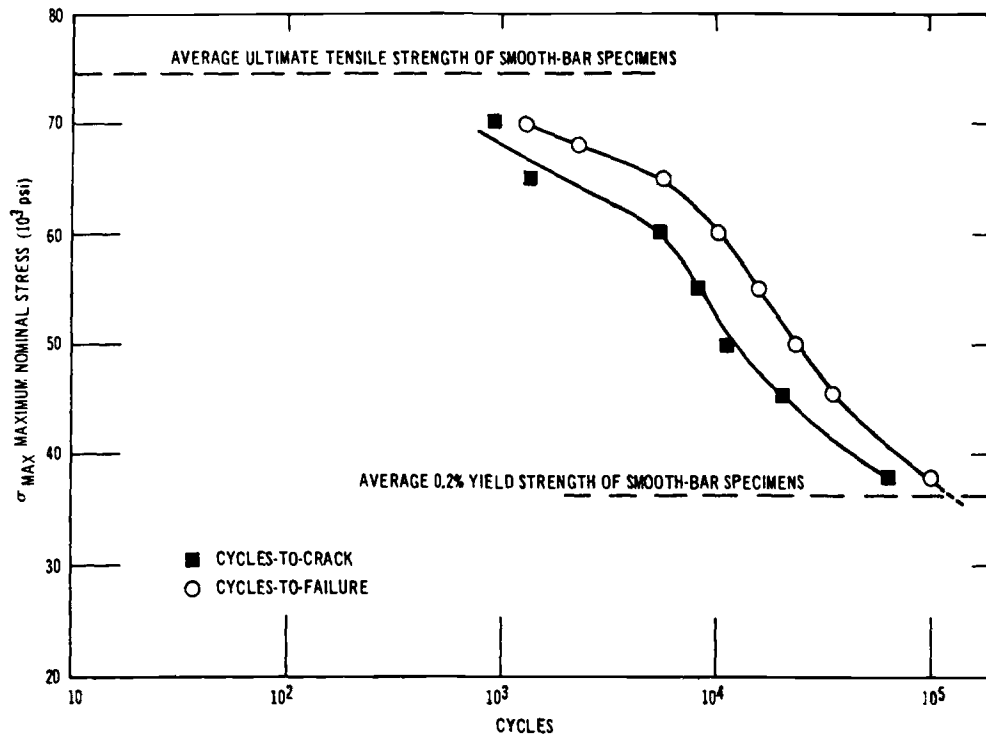
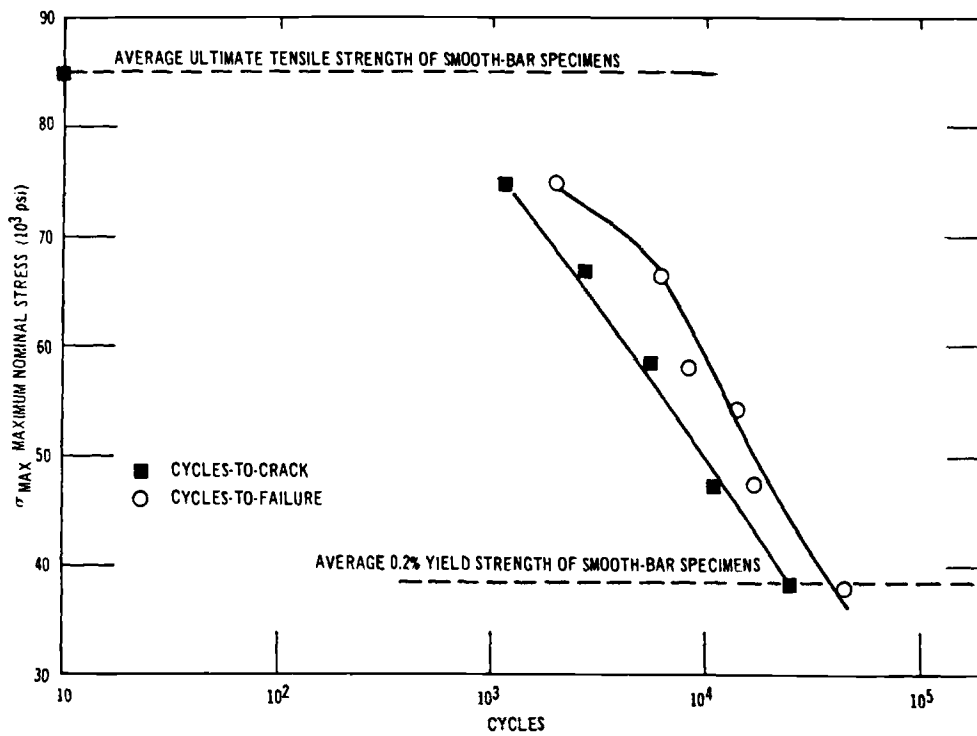


FIG. 71-4-23 – Low-cycle fatigue test results of edge-notched flat-plate specimens.



FLUCTUATING TENSION LOADING. MINIMUM STRESS 4×10^3 psi. MATERIAL: 2 1/4 Cr-1 Mo ALLOY STEEL

FIG. 72-5-23 – Low-cycle fatigue test results of edge-notched flat-plate specimens.



FLUCTUATING TENSION LOADING. MINIMUM STRESS 4×10^3 psi. MATERIAL: TYPE 304 STAINLESS STEEL

FIG. 73-6-23 – Low-cycle fatigue test results of edge-notched flat-plate specimens.

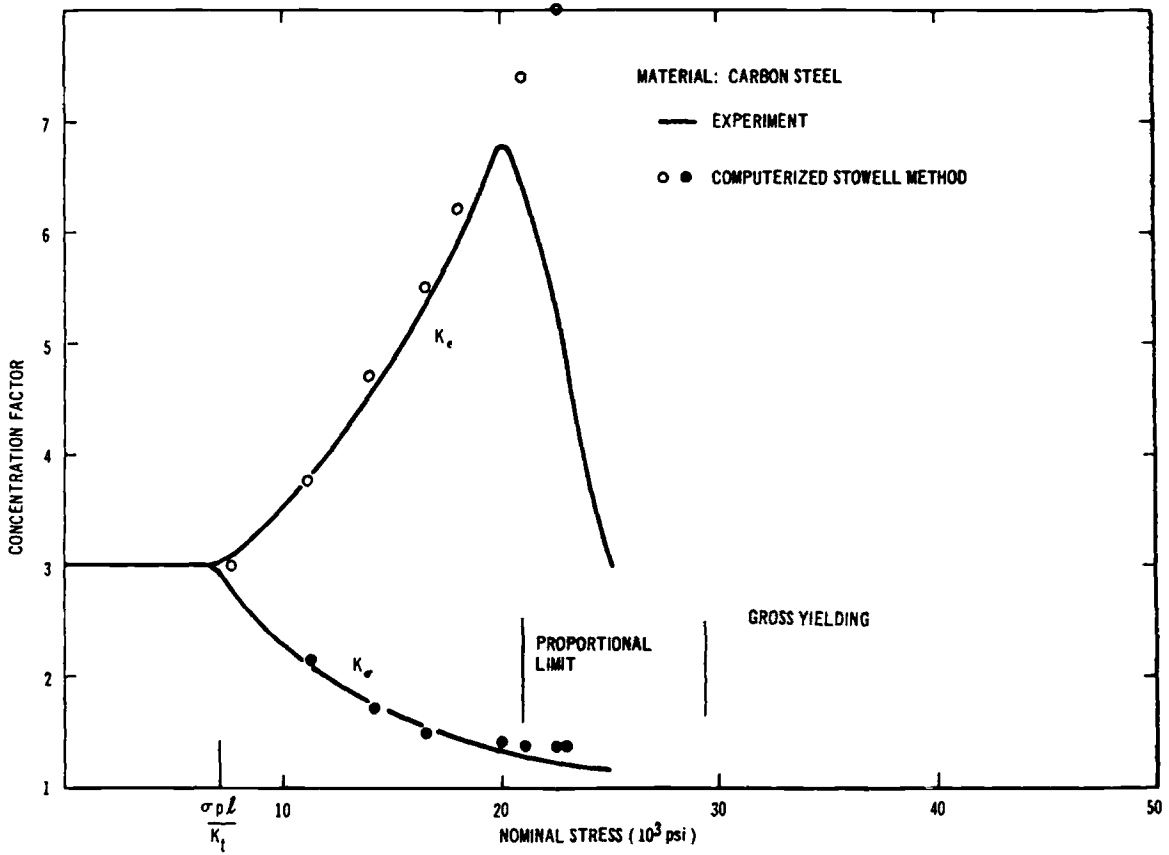


FIG. 74-8-23 – Comparison of experimentally and theoretically (Stowell method) determined stress– and stress-concentration factors versus the applied nominal stress.

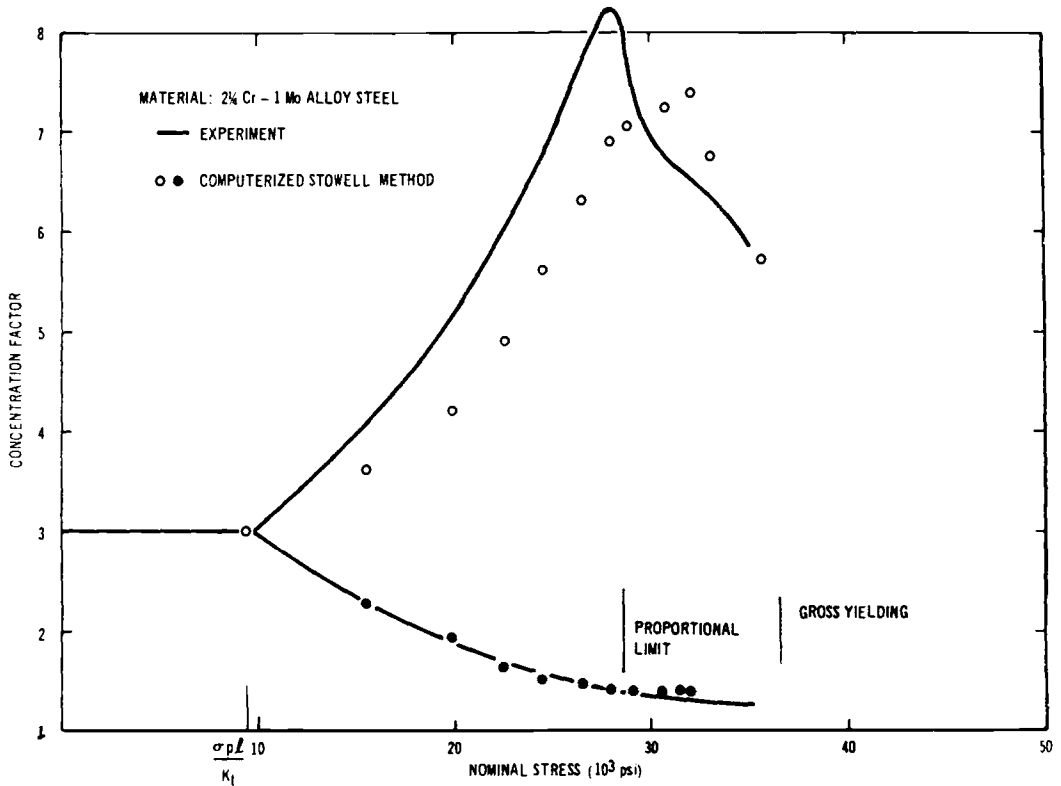


FIG. 75-9-23 – Comparison of experimentally and theoretically (Stowell method) determined stress– and strain-concentration factors versus the applied nominal stress.

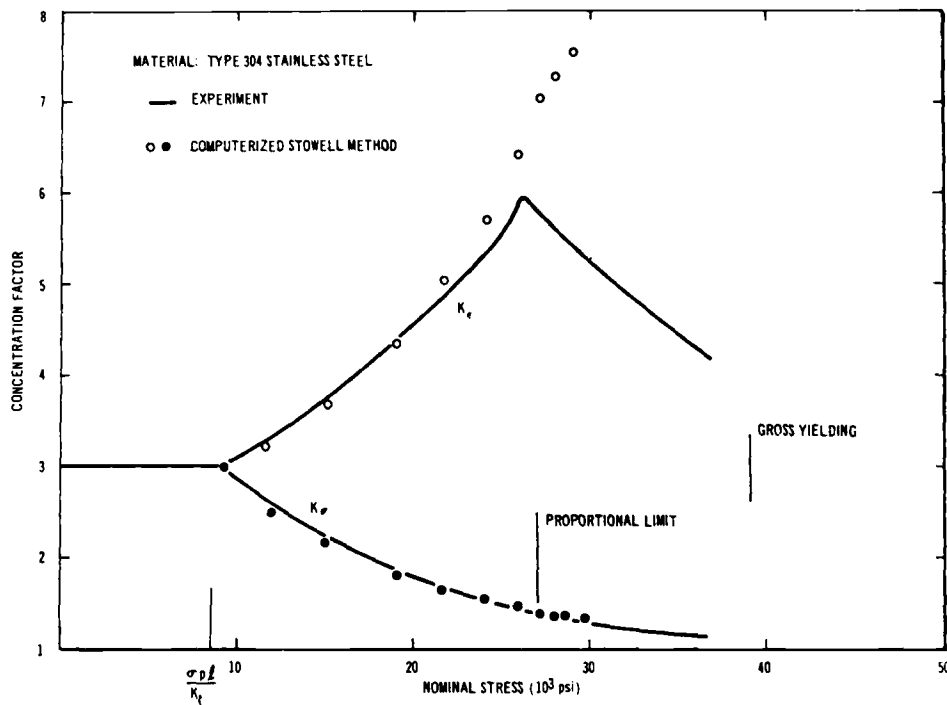


FIG. 76-10-23 – Comparison of experimentally and theoretically (Stowell method) determined stress- and strain-concentration factors versus the applied nominal stress.

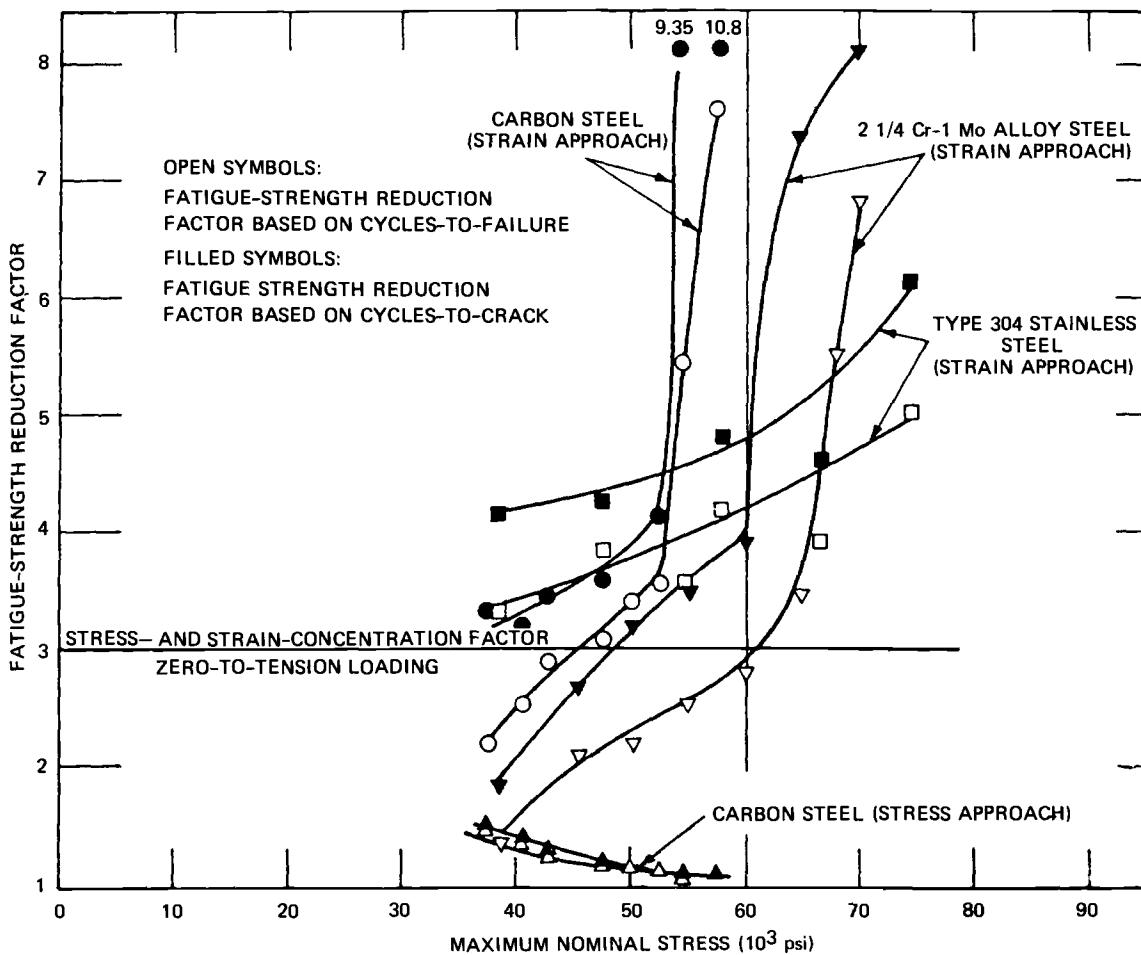


FIG. 77-11-23 – Fatigue-strength-reduction factors, stress and strain basis, for cycles-to-crack and cycles to failure versus applied maximum nominal stress. Edge-notched flat-plates, $K_t = 3$, zero-to-tension loading.

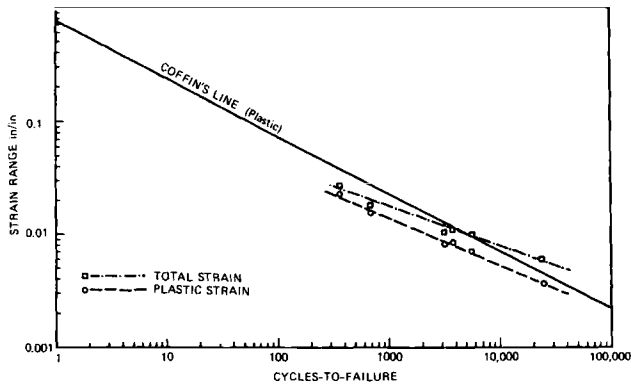


FIG. 78-5-25 – Total strain range and plastic strain range versus cycles-to-failure for completely reversed strain controlled low cycle fatigue tests. Material: Type-304 stainless steel.

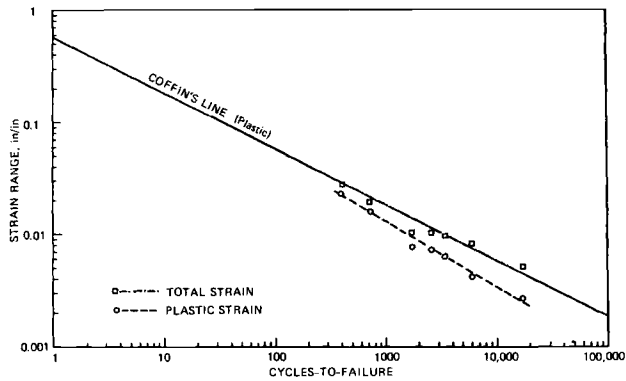


FIG. 79-6-25 – Total strain range and plastic strain range versus cycles-to-failure for completely reversed, strain controlled low cycle fatigue tests. Material: 2 1/4 Cr - 1 Mo alloy steel.

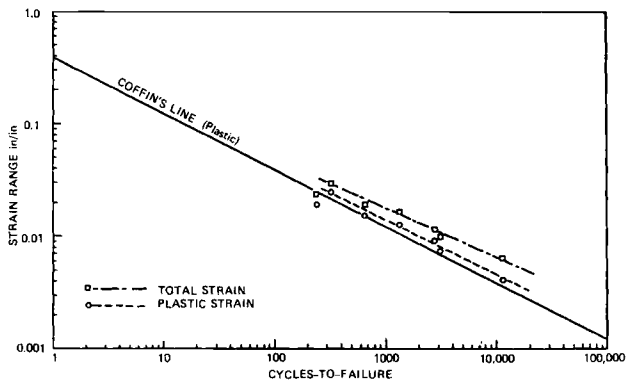
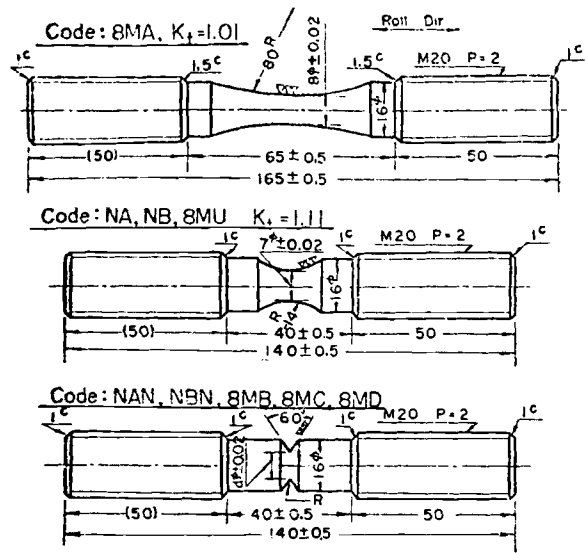


FIG. 80-7-25 – Total strain range and plastic strain range versus cycles-to-failure for completely reversed, strain controlled low cycle fatigue tests. Material: Carbon steel.

cycles and in some cases did not exceed 10^2 cycles. The specimens were continuously observed with the aid of a magnifying glass to define N_C . Figs. 82-8-15 and 83-9-19 show some typical results of LCF tests. Apparently test



Code	NAN	NBN	8MB	8MC	8MD
d	7	7	8	8	8
R	0.6	0.6	2.4	0.6	0.25
K_t	2.35	2.35	1.57	2.48	3.48

R : Notch Radius

K_t : Theoretical Stress Concentration Factor

FIG. 81-1-19 – Details of specimen.

results for unnotched specimens, $k_t = 1$, were not reported in the paper.

Iida introduces the following ratio of strain amplitudes. "Total diametral strain amplitude for an unnotched specimen corresponding to a given N_C divided by the local, total diametral strain amplitude for a notched specimen for the same N_C ." He plots this ratio with k_t as a parameter against cyclic life N_C and N_f in Fig. 84-24-19. It is seen that this ratio is always larger than the "ESCF" k_t and that its magnitude depends on k_t .

Iida calls this ratio fatigue strength reduction factor derived on the basis of strain controlled fatigue tests. This factor is similar to the factor Q_C^{1a} discussed in F.1. (Krempel R 27). It points out that, according to experiments, for a given k_t , to cause failure in the same number of cycles the local diametral strain in the notch root is a number of times smaller than the diametral strain in an unnotched specimen. This has been also discussed in F.1.

The author plotted, in Fig. 85-25-19, the relationship between the "ESCF" k_t and N_C using as a parameter different total strain amplitudes at the notch root. In the same figure he plotted also the "TSCF" k_t vs. life ratio R_L for different strain amplitudes (solid lines). The life ratio R_L is defined as the ratio of N_C for unnotched specimen to N_C for notched specimen with a fixed k_t for a given total strain amplitude. It is seen that life ratio R_L is a function of total strain amplitude and of "ESCF" k_t .

F.5. – Snow, et al, in R. 45 point out that in the fatigue analysis of structures the largest uncertainty is the fatigue strength reduction factor which can be used to represent the weakening effect of stress raisers. The designer should recognize that unless the "FS-th RF" has been deter-

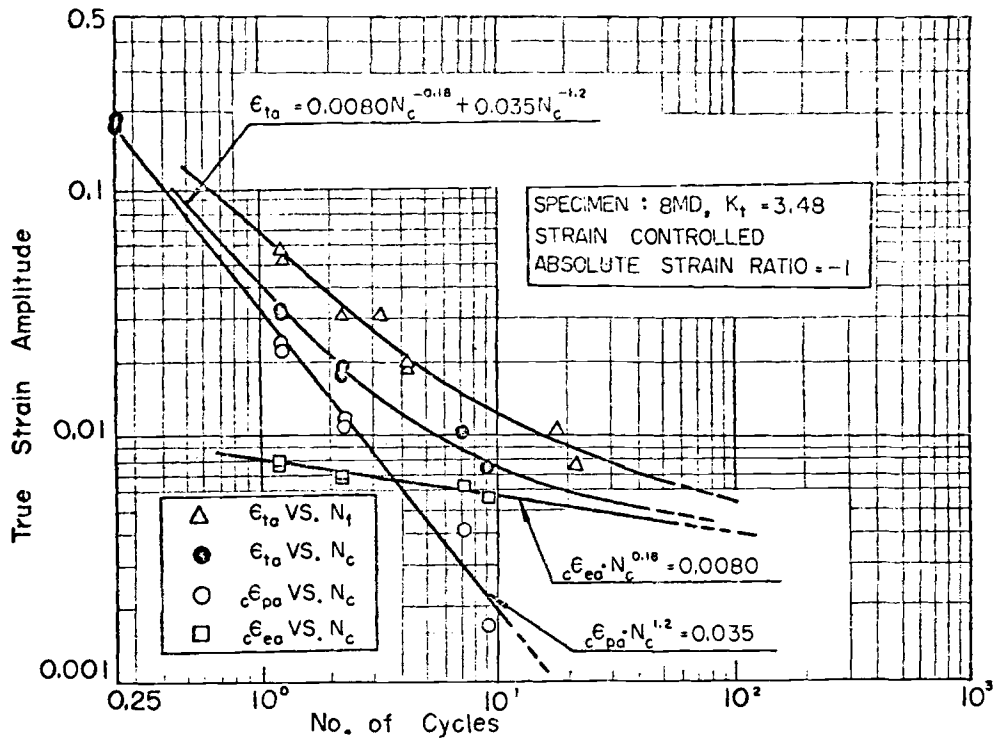


FIG. 82-8-19 – Relation between cycles and true strain amplitude (8MD).

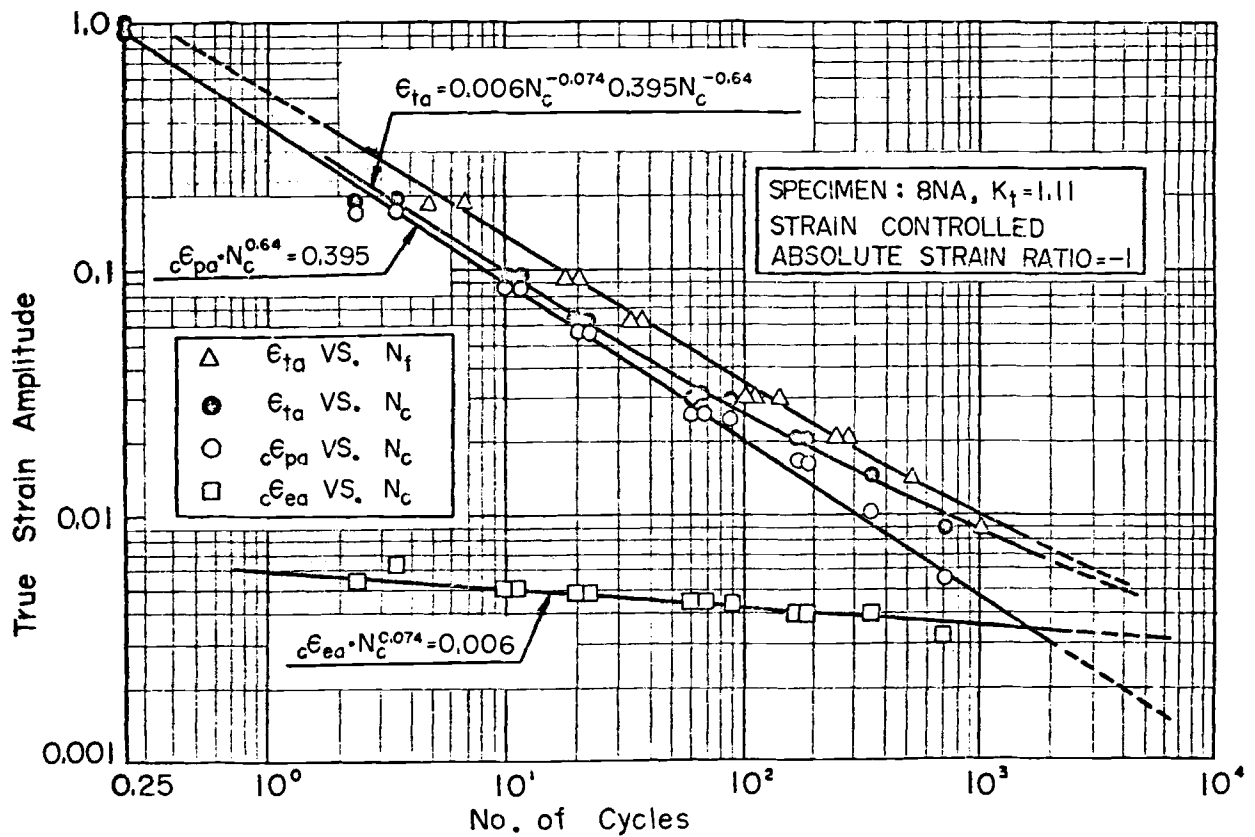


FIG. 83-9-19 – Relation between cycles and true strain amplitude (8NA).

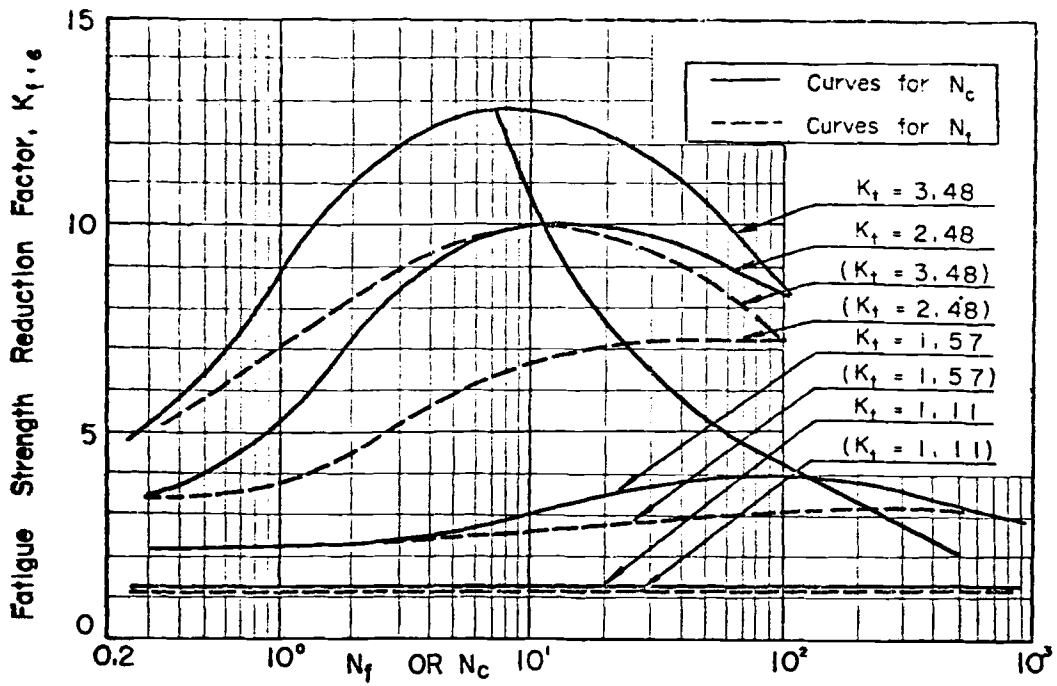


FIG. 84-24-19 – Relation between cycles and fatigue strength reduction factor.

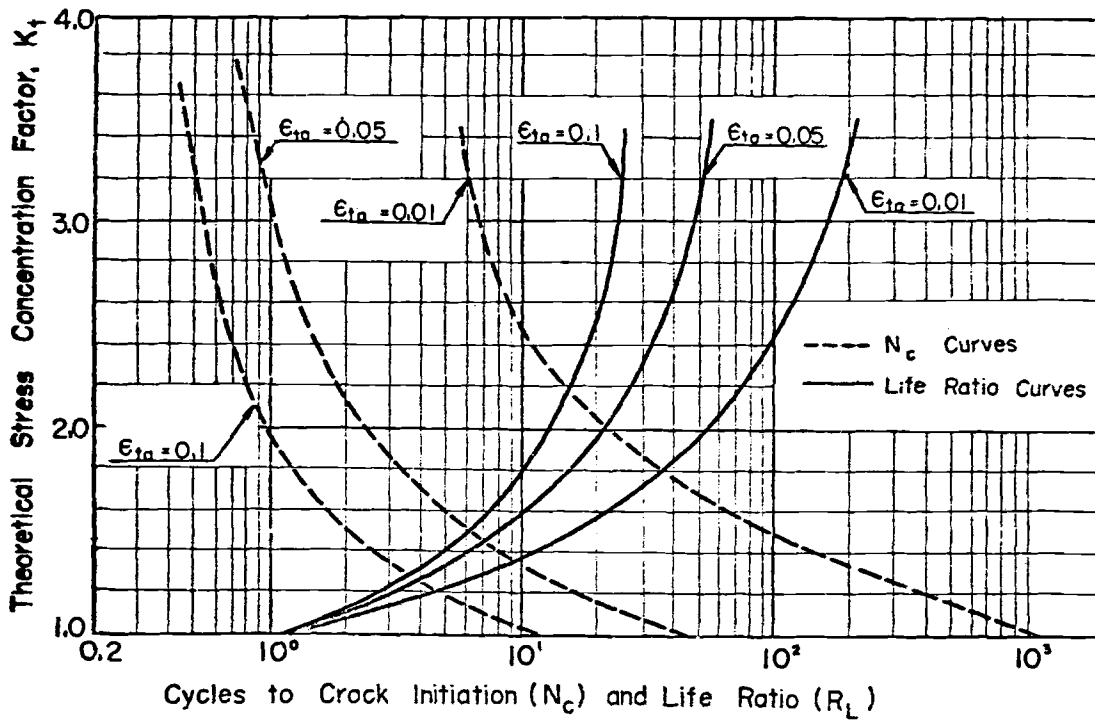


FIG. 85-25-19 – Relation between theoretical stress concentration factor and cycles to crack initiation or life ratio.

mined from experiments on a member of similar geometry, material and size to that of the prototype it should not be expected to give a precise estimate of fatigue life.

The authors describe the results of axial and bending, room temperature LCF tests on Ni – Cr – Fe alloy 600 (Inconel) and on low-alloy steel (A302B). Tests performed on flat, unnotched specimens were strain controlled. The notched specimens were singly and doubly edge-notched. The paper does not indicate clearly how the notched specimens were controlled in cyclic tension-compression and in cyclic bending.

The authors discuss a fatigue strength reduction factor which is shown in their Fig's. 6 and 7 but which again was not clearly defined. They compare this factor with other "FS-th RF" derived by Krempl in R. 23, Sec. F. 3. and by Iida in R. 15, Sec. F. 4 and conclude that for a good quantitative understanding of the laws governing fatigue life in the low-cycle range a much more detailed study of the phenomenon is required than was made in any of the three investigations. In the same time the authors state that the tests described in their paper are of more practical significance than those which were reported in R 23 and R 15.

In addition, they also draw a conclusion from their own tests that under conditions of strain cycling, at nominal strain levels representative of good design practice, the use of a high elastic stress concentration factor k_t as an estimate of a "FS-th RF" can be grossly over-conservative.

The reviewer would have liked to discuss in more detail the results of reported fatigue tests and to review the significance of the calculated "FS-th RF" reported in this paper, but the complexity of the paper interfered with the aim.

F.6. – Krempl in R 29 and R 28 answers the criticism by Snow et al, R 45, (see F. 5) of the fatigue test results described by Krempl in R 23, see F. 3.

He points out that different magnitudes of "FS-th RF" are to be expected because the materials are different and also because the test procedures and test specimens were considerably different. He concludes that the differences in "FS-th RF" may be explained quantitatively if the many differences which occur in the separate test series are properly recognized.

SECTION G
**FATIGUE STRENGTH REDUCTION FACTORS ON
 STRESS BASIS. RESULTS OF LCF TESTS**

G.1. — Ilg in R. 20 describes LCF tests at room temperature on notched and unnotched sheet specimens (0.090 in. thick) of 2024-T3 and 7075-T6 aluminum alloys and on SAE 4130 steel, 0.075 in. thick. The sheets were edge-notched and the "ESCF" k_t was equal 2 and 4. The tests were of the tension-compression type, controlled by the cyclic maximum nominal stress \bar{S}_{max} across the net section of the notched specimens. The tests on *unnotched* specimens were also *stress controlled*.

In addition to a large number of completely reversed tension-compression tests, with load ratio $R = -1$, there were tests with mean cyclic nominal stresses \bar{S}_m equal to 20,000 psi and 50,000 psi which resulted in varying load ratios including $R = 0$ and $R \geq 0$. LCF tests were performed in the life range of 2 to 10,000 cycles, however, previously published data have been included to extend the data to 10^7 cycles.

Figs. 86-4-20, 87-5-20, 88-6-20 present fatigue test results obtained with the 2024-T3 aluminum-alloy sheet specimens. Figs. 89-10-20, 90-11-20, 91-12-20 show test results for the normalized, SAE 4130 steel sheet specimens. The ordinates are cyclic maximum stresses and the abscissae define fatigue life from 1 to 10^7 cycles. Figs.

86-4-20 and 89-10-20 summarize test results for unnotched specimens and load ratio $R = -1$ for 2024-T3 aluminum and SAE 4130 steel, respectively. Figs. 87-5-20 and 90-11-20 summarise test results for specimens with "ESCF" $k_t = 2$, for the two materials and Figs. 88-6-20 and 91-12-20 summarize test results for $k_t = 4$. Each of the four figures for the notched specimens contain two curves, one for load ratio $R = -1$ and the other for a nominal mean stress $\bar{S}_m = 20,000$ psi. In addition to the above six figures, the authors present six more figures for hardened SAE 4130 steel and for aluminum alloy 7075-T6 (not reproduced). Ilg points out that S-N curves are concave upward in the long-life range, have a reversal of curvature at an inflection point to concave downward in the short-life range. The tensile strength of notched specimens sometimes exceed that of notched specimens. In this investigation for alloy 7075-T6 the notched specimens had somewhat higher tensile strength than the unnotched specimens, however, for the case of alloy 2024-T3 the reverse was observed. For the 4130 steel the notched specimens had a higher tensile strength than the unnotched.

Using the test results, the author calculated K_f the

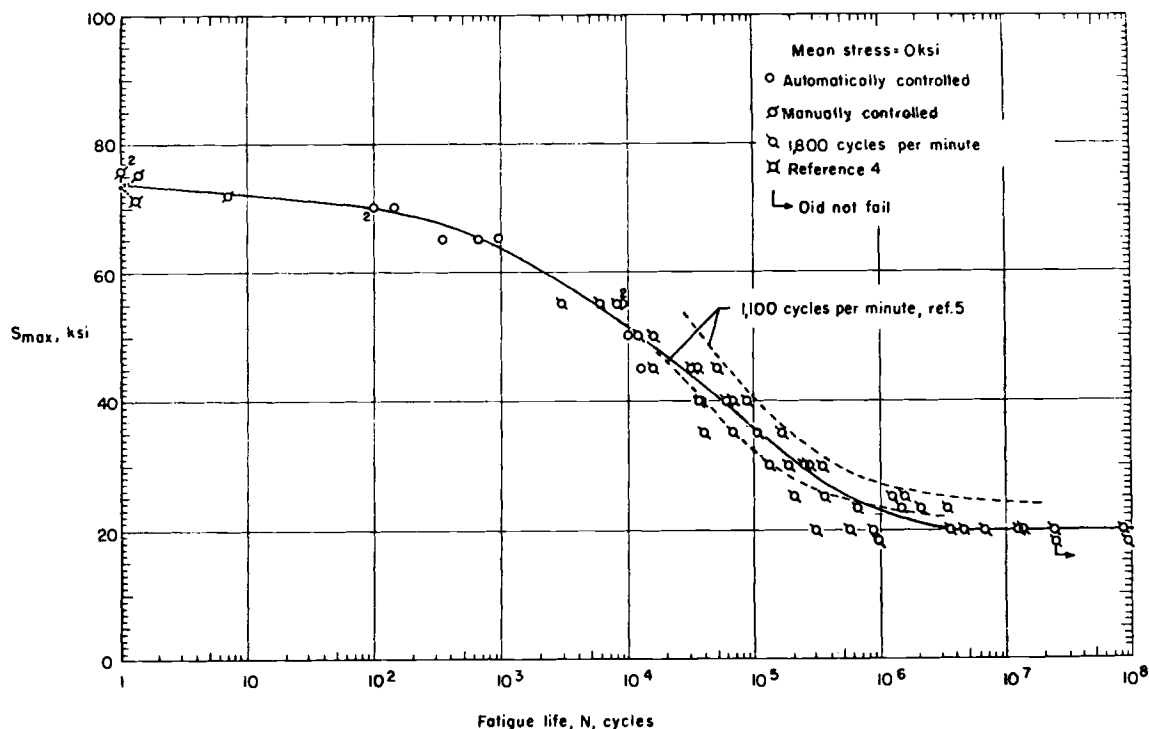


FIG. 86-4-20 — Results of axial-load fatigue tests on unnotched 2024-T3 aluminum-alloy sheet specimens. $K_T = 1.0$.

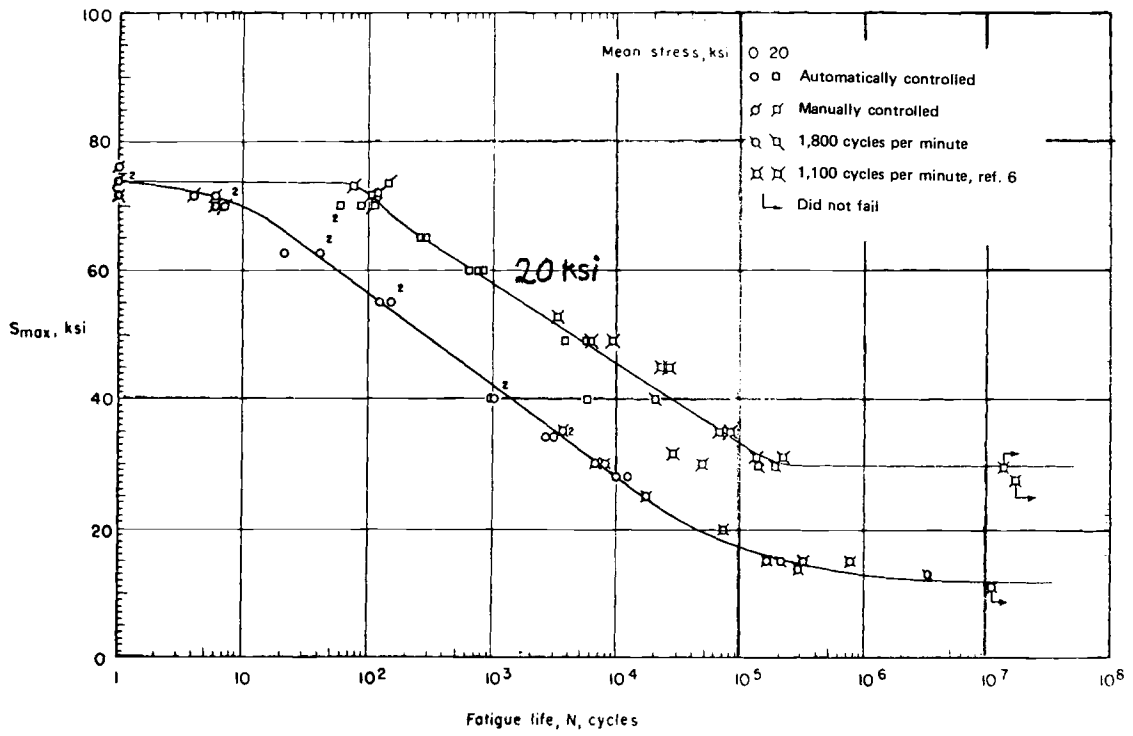


FIG. 87-5-20 – Results of axial-load fatigue tests on notched 2024-T3 aluminum-alloy sheet specimens. $K_T = 2.0$.

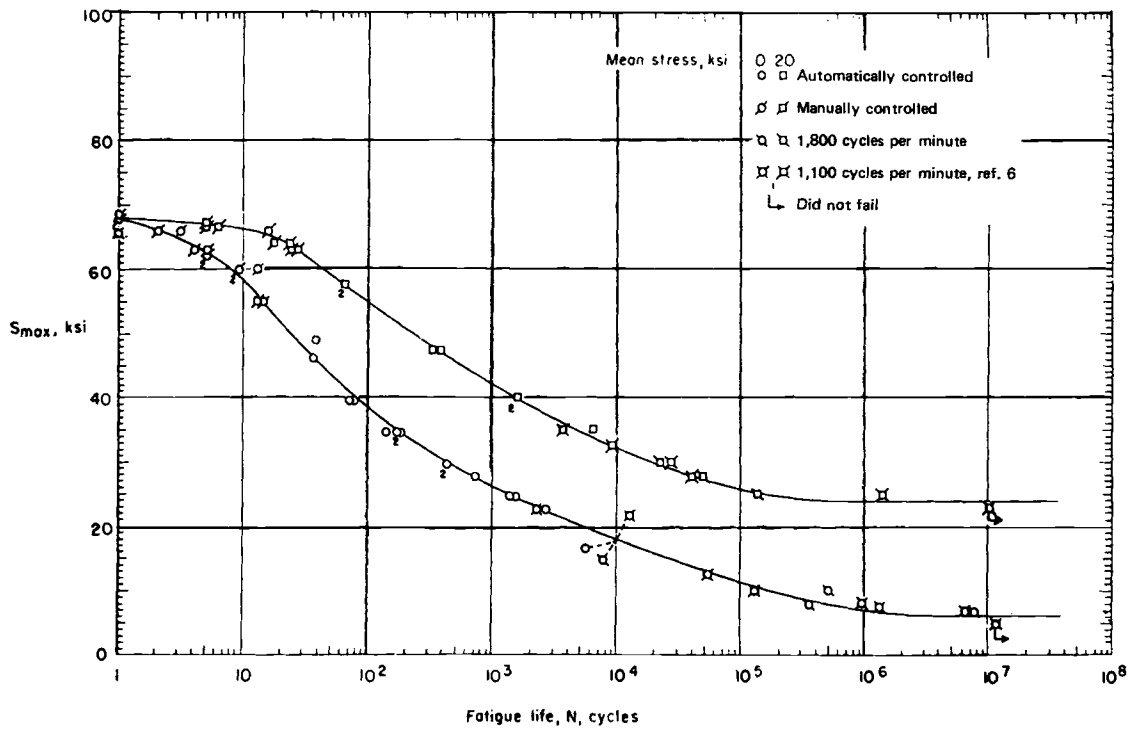


FIG. 88-6-20 – Results of axial-load fatigue tests on notched 2024-T3 aluminum-alloy sheet specimens. $K_T = 4.0$.

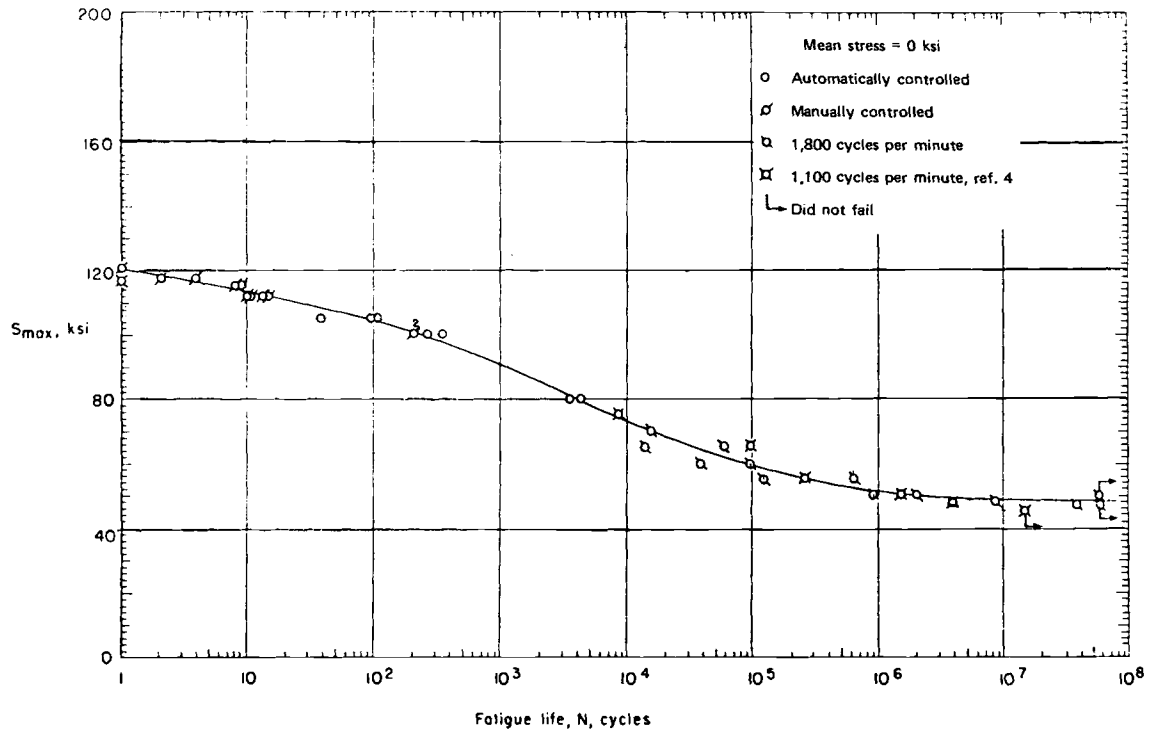


FIG. 89-10-20 - Results of axial-load fatigue tests on unnotched normalized SAE 4130 steel sheet specimens. $K_T = 1.0$.

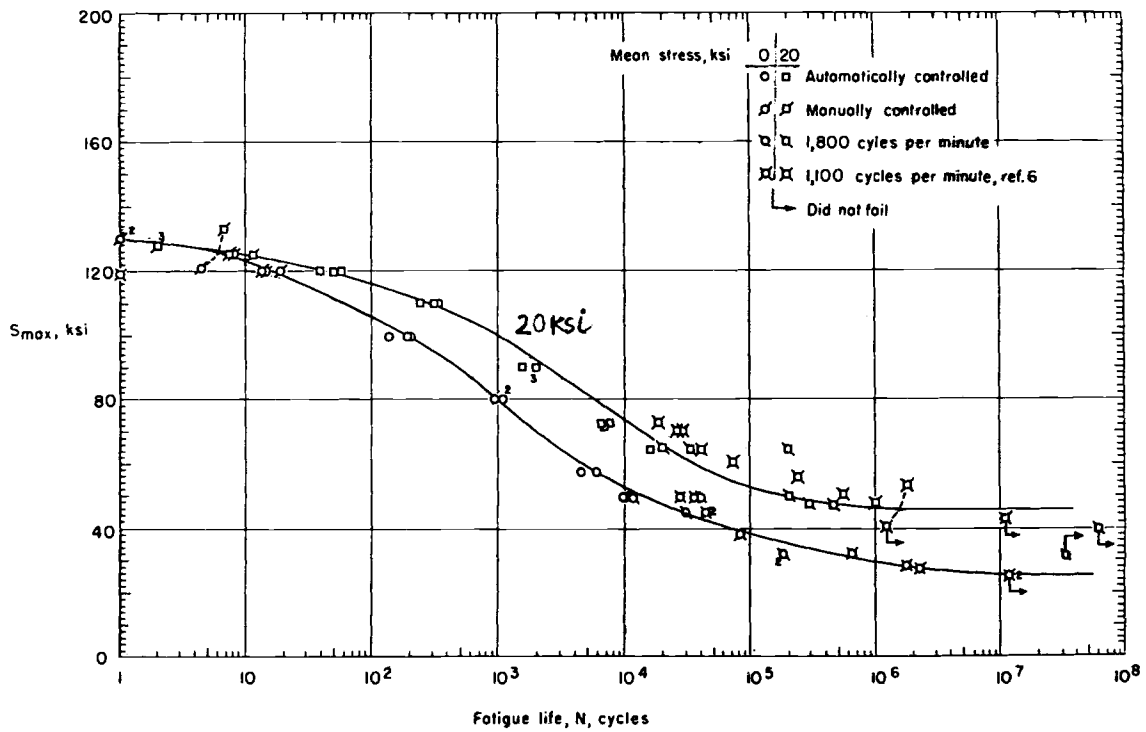


FIG. 90-11-20 - Results of axial-load fatigue tests on notched normalized SAE 4130 steel sheet specimens. $K_T = 2.0$.

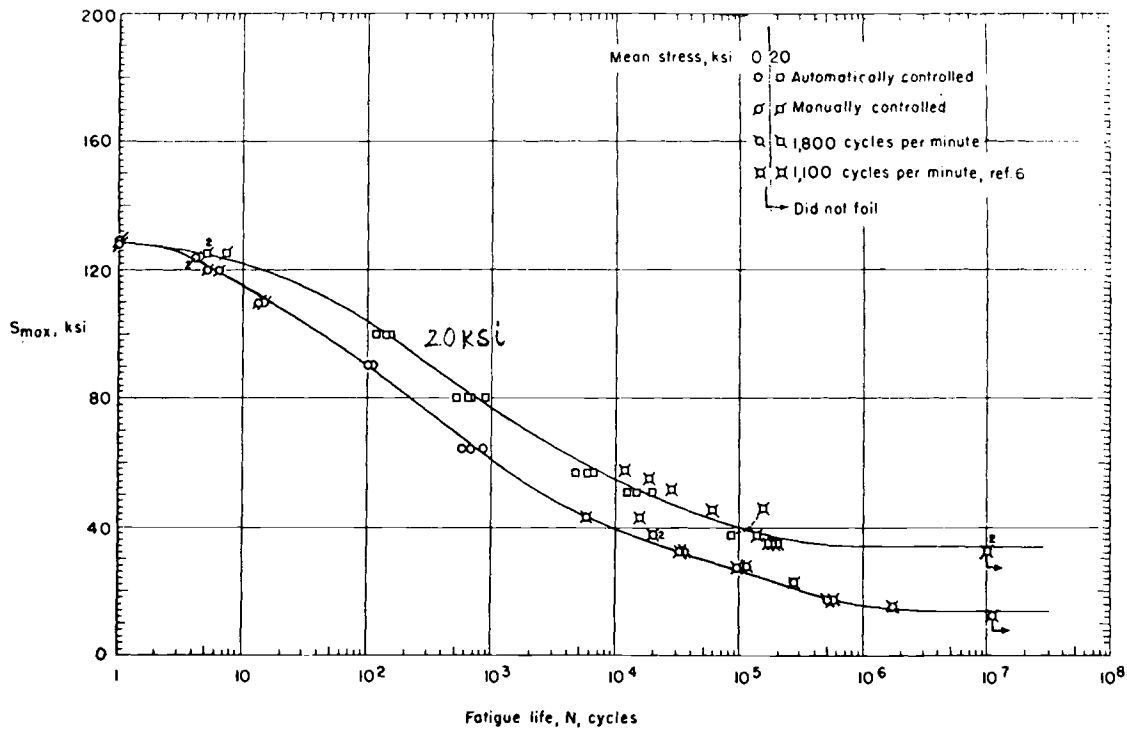


FIG. 91-12-20 – Results of axial-load fatigue tests on notched normalized SAE 4130 steel specimens. $K_T = 4.0$.

fatigue strength reduction factor to fracture “FS-th RFF”. Because the data were derived from *stress controlled* fatigue tests on both unnotched and notched specimens, the factor K_f is defined on stress basis and is different than the factor Q discussed in section F and which was defined on strain basis.

Factor K_f was calculated as the ratio of \bar{S}'_{max} , maximum stress in the unnotched specimen to \bar{S}_{max} , maximum nominal stress in the notched specimen for the same fatigue life

$$K_f = \frac{\bar{S}'_{max}}{\bar{S}_{max}}$$

The calculations were made only for load ratio $R = -1$ and K_f was plotted as a function of \bar{S}_{max} in Figs. 92-16a-20 and 93-16b-20. In each of the four figures (a, b, c, d) for the four materials there are two curves shown for $k_t = 2$ and 4. It is seen that K_f reaches a maximum for very small values of \bar{S}_{max} , however this maximum is smaller than “ESCF” k_t . Also K_f decreases with increasing \bar{S}_{max} and when \bar{S}_{max} reaches the tensile strength K_f approaches one. Note that the width of the scatter-band decreases with increasing nominal stress. It should be pointed out that the author did not attempt to analyze the effect of mean stress on cycles to fracture.

G.2. – Nachtigall, et al, in R. 37 discuss fatigue life of four metals in ambient air, liquid nitrogen and liquid helium at 70°F, -320°F and -452°F. The metals tested were 2014T6 aluminum alloy, Inconel 718, SA1-2.5 Sn titanium alloy and AISI Type 301 stainless steel. The notched and unnotched sheet specimens were tested in

pulsating tension with a load ratio $R = 0.14$. The notched specimens had a rather large “ESCF” $k_t > 17$.

The relationship between the maximum nominal stress \bar{S}_{max} and life to fracture for the four metals is shown in Fig. 130-4abcd-37. It is seen that decreasing the temperature from 70°F to -320°F resulted in increased fatigue strength for all the four metals. Inconel 718 and Type 301 stainless steel exhibited the highest fatigue strength and the two light metal alloys the lowest.

The authors calculated K_f , the fatigue strength reduction factor to fracture, on stress basis. It is shown in Fig. 131-6-37 for 2014-T6 aluminum alloy and for Inconel 718 for tests at three temperatures, 70°F, -320°F and -452°F. K_f was calculated as the ratio of maximum stress for the unnotched specimens to the maximum nominal stress for notched specimens, for the same life to fracture.

The tensile notch strength factor, that is the ratio of tensile strength for the unnotched and notched specimens, was plotted at 1/2 cycle. The authors state that up to approximately 50 to 100 cycles the “FS-th RFF” was nearly the same as tensile notch strength factor for all materials at all temperatures. With increasing cyclic life the factor K_f was increasing and at room temperature at 10^4 cycles K_f is equal to 3 for 2014-T6 aluminum alloy and equal to 2 for Inconel 718. It appears that for fatigue lives of the order 10^6 cycles the factor K_f is about 3 for Inconel 718 and about 5 for 2014-T6 aluminum alloy.

Note, that these are rather small values considering that the “ESCF” k_t is larger than 17. The above results are for pulsating loads with load factor $R = 0.4$ and not for completely reversed loads.

G.3. — Bell, et al, in R.2 describe axial fatigue tests of unnotched and notched 18 Cr - 9 Ni steel sheet 0.039 in. thick. The load ratio varied widely from -1.0 to +0.91 and fatigue life varied from 10 to 10⁷ cycles. The notched specimens had three 1/8 in. dia. drilled holes with "ESCF" $k_t = 2.44$. The authors were investigating the effect of mean stress on the fatigue life of notched specimens subjected to axial load cycling. Tests were conducted on Haigh machine for cyclic life in the range from 5 x 10³ to 10⁷ cycles at 3000 c.p.m. In the range from 10 to 10⁵ cycles, tests were carried out on a Schenck axial-load fatigue machine at about 10 c.p.m.

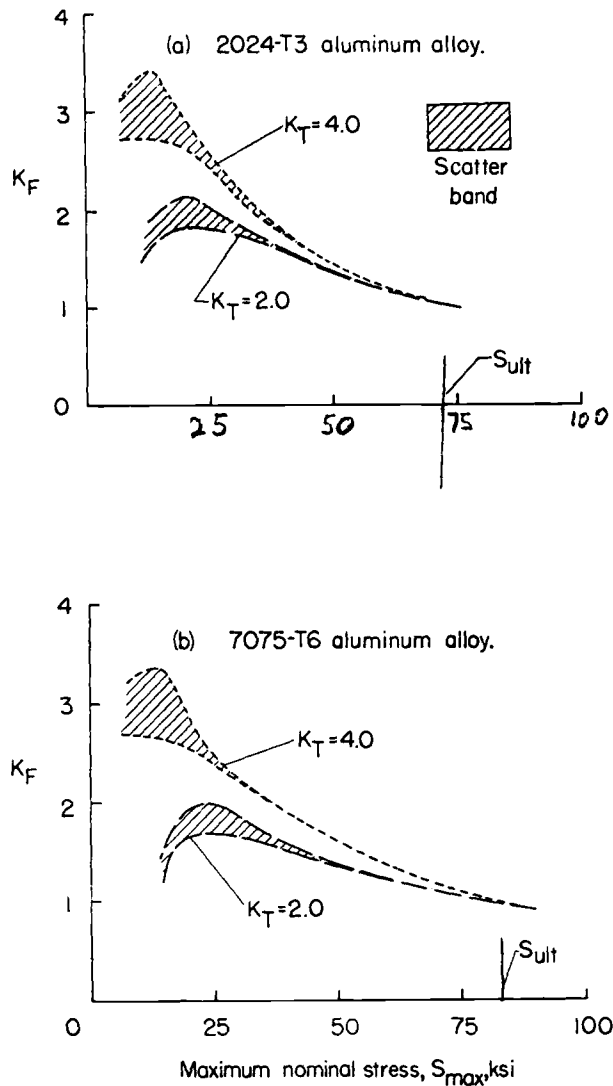


FIG. 92-16ab-20 — Variation of K_F with maximum nominal stress of notched specimen. $R = -1$.

Tests were conducted at values of load ratios $R = -1.0, -0.46, +0.075, +0.33, +0.5, +0.725$ and $+0.91$.

The results of fatigue tests on both fatigue machines are plotted, for values of R as a parameter, as curves of maximum nominal stress against cycles to fracture in Fig. 94-3-2 for unnotched and in Fig. 95-5-2 for notched specimens. Above figures provided a basis for detailed

analysis of various quantities, which is shown in Figs. 96-7a-2 and 96-7b-2 for unnotched and notched specimens respectively. In these figures the cyclic stress amplitude (nominal for notched specimens) is shown as a function of mean imposed stress for various values of cyclic life. It is seen that for very long cyclic life the curves for unnotched specimens are similar in shape to the well-known curves devised by Goodman, Soderberg and others.

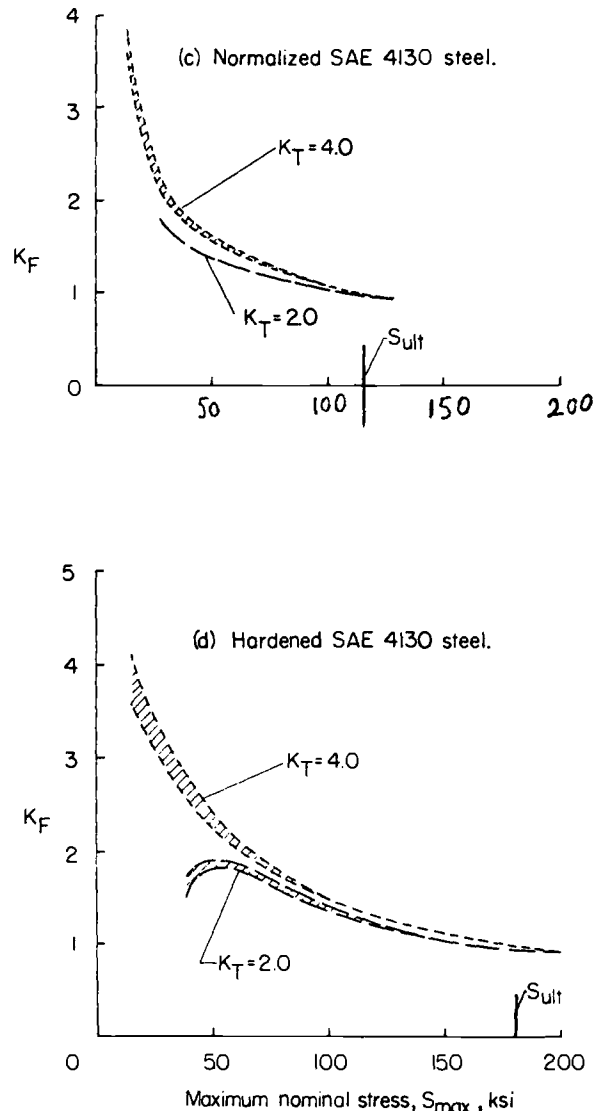


FIG. 93-16cd-20 — Figure 92 concluded.

The authors have analyzed a number of approaches designed to derive the cyclic life curves for the notched specimens shown in Fig. 97-7b-2 from the unnotched data in Fig. 97-7a-2. They came to the conclusion that none of the investigated approaches were satisfactory. Instead, the authors proposed a modified fatigue strength reduction factor to fracture K_{fm} which includes the influence of various mean stresses. The proposed definition is as follows

$$K_{fm} = \frac{\text{Max. cyclic stress amplitude for unnotched specimen}}{\text{Max. cyclic nominal stress amplitude for notched specimen}}$$

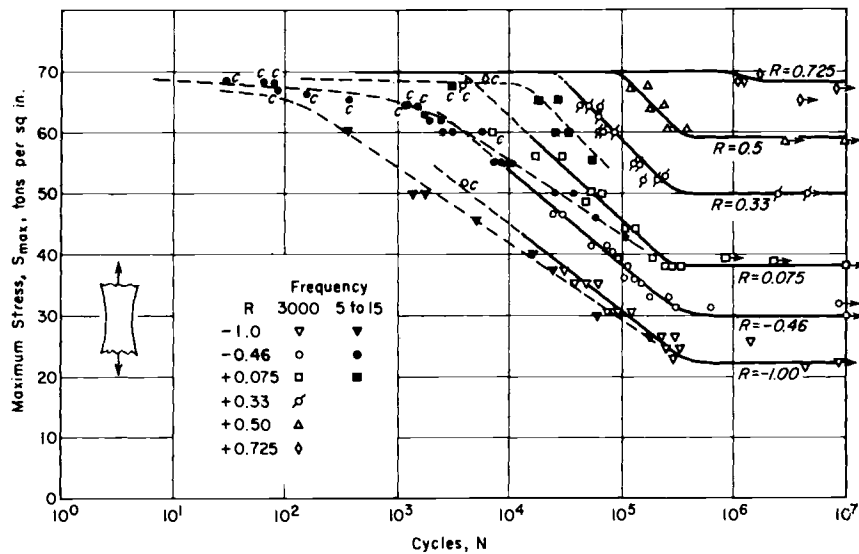


FIG. 94-3-2—*S-N* curves for various stress ratios, unnotched specimens.

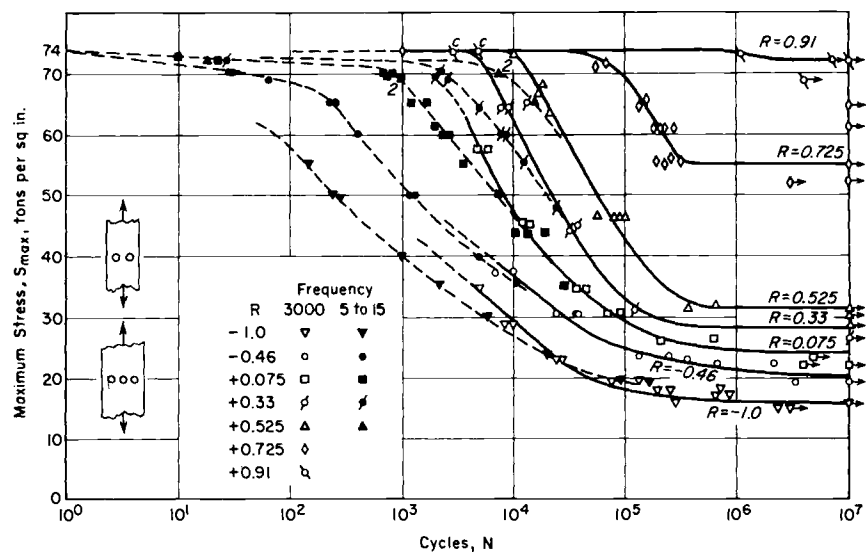


FIG. 95-5-2—*S-N* curves for various stress ratios, notched specimens.

The above ratio is for the same mean stress for the unnotched and notched specimens and for the same cyclic life.

The authors state that the above definition results in curves of the simplest form for graphical representation. The “FS-th RFF” K_{fm} calculated in the above manner is shown in Fig. 98-9-2 as a function of cyclic life for different mean stresses and for $k_t = 2.44$. Note that for $R = -1$. ($S_m = 0$) K_{fm} varies from approximately 1.0 at one cycle to a maximum of about 1.6 at 30×10^3 cycles and then decreases.

The authors state that until there is more information about the localized stress and strain conditions, it is not possible to predict accurately notched fatigue data from unnotched fatigue tests. However, if the notched fatigue curve is known for zero mean stress ($R = -1$), curves for

other mean stresses might be possibly derived using an approach proposed by the writers.

G.4 – Wellinger, et al, in R. 53 (in German) describes fatigue tests performed at room temperature on unnotched and notched specimens from a German low-alloy steel (34 Cr Ni Mo 6) heat treated to three different strength levels. The notched specimens were cylindrical (24 mm dia.), some had deep circumferential notches with “ESCF” $k_t = 1.6, 2.4, 5.2$ and 8.1 , and others had shallow notches with $k_t = 1.4$ and 4.2 .

Two series of tests were made, with fully reversed tension-compression, load ratio $R = -1$, and with pulsating tension, $R = 0$. The life range extended from 1 cycle to 10^7 cycles. In some tests cycles to crack initiation were observed. Fig. 99-18-53 is interesting. It shows the ratio of N_c to N_f cycles to fracture as a function of “ESCF” k_t . For unnotched

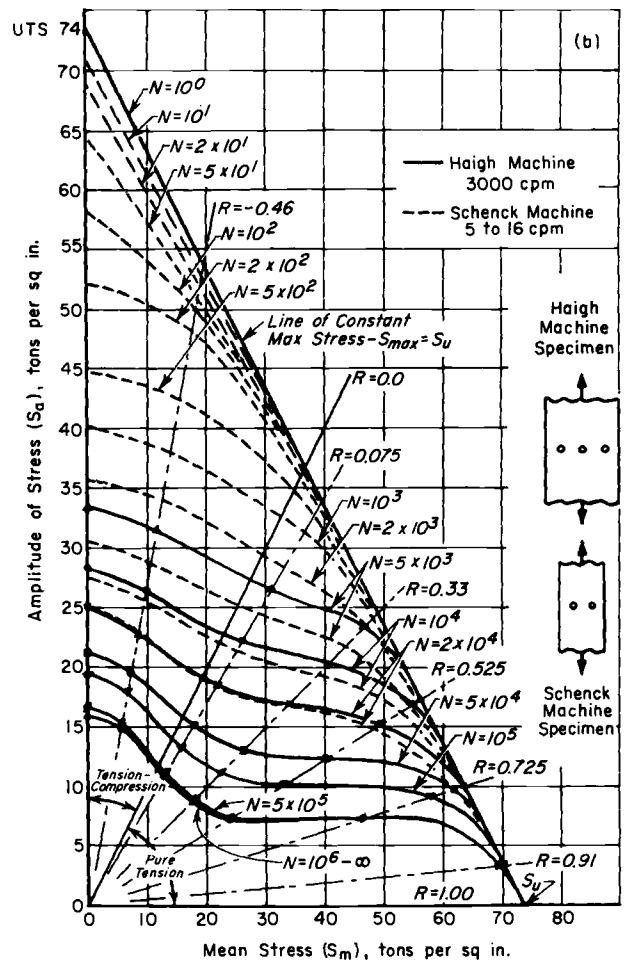
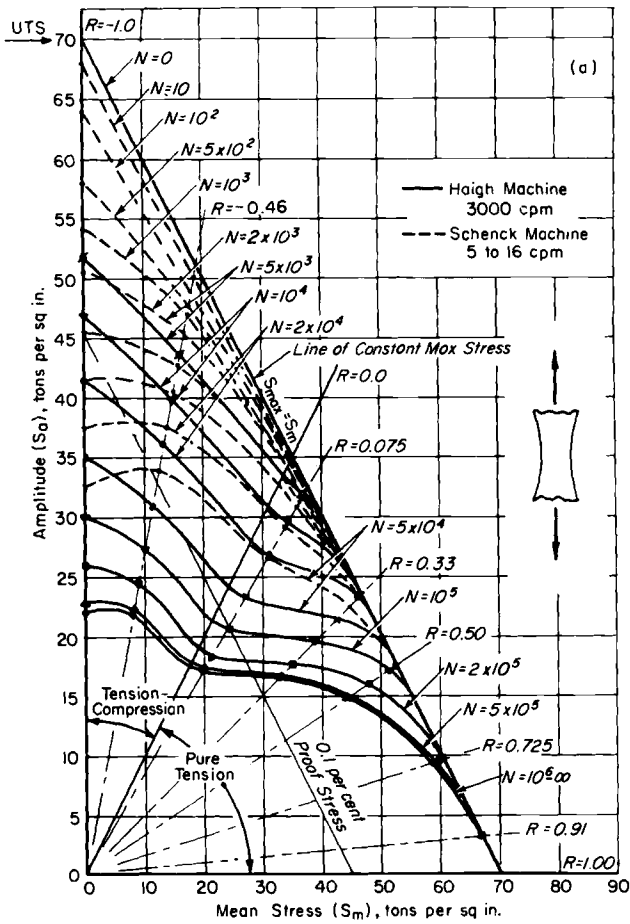


FIG. 96-7a-2 - $S_a - S_m$ curves for fatigue specimens.

FIG. 97-7b-2 - Fig. 96 continued.

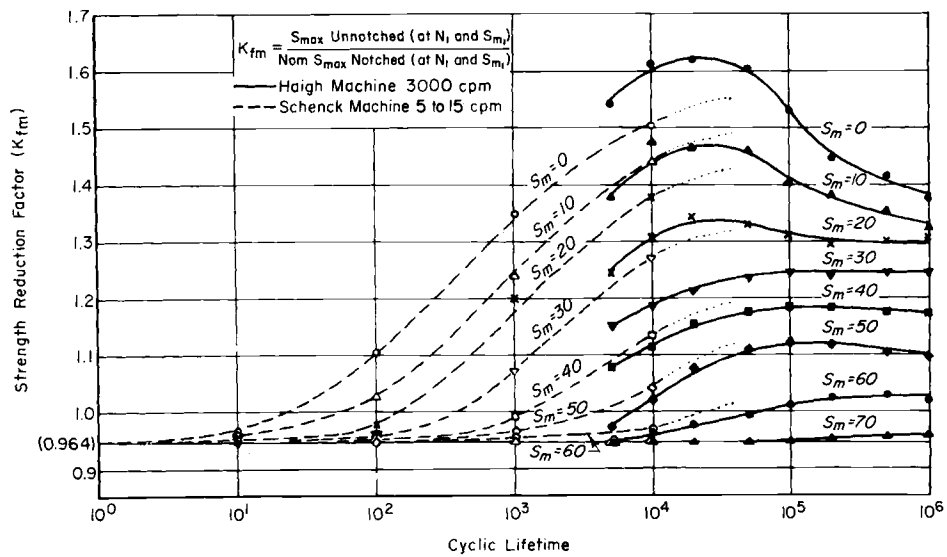


FIG. 98-9-2 - Strength reduction factor (k_{fm}) versus cyclic lifetime.

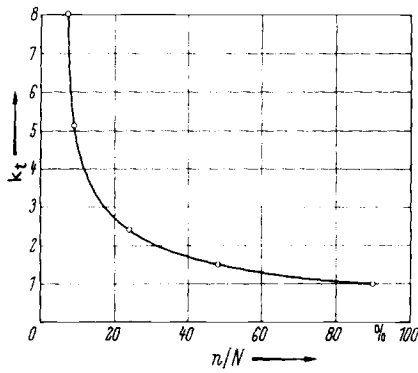


FIG. 99-18-53 – Crack initiation in relation to the elastic stress concentration factor and to the number of cycles to fracture for reversed tension-compression loading and for pulsating tension. (34Cr Ni Mo 6 steel in three different hardness levels).

specimens ($k_t = 1$) the ratio may be as high as 0.9, for sharp notches, as low as 0.08. This ratio appear to be the same for load ratios $R = 0$ and $R = -1$.

Some of the test results with completely reversed tension-compression are shown in Fig. 100-7-53. It shows the cyclic stress amplitude as a function of cyclic life up to 10^7 cycles for “ESCF” $k_t = 1, 2.4, 5.2$ and 8.1 . Besides k_t

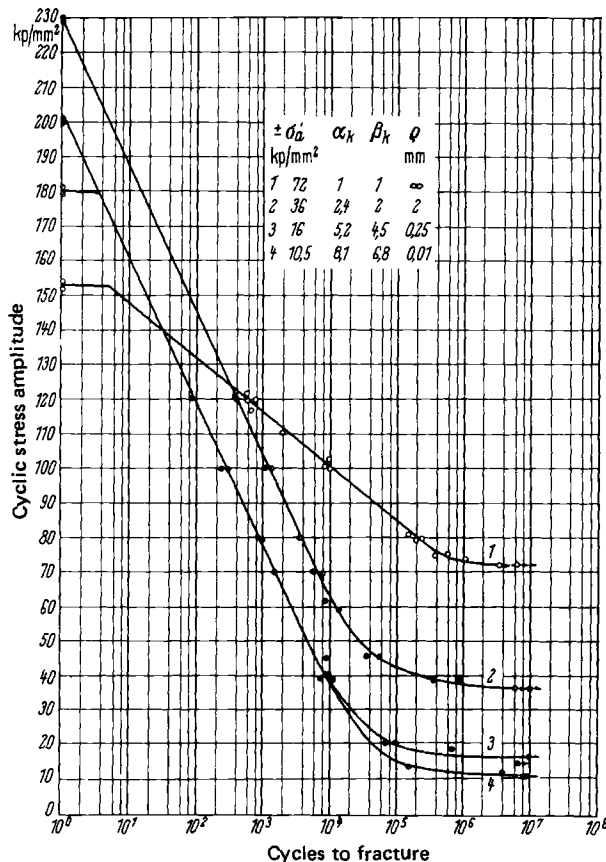


FIG. 100-7-53 – Reversed tension-compression fatigue tests on specimens of 34 Cr Ni Mo 6 steel in hardness level H3. (12/24 mm dia. ; $\sigma_m = 0$).

the table in the figure includes the “FS-th RF” k_f which is lower than k_t .

The authors have calculated $\frac{1}{K_f}$, the inverted fatigue strength reduction factor to fracture on stress basis K_f .

$\frac{1}{K_f}$ was plotted as a function of cyclic life for the deep and shallow notches in Figs. 8 and 9, which are not reproduced because of their complexity. The authors indicate in Fig. 101-10-53 that, although specimens with shallow and deep notches and with same k_t have the same endurance limit, the low-cycle life is shorter for shallow notches.

This paper has 22 figures, mostly rather complex and in addition the text is not always clear. It is of interest that the authors list only German literature references pertaining to low-cycle fatigue. The very many papers on this subject published in the U. S. and United Kingdom are not mentioned.

Another paper by Wellinger, et al, R. 52 was recently translated into English.

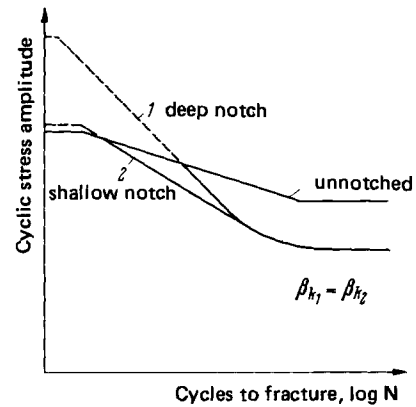


FIG. 101-10-53 – Fatigue diagram for specimens with shallow and with deep notches of the same elastic stress concentration factor.

SECTION H

FATIGUE STRENGTH REDUCTION FACTORS IN BENDING.

H.1. — Hickerson, et al, in an elaborate and complete paper, R. 17, report on LCF tests performed at Lehigh University under the sponsorship of Pressure Vessel Research Comm. (PVRC). These tests were intended to provide information on the influence of notches, holes and fillets on room temperature fatigue life of three pressure vessel steels A201A, A302B and A517F. The tests were performed on the widely used "Lehigh" cantilever-type specimen which provides nearly complete transverse restraint in the center of the reduced test section and therefore, induces in the specimen a 2 to 1 biaxial stress state. See Fig. 102-1-17. Three discontinuities common in pressure vessel design elements were

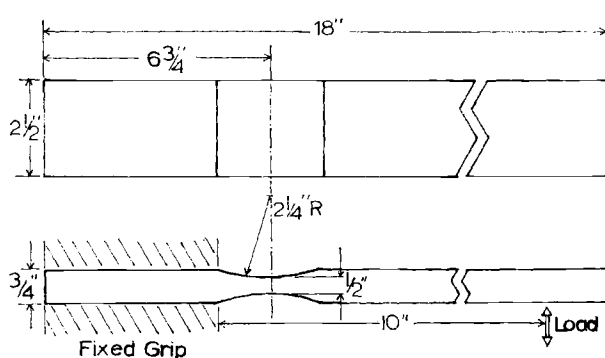


FIG. 102-1-17 — *Lehigh fatigue specimen.*

simulated -45° shallow notches with "ESCF" k_t from 1.4 to 5.0, sharp-edged surface hole with $k_t = 2.2$ and a fillet with $k_t = 2.1$. Specimens containing stress raisers were basically the same as the standard unnotched specimens and the desired geometrical configuration was machined in the reduced section only on one side of the specimen while the other side was unchanged. See Fig. 103-2-17. For specimens with the 1/2 in. deep, 1/2 in. dia. hole, strain measurements were taken in the minimum section at a point midway between the hole and the edge.

Fatigue testing was controlled by the imposed nominal total strain range $\overline{\Delta e}_n$ which was measured on the unnotched side of the specimen. Specimens were tested in repeated nominal bending tension, $R = 0$, repeated nominal bending compression and in fully reversed nominal bending, $R = -1$.

Failure of the specimens was considered from two aspects — macrocracking and complete fracture. Fracture was defined as the point at which the load on the specimen was essentially zero, this usually coincided with complete separation of the specimen into two parts.

Macrocracking in the case of the plain and notched specimens tested in pulsating tension, $R = 0$, was defined as the point at which the load on the specimen dropped to 85% of its initial value. For the definition of macrocracking of other notched specimens see the original paper.

The imposed total nominal strain range for notched specimens measured on the unnotched side is designated $\overline{\Delta e}_n$ and the corresponding total strain range for the unnotched specimens is designated $\overline{\Delta e}$.

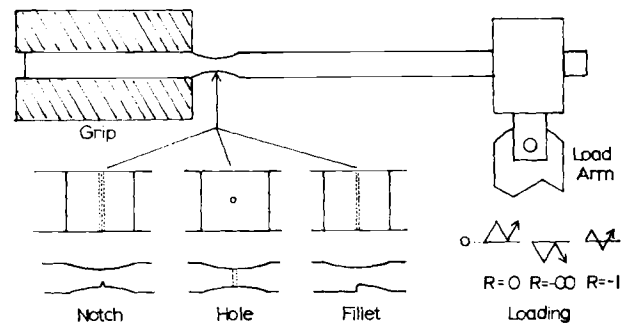


FIG. 103-2-17 — *Stress raisers and loading cycles studied.*

The authors introduced two fatigue strength reduction factors, one for macrocracking Q_{bc} and another for fracture Q_{bf} . These "FS-th RF" were defined as follows:

$$Q_{bc} = \frac{\overline{\Delta e}}{\overline{\Delta e}_n} \text{ for macrocracking}$$

$$\text{and } Q_{bf} = \frac{\overline{\Delta e}}{\overline{\Delta e}_n} \text{ for fracture.}$$

In both cases, the imposed strain ranges $\overline{\Delta e}$ and $\overline{\Delta e}_n$ are for the same number of cycles. For discussion of other "FS-th RF" see Section F.1.

After a large number of fatigue tests were completed the authors plotted curves of total imposed strain range as a function of cycles to crack initiation and to fracture, for the unnotched, notched, holed and filleted specimens. The cycles to failure range from 1500 to 100000. Using this data the "FS-th RF" Q_{bc} and Q_{bf} were calculated and plotted as a function of cyclic life for the three materials and for the several notches in repeated tension, repeated compression, and in totally reversed bending.

The authors compare factors Q_{bc} and Q_{bf} with elastic stress or strain concentration factor k_t . Probably it would have been more logical to compare Q_{bc} and Q_{bf} with a fatigue strength reduction factor k_f which includes the effect of size and notch sensitivity on fatigue endurance and which is usually less than k_t .

The authors discuss extensively, with the help of eleven figures, the behavior of the experimentally determined "FS-th RFF" Q_{bc} and Q_{bf} . Here only some of the more important results will be mentioned.

The fracture behavior of specimens with notches in repeated tension, $R = 0$, is similar for the three steels although the actual values of Q_{bf} vary. This may be seen from Figs. 104-3-17, 105-4-17 and 106-5-17. Factor

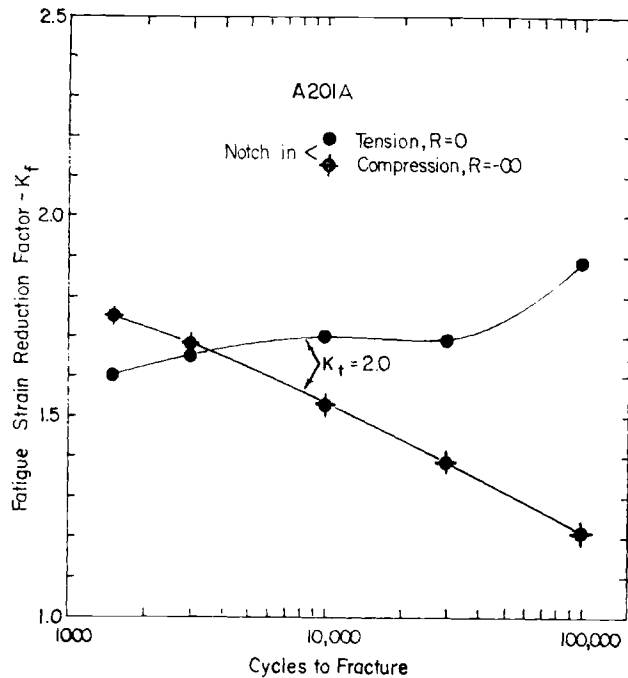


FIG. 104-3-17 – Notched fatigue strain reduction factors for fracture of A201A.

Q_{bf} is low in the low-cycle region, is substantially less than k_t , but rises in the higher cycle region.

Figs. 107-6-17 and 108-7-17 which show factor Q_{bc} for macrocracking shows the same trends as the other figures, but the Q_{bc} values are displaced to levels above k_t for A302B and close to k_t for A517F. The authors suggest that the substantial increase in factor Q_{bc} as compared with factor Q_{bf} be given consideration in component design.

The results of fatigue tests in reversed bending, $R = -1$, are shown for macrocracking and for fracture in Fig. 109-8-17 for steel A302B and in Fig. 110-9-17 for steel A517F. It is seen that factor Q_{bc} exceeds factor Q_{bf} in the whole range of cycles but does not rise in the high-cycle region.

The authors provide a convenient table Fig. 111-T5-17 which summarizes general relationship between factors Q_{bc} , Q_{bf} and "ESCF" k_t for notched specimens, for $R = 0$, $R = -1$, and $R = -\infty$.

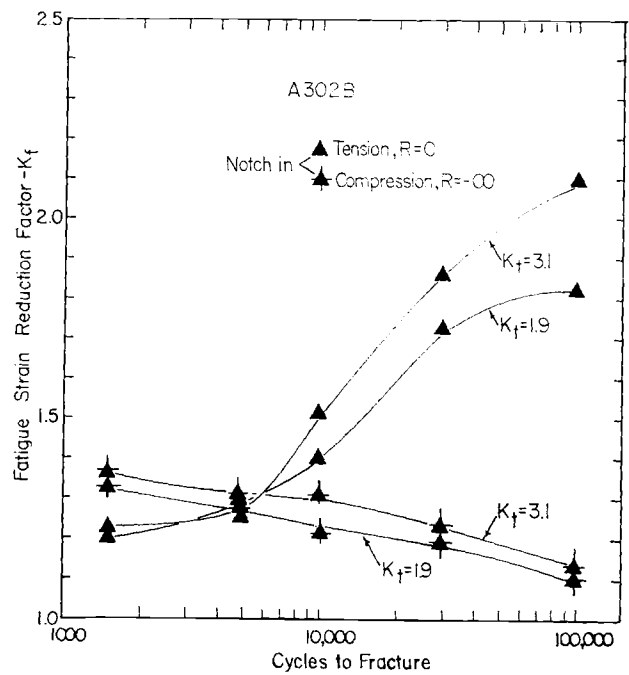


FIG. 105-4-17 – Notched fatigue strain reduction factors for fracture of A302B.

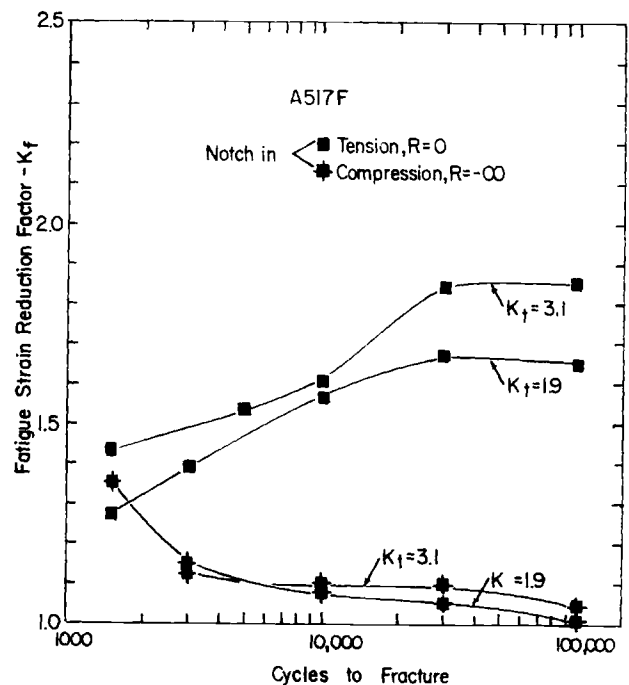


FIG. 106-5-17 – Notched fatigue strain reduction factors for fracture of A517F.

The results of a series of fatigue tests on steel A517F to determine how factors Q_{bc} and Q_{bf} vary with "ESCF" k_t are shown in Figs. 113-11-17 and 113-10-17, respectively. As previously, factor Q_{bc} exceeds factor Q_{bf} in all cases. In approximately the same order, higher values of k_t result in higher values of Q_{bc} and Q_{bf} .

The "FS-th RFF" Q_{bf} for notches in compression is shown in Figs. 104-3-17, 105-4-17 and 106-5-17. The

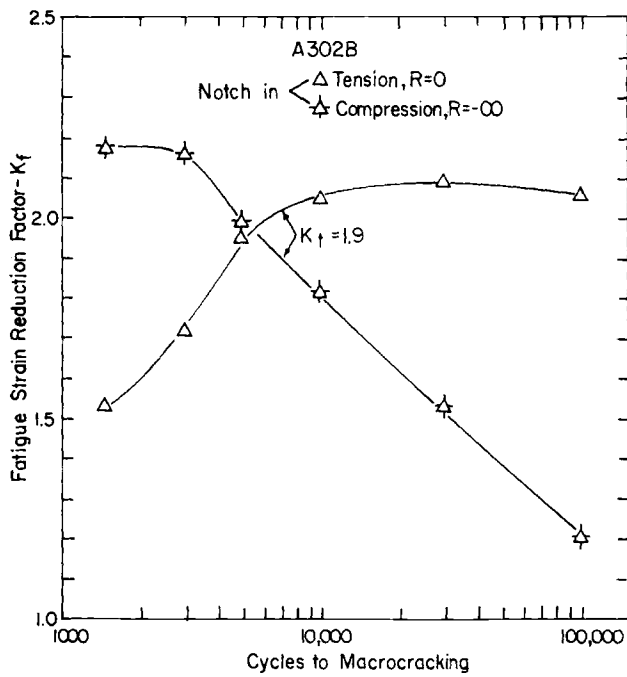


FIG. 107-6-17 – Notched fatigue strain reduction factors for macrocracking of A302B.

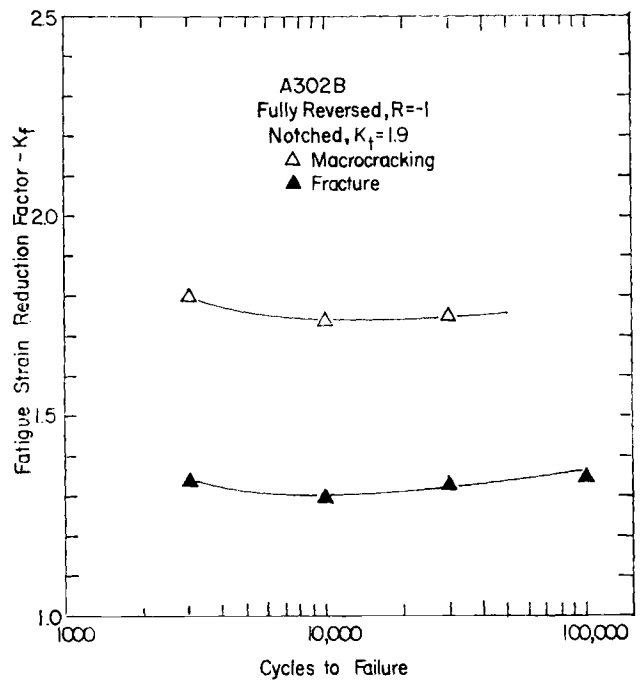


FIG. 109-8-17 – Notched fatigue strain reduction factors for A302B in reversed bending.

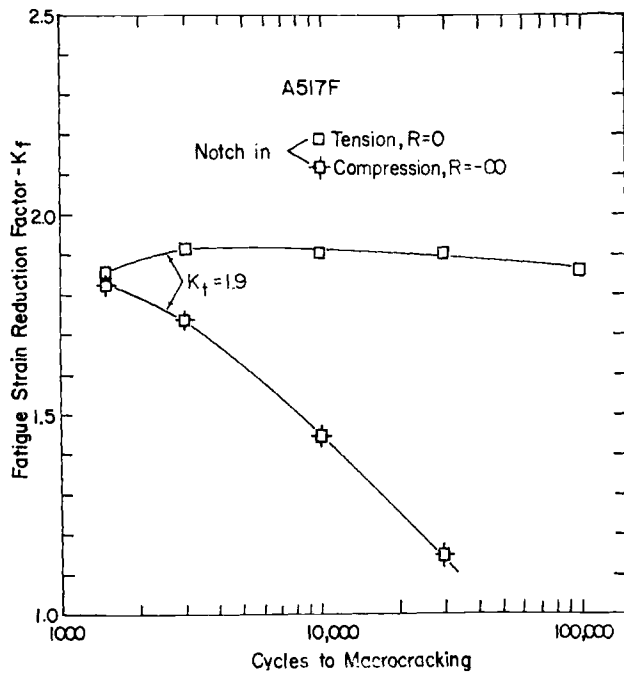


FIG. 108-7-17 – Notched fatigue strain reduction factors for macrocracking of A517F.

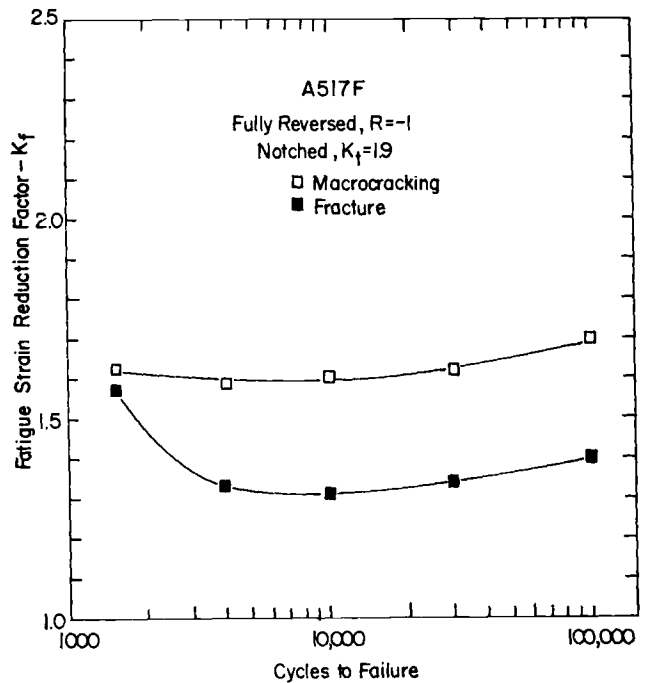


FIG. 110-9-17 – Notched fatigue strain reduction factors for A517F in reversed bending.

Table 5—General Relationship Between K_t and K_f for Notched Specimens

Loading condition	5000 cycle life		100,000 cycle life	
	Macrocracking	Fracture	Macrocracking	Fracture
$R = 0$	$K_f < K_t$	$K_f \ll K_t$	$K_f \cong K_t$	$K_f = K_t$
$R = -1$	$K_f < K_t$	$K_f \ll K_t$	$K_f < K_t$	$K_f \ll K_t$
$R = -\infty$	$K_f \cong K_t$	$K_f \ll K_t$	$K_f \cong 1.0$	$K_f \cong 1.0$

FIG. 111-T5-17

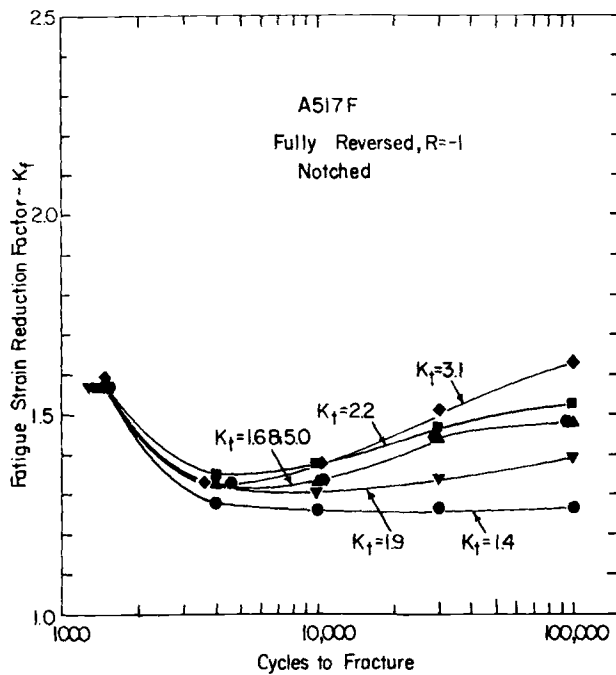


FIG. 112-10-17 - Variation of K_f for fracture with K_t for A517F.

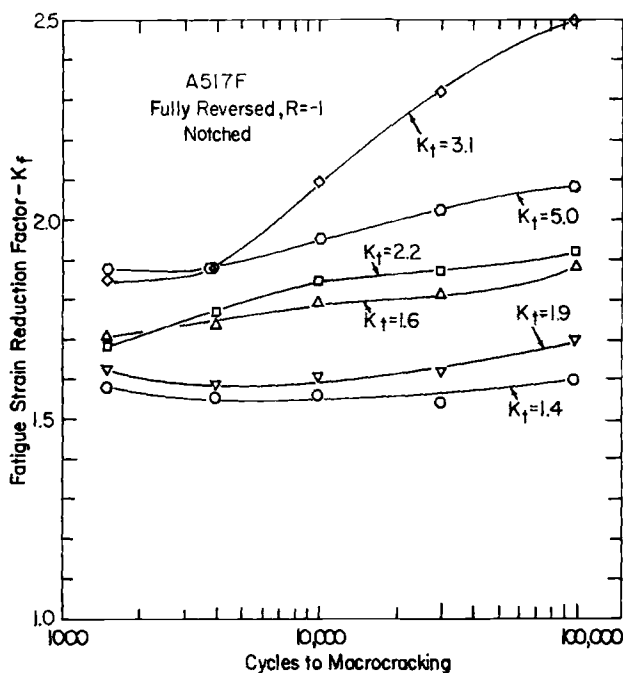


FIG. 113-11-17 - Variation of K_f for macrocracking with K_t for A517F.

fact that a notch in compression can shorten low-cycle fatigue life is an indication that plastic strains present at the root of the notch cause tensile strain to occur. The authors state that, as the nominal strain range is increased, the local plastic strain at the peak of the load cycle will be sufficiently large to produce reversed bending conditions. Therefore, in large strain range tests the compression notch is, in fact, in compression only during the first half of the cycle, and thereafter will be alternately

in tension and compression. Similarly, the tension notch will not be in tension alone after the first half cycle. Therefore, at high strain ranges and short cycle lives the curves for the two loading conditions must approach on another, as observed. For additional informative discussion the reader is referred to the original paper.

Fig. 114-12-17 shows factors Q_{bc} and Q_{bf} for the sharp-edge hole, $k_t = 2.2$, for completely reversed loading,

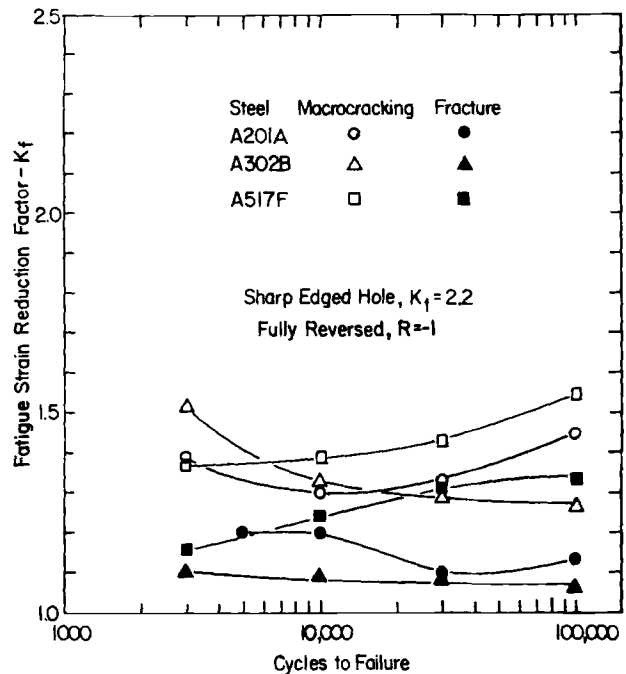


FIG. 114-12-17 - Fatigue strain reduction factors for sharp-edged holes in A201A, A302B, and A517F.

$R = -1$. Typical values of Q_{bf} fall below 1.3 and for Q_{bc} fall below 1.6.

Fig. 115-13-17 shows factors Q_{bc} and Q_{bf} as a function of cyclic life for steel A517F with holes, $k_t = 2.2$, fillets, $k_t = 2.1$, and with notches, $k_t = 2.1$. It seems that the factors Q_{bf} for the notched and filleted specimens have quite similar values. However, factor Q_{bc} for the filleted specimens is well above that for the notched specimens and for the whole cyclic range is close to $k_t = 2.1$, which was measured photoelastically for this configuration. The authors state that this result is in agreement with the generally reported observation that fillets commonly become sites for crack initiation in fatigued components.

The results of this investigation indicate that the "FS-th RFF" Q_{bf} seldom reaches or exceeds "ESCF" k_t in either the high or low-strain regions and, in fact, for a notch in nominal repeated tension it decreases in the low-cycle region. The authors state that the above results do not agree with the results of the current PVRC study with full-scale pressure vessels where factors Q_{bf} were found to be much larger, between 7.1 and 3.4. They point out that the growth of fatigue cracks is independent of the initiating notch, flaw or defect. The growth depends on the material, on the imposed total

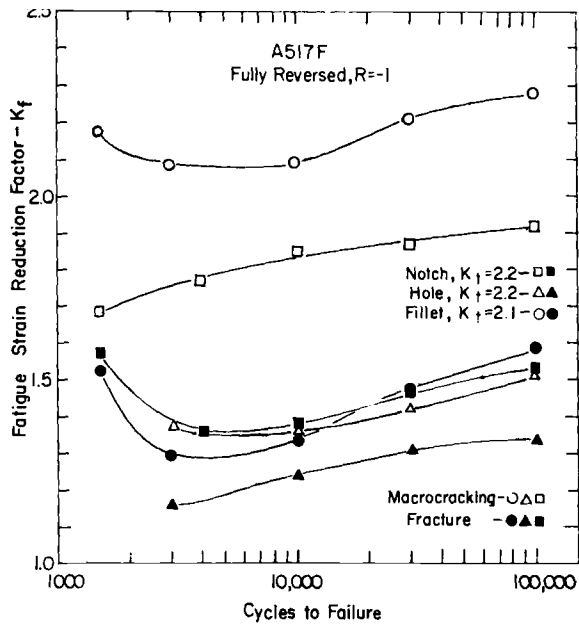


FIG. 115-13-17 – Comparison of K_f for notches, holes and fillets in A517F.

strain range, on the character of loading cycle with repeated tension, $R = 0$, producing the highest propagation rates. Also, at the highest strain ranges the three types of loading cycles ($R = 0, -1, -\infty$) converge, since extensive plastic flow reduces all the tests to the fully reversed type, $R = -1$. This is shown in Fig. 116-14-17 for steel A517F and in Fig. 117-15-17 for steel A302B. In these

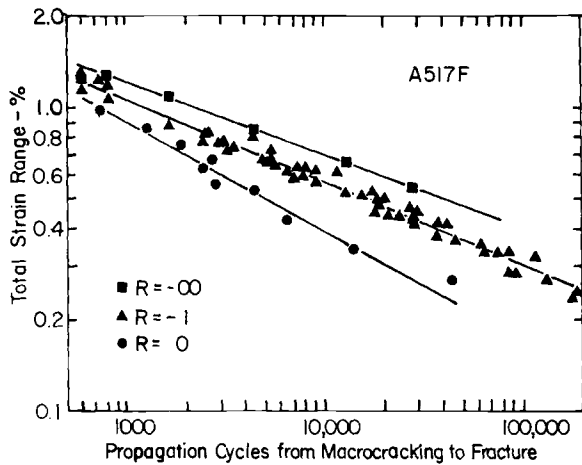


FIG. 116-14-17 – Relationship between strain range and crack propagation cycles for notched specimens of A517F.

figures the nominal total strain range is plotted as a function of propagation cycles from macrocracking to fracture for the three types of loading.

For the three materials, the authors collected all available data defining the number of cycles from macrocracking to fracture for repeated tension loading, $R = 0$. The data were plotted in Fig. 118-16-17 against local macroscopic strain range experienced at or near the

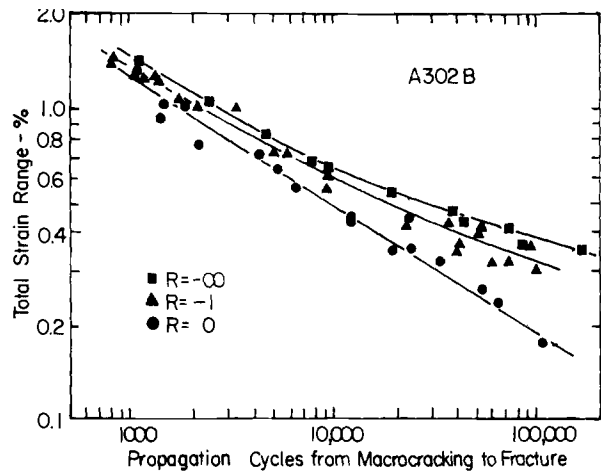


FIG. 117-15-17 – Relationship between strain range and crack propagation cycles for notched specimens of A302B.

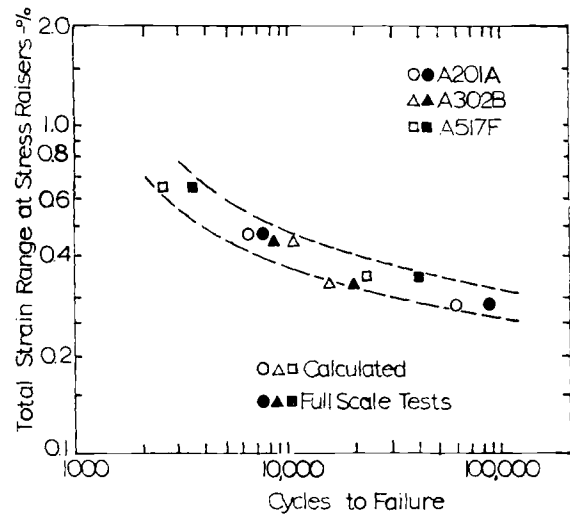


FIG. 118-16-117 – Comparison of measured pressure vessel fatigue life with that calculated from crack propagation in notched tests.

fracture site. In the same figure they have plotted similar data obtained from the full-scale vessel tests. The authors state that the general order of agreement of the two sets of data are close enough to demonstrate that the low-fatigue lives of the full-scale vessels may be attributed to the existence of sharp crack-like flaws that are present even before testing has begun. In other words, it appears, that the causes of the exceptionally high values of “FS-th RFF” Q_{bf} , obtained in the full-scale tests are not macroscopic stress raisers first producing cracks and then propagating them, but are rather macroscopic stress raisers propagating already existing cracks.

The authors conclude that laboratory test data pertaining to crack growth can be used, with further refinement, to predict the behavior of full-scale vessels.

H.2 – Baron, et al, in R. 1 report on “LCF” tests performed at room temperature on a 3% Ni, Cr, Mo grooved plate 1.5 in. wide, 0.286 in. thick, machined from a heat treated forging. The dimensions of the specimen are shown in Fig. 119-1-1. The transverse groove is one inch

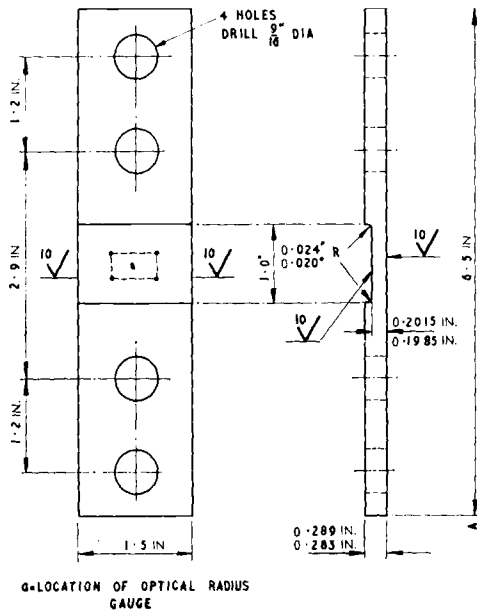


FIG. 119-1-1 – Test specimen with 0.02-in.-radius fillets.

wide, 0.085 in. deep, and the small fillet radii are 0.004, 0.02, and 0.04 in. The corresponding “ESCF” k_t were obtained photo-elastically as 2.8, 2.0 and 1.6, respectively. The largest fillet was produced with a 3 in. radius grinding wheel and k_t was practically equal to 1.0.

The specimens were tested in repeated bending, $R = 0$. The modified Schenck fatigue machine produced a uniform bending moment over central 2 in. of the specimen. The imposed total (elastic + plastic) strains were measured over a 0.3 in. gauge length in the center of the groove. Note that the measured strains are not local strains (near the fillets) and must be considered nominal.

The end point of each test was taken to be the life at which a crack first became visible in one of the fillets when viewed under magnifying glass.

The effect of varying fillet radius, $k_t = 1, 1.6, 2.0$ and 2.6 is shown in Fig. 120-3-1. The fatigue strength reduc-

tion factors to cracking Q_{bc} were derived by dividing the total strain range for a given cyclic life N_c with a 3 in. radius (unnotched) by the nominal, total strain range for the same life with a smaller radius. This calculated factor was tabulated in Fig. 121-T III-1. The table indicates that Q_{bc} tends to decrease with increasing life.

TABLE III

Fillet Radius, in.	Stress-Concentration Factor (k_t)	Effective Strain-Concentration Factor in Fatigue (K_f) for a Life of:		
		3000 cycles	10,000 cycles	30,000 cycles
0.004	2.8	2.6	2.5	2.3
0.02	2.0	2.0	2.0	1.8
0.04	1.6	1.8	1.7	1.6

FIG. 121-T111-1

The authors conclude that in short-life, strain-controlled fatigue the “FS-th RFC” Q_{bc} is practically equal to the “ESCF” k_t . The smallest radius gave the greatest difference between the two. They state that this is rather surprising and they quote some previous work on strain concentrations in support of their conclusion.

H.3. — Coles, et al, in R. 5 describe “LCF” tests at 565°C on 1% Cr, Mo, V steel beams in reversed bending at one cycle per minute. The 0.2 in. deep beams were notched only on one side and the notches were 0.020 in. deep transverse grooves with various root radii which resulted in elastic stress concentration factors $k_t = 2.8, 3.1, 3.6$ and 4.7 shown in the table in Fig. 122-21-5.

The authors point out that a notch in a specimen subjected to plastic strain under bending conditions changes the strain distribution considerably and the notched section tends to act as a plastic hinge. It was not feasible to take account of these local effects and the imposed strain amplitude in Fig. 122-21-5 is the strain measured in an unnotched specimen whose ends were subjected to the same angular deflection. The plotted strains must be regarded as “nominal” and the interpretation of results is accordingly restricted.

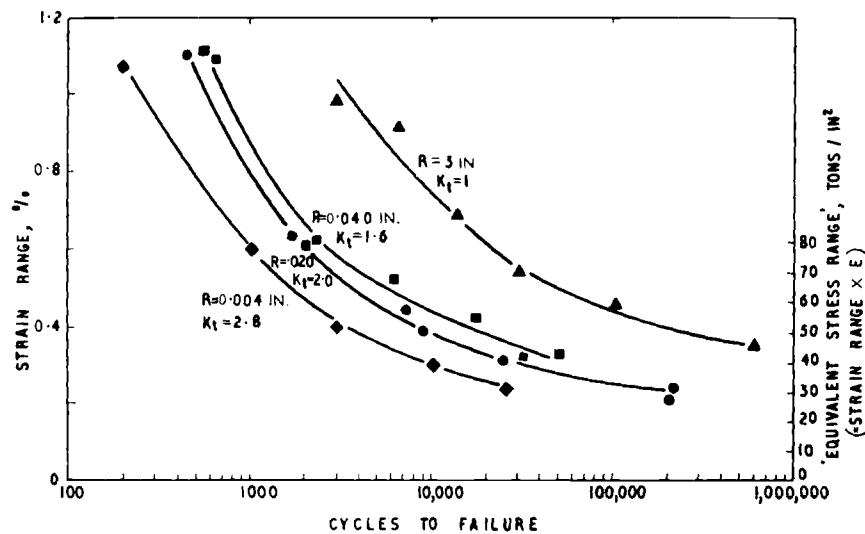


FIG. 120-3-1 – Effect of fillet radius. Specimens machined from the 3% Ni-Cr-Mo steel forging. (Yield strength 47 tons/in.²).

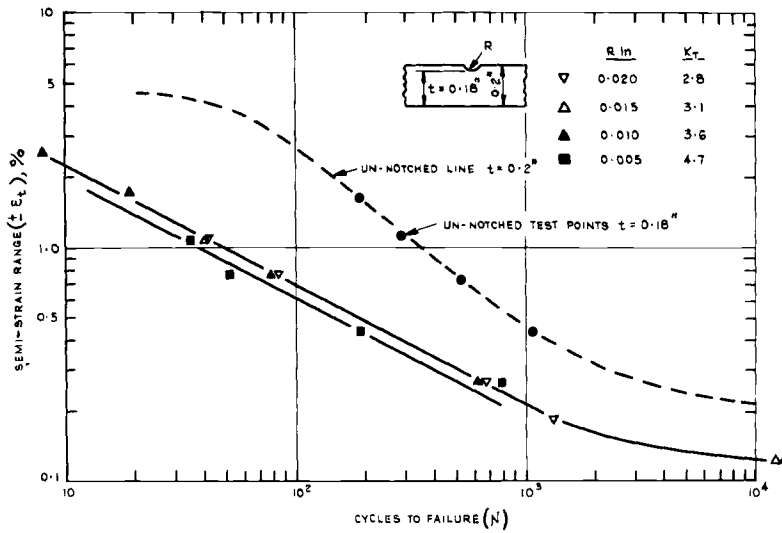


FIG. 122-21-5 – Effect of notches on cycles to failure for 1 c/m continuous-cycling tests on forged 1 Cr–Mo–V Al at 565°C.

The test results are plotted in Fig. 122-21-5 together with comparable results for unnotched specimens. The notches apparently caused substantial reduction in cycles to fracture e.g. from 110 to 8 cycles at $\pm 2.5\%$ strain and from over 20,000 cycles to 900 cycles at $\pm 0.2\%$ strain. Also, the maximum reduction in nominal strain range at fracture occurred at a life of about 100 cycles and nu-

merically exceeds the “ESCF” k_t . Note that variations in root radius had little effect on the resulting strength reduction.

The authors state that the notch effect may be less pronounced in situations where the notch is so small in relation to the component thickness that there is no tendency for a plastic hinge to develop.

SECTION I
MISCELLANEOUS STUDIES ON EFFECT OF
NOTCHES IN LOW-CYCLE FATIGUE

I.1. — Manson, et al, in R. 33 present the results of an exploratory study developed to permit a simple analysis of the fatigue process in hourglass shaped specimens with simple machined notches subjected to uniaxial reversed loading at room temperature. The study is limited to and presents preliminary results for the estimation of crack initiation and propagation to failure for two materials annealed 4340 steel and 7075-T6 aluminum. The investigation was conducted to determine the degree of validity that could be expected when highly simplified assumptions were made with regard to three major facets of the fatigue problem of notch specimens: (a) the determination of the strain at the root of the notch, (b) the number of cycles required to develop a crack of engineering size, and (c) the number of cycles required to propagate the crack of engineering size to complete fracture.

The above was quoted verbatim from the paper.

The crack which defined initiation was taken as a surface crack ranging from 0.006 to 0.010 inch long, which was found experimentally to be about 0.003 in. deep.

The authors state that an approximate analysis has been developed whereby the number of cycles required to start an engineering size crack and the number of cycles required to propagate this crack to failure could be estimated for a notched specimen from a knowledge of the fatigue behavior of unnotched specimens. Reasonably good agreement with experimental results were obtained for the two materials and the two notch configurations tested. Further evaluation with more materials and a wider range of notch geometries is desirable. The effect of cyclic strain hardening or softening on the crack propagation stage also requires further evaluation.

The specimens used had a conventional circular hourglass shape with a minimum diameter of 1/4 in. Slot notches, 0.010 in. deep with radii 0.008 and 0.025 in. were machined into the specimens. The "ESCF" were $k_t = 3$ and 2 respectively. The measured fatigue strength reduction factors for 10^6 cycles were 2.9 and 2.0 for the 4340 steel and 2.9 and 1.7 for the 7075-T6 aluminum.

The authors made an important assumption that the crack will be initiated in a notched specimen in a number of cycles dependent only on Δe , the calculated, local strain range at the root of the notch. The number of cycles to initiate a crack in the notched specimen is assumed to be the same number of cycles required to initiate a crack in an unnotched specimen subjected to the same local strain range. Note that although the above assumption is plausible it may not be generally valid, 3. g. see discussion in Sections F. 1. and F. 4.

In order to calculate Δe , the plastic strain concentration factor "PS-n CF" q_p must be known. The factors

q_p were calculated using two approaches, previously discussed in Sections D and E, the "SHO" and the Neuber approach. This paper contains discussion of the two methods and also a new graphical procedure to determine q_p . It is important to note that cyclic stress-strain diagrams, see Section C, were used instead of monotonic diagrams. The local strain range in the notch root is $\Delta e = \bar{\Delta e} \cdot q_p$.

The authors assume that for a notched specimen the crack propagation period for a given strain range depends to a first approximation on the applied strain range only and not on the strain-concentration factor imposed; the crack propagates under a strain-concentration essentially unrelated to the strain concentration that caused it to form. This strain concentration which controls propagation depends largely on the crack itself and not on the geometric conditions existing prior to the development of the crack.

The authors point out that even though the higher stress concentration factors have a considerable effect in reducing the crack initiation periods, the crack initiation period for notched specimens is generally a relatively small part of the total life. Thus, only to a minor extent does the sum of the two components, initiation and propagation, reflect the differences introduced by the higher nominal stress concentration. This observation is in agreement with the general experimental finding that increasing the nominal stress concentration factor for a notch does not produce a correspondingly large decrease in fatigue life in the low cycle range. In fact, as the nominal stress concentration factor is increased, a value is reached beyond which further decrease in total life is negligible. The above was quoted verbatim.

There are many curves presented in this informative paper and for further details and discussion the reader is referred to the original paper. Appendix B is a sample calculation for an annealed 4340 steel-notched specimen with $k_t = 2$ and imposed nominal axial strain range of 0.008 in. per in.

Also for further discussion of propagation of cracks in notched specimens the reader is referred to Section 1.2. and to Price, et al, R. 59.

I.2. — Dawson, et al, in R. 9 report on push-pull "LCF" tests at elevated temperature (600°C) on notched cylindrical specimens, 0.2 in. dia., of type 316 steel. The notches were machined from one side at a tangent to the specimen circumference. The notched depth quoted is the maximum depth. The details of each notch and the associated "ESCF" are shown in Fig. 123-T11-9. The authors state that this type of notch was chosen to minimize the increase in the nominal stress as compared with a plain specimen, so that a given cross-head displacement

TABLE II.—Details of Notched Specimens

Notch Depth, in.	Elastic Stress-Concentration Factor for Different Root Radii (ρ), in.			Notch Angle (θ)
	$\rho=0.002$	$\rho=0.003$	$\rho=0.004$	
0.001	2.4	2.1	1.8	} 30°
0.002	2.6	2.3	2.2	
0.004	3.1	2.6	2.5	
0.008	3.75	3.2	2.9	
0.016	4.2	3.7	3.2	
0.004	1.8	—	—	} 90°
0.008	2.6	—	—	

FIG. 123-T11-9

might be considered to give the same nominal strain.

The data were obtained at two nominal strain ranges away from the notch, $\pm 0.325\%$ and $\pm 1.26\%$. The cycles to fracture are shown in Fig. 124-10-9 as a function of notch depth for four different notches including variations in root radii and in the notch included angle. In addition, data for unnotched specimens at the same

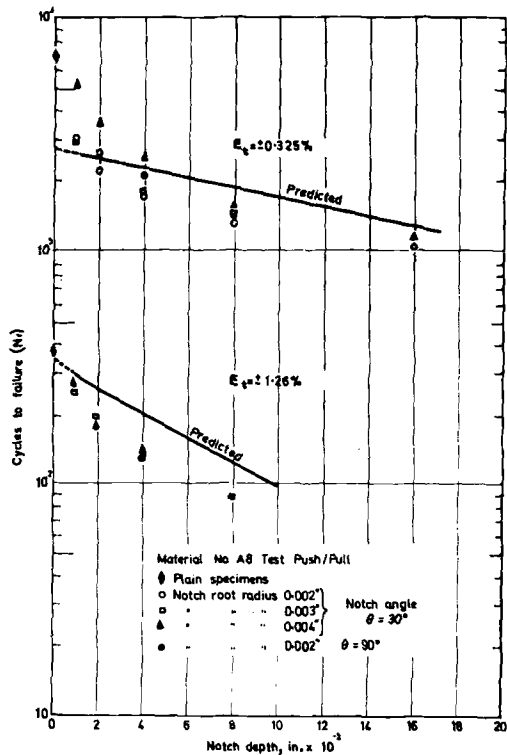


FIG. 124-10-9 – Effect of notch depth and form on endurance of Type-316 steel.

nominal strains are included. It is seen that increasing the notch depth and reducing the root radius lowers the cycles to fracture.

The authors state that when the strain at the notch root is large, e. g. $\pm 1.26\%$, nominal imposed strain, the cyclic life is relatively unaffected by root radius. Also, at the lower imposed strain, for notch depth less than

0.006 in., an increase in the notch-root radius raises cyclic life even to the extent that a specimen fracturing in 5000 cycles required 50% of its life to initiate a crack.

Fractographic examination showed that with one exception the initial stage of cracking was absent so that the cyclic life of the notched specimens were determined by crack propagation alone. This later concept did not predict the lives of the notched specimens too well, the actual life usually being less than predicted. For additional discussion of the above concept see the original paper and also Price, et al, in R. 59.

I.3. – Peterson in R. 40 discusses elasto-plastic relations in notches and the “PS-n CF” q_p which is derived by the “SHO” method. Fig. 40-24-40 is interesting. It shows q_p as a function of nominal stress. Note that q_p exhibits a maximum when the nominal stress reaches the yield stress.

Peterson developed an analytical method for estimating the life of notched members in the finite life region. This method is discussed by the author in the Appendix to R. 40. It uses an analytical expression for the cyclic stress-strain diagram and an iterative procedure for the determination of “PSCF” q_p and is based on the “SHO” method.

It appears that the suggestion use the “cyclic stress-strain diagram” instead of the “monotonic” for the determination of q_p was first made by Peterson in this paper.

The results of applying this method to notched members of normalized SAE 4130 steel tested at room temperature are shown in Fig. 125-26-40. For the details of this rather complex figure and for the analytical method developed by Peterson the reader is referred to the original paper.

To help the designer, Peterson prepared a chart for the SAE 4130 steel based on results of his analytical method. This chart is shown in Fig. 126-29-40. The factors k_f refer to any notch geometry that has the specified k_f value at the endurance end of fatigue life. In Fig. 127-30-40 the same curves are shown in dimensionless form, together with similar curves for two other widely different steels.

I.4. – Peterson in R. 41 continues the analysis of the effect of notches which he discussed in R. 40. He added Fig. 128-6-41 which shows the ratio

$$\frac{\text{Plastic Strain Conc. Factor } q_p}{\text{Fatigue Strength Reduction Factor } k_f}$$

for three steels as a function of cyclic life with elastic stress concentration factor as a parameter. He points out that the maximum value of the ratio $\frac{q_p}{k_f}$ is about

2 in the low-cycle life range and 1 in the high-cycle, endurance range. The author does not explain sufficiently clear how the above seven curves were derived.

Peterson suggests that until further work is carried out the curves shown in this figure be used for design purposes. The reviewer assumes that the curves are for room temperature and that cyclic stress diagrams were used for their determination.

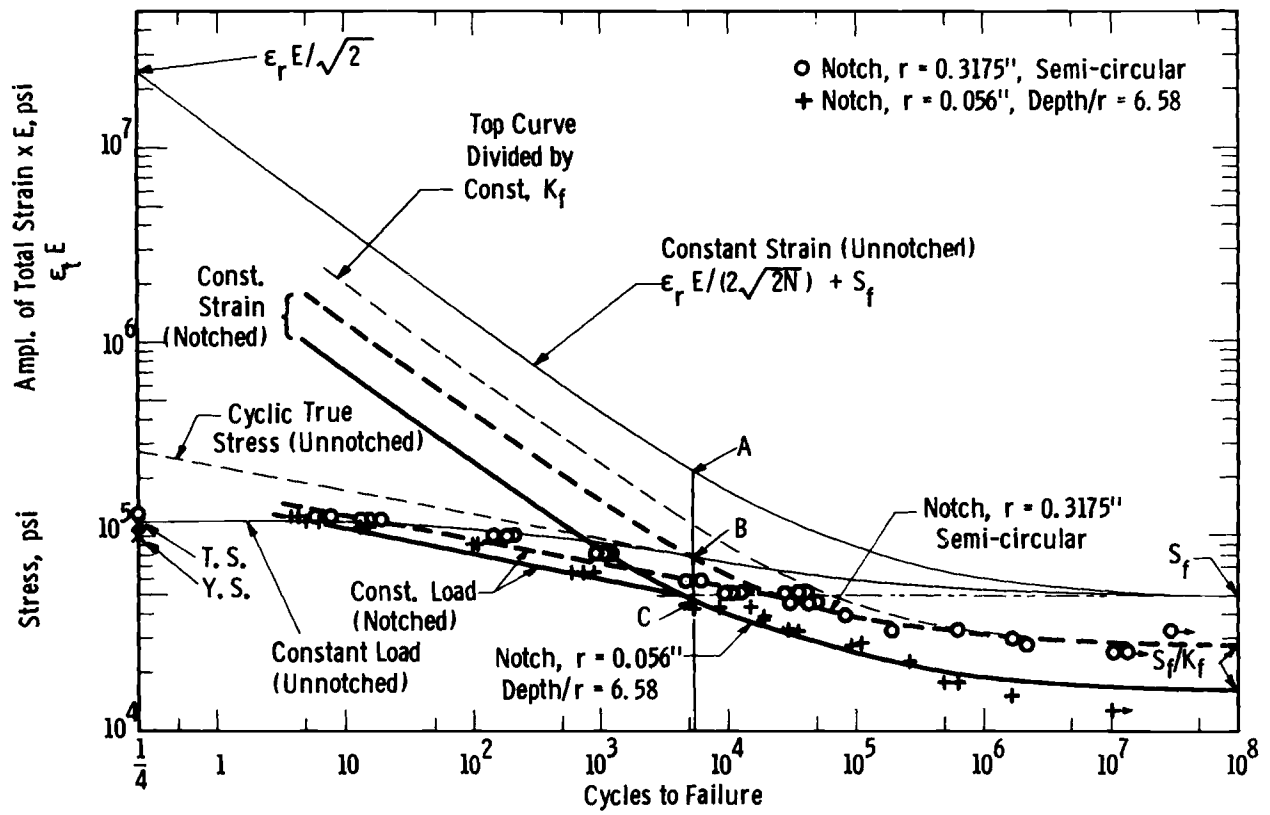


FIG. 125-26-40 – Application of analytical method to notched specimen of SAE 4130 normalized steel—alternating axial load (data from Illg (13), see also Fig. 9).

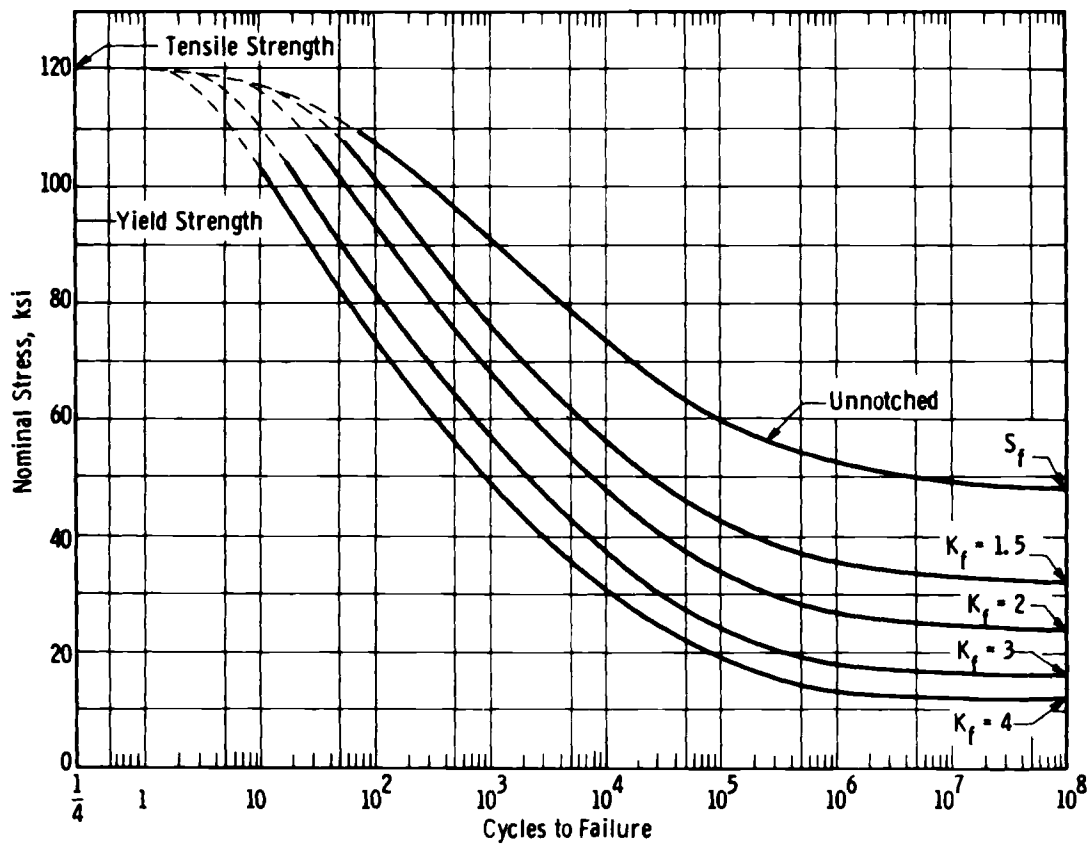


FIG. 126-29-40 – Design chart for SAE 4130 normalized steel; axial loading; zero mean load.

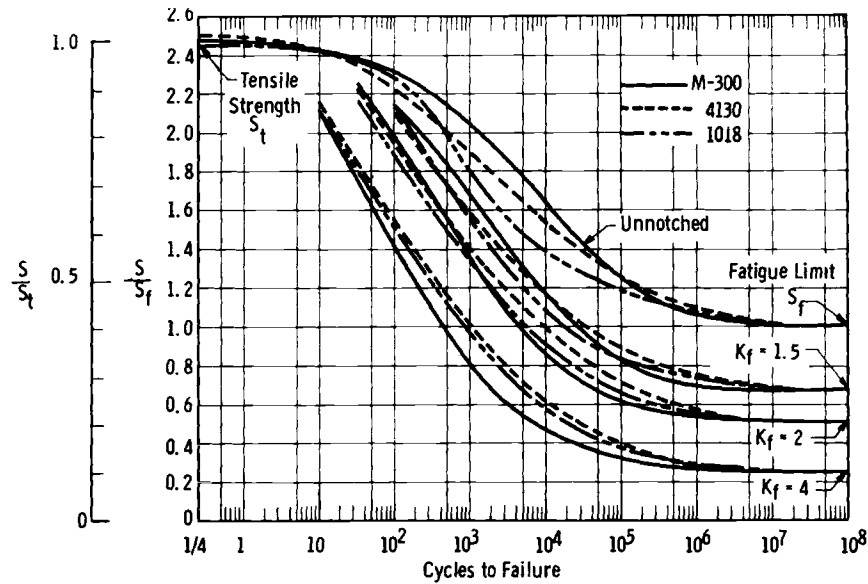


FIG. 127-30-40 – Comparison of design curves for three steels; axial loading; zero mean load.

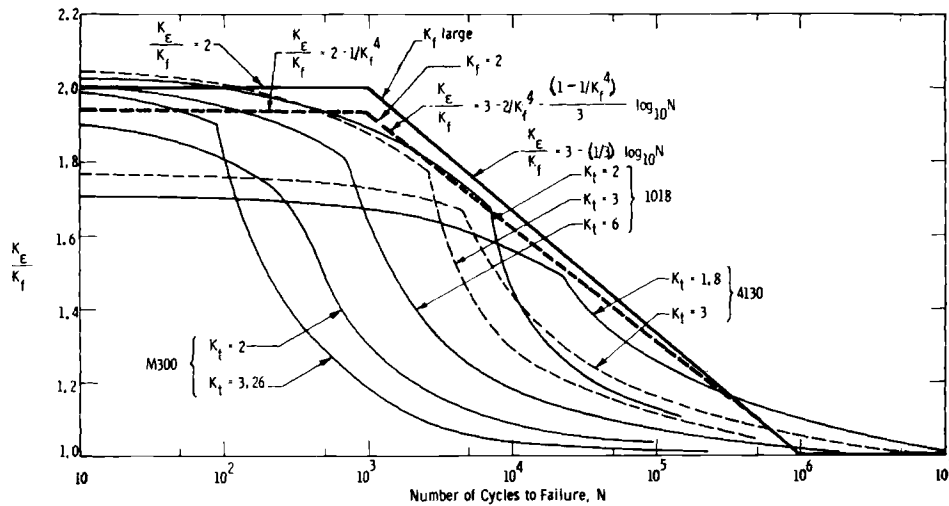


FIG. 128-6-41 – Variation of strain concentration factor as a function of the number of cycles to development of small crack.

The last short chapter pertains to crack propagation in a low carbon steel plate.

I.5 – Picket, et al, in R. 42 are concerned with “LCF” life of pressure vessels. The authors have proposed a method for predicting the “LCF” life of full-size pressure vessels based on tests performed at the Southwest Research Institute and other laboratories. The method separates crack initiation from crack propagation and uses the “SHO” approach for the determination of localized strain. Because this is an elaborate paper which requires a great deal of attention, it will not be reviewed here and the reader is referred to the original paper for particulars of the analysis.

I.6 – Manson et al in R. 33, see I.1 describe a notch configuration which was used for experimental investigations of notched specimens in Low-Cycle Fatigue. The specimen had a conventional circular hourglass shape. In the minimum section there are two tangentially located (slanted) notches placed symmetrically on opposite ends of the same diameter. See Fig. 132-3-33. The controlling nominal Total Strain Range is measured across a diameter on the surface of the minimum section which was not notched. Similar, but very shallow and sharp notches were described by R. A. T. Dawson et al in R. 9, see I.2.

SECTION J PROPOSED FUTURE WORK

J.1. — Langer in R. 31 states that unwarranted conclusions are too often drawn from inadequately analyzed "LCF" tests of notched specimens. See discussion in section F. 5. He hypothesizes that a set of five significant parameters determine the number of cycles required to initiate and to propagate a crack in an *unnotched* specimen. They are: 1) Total strain range, 2) Prestrain or cumulative value of monotonically increasing strain, 3) Mean stress. After the crack has initiated its rate of growth is determined by 4) Range of fluctuation of stress intensity factor K_I . 5) Mean value of K_I during the cycle. The author presents justifications for the choice of the above five parameters.

For notched specimens the fatigue process is to be studied in two phases, crack initiation and crack growth. The initiation is determined by the local strain range, by the mean local strain and by the mean stress in the notch apex.

Detailed elasto-plastic analysis considering strain hardening, loading, unloading and re-loading is feasible at the notch root. The analysis must be carried for a number of cycles to determine whether or not shakedown occurs. If it does not occur, the rate of monotonic strain increase must be determined. When the analysis has been completed the cycles to crack initiation can be determined by reference to available fatigue data for unnotched specimens. In the reviewer's opinion the equivalence of local strain range in the notch and in an unnotched specimen in respect to cyclic life is a tacit assumption. For instance, R. 26, 23 and 19 indicate that the above assumption may not be justified. After the crack has initiated, its rate of growth is determined by the stress intensity factor K_I .

Langer proposes to check the validity of the hypotheses by a series of tests on a notched specimen shown in Fig. 129-2-31. This is a compact tension specimen used in fracture mechanics for crack-growth studies. The notch radius can be varied to result in a series of elastic concentration factors K_t . Also, the slot width t should be large enough to prevent closing at the largest compressive load. Langer states that the primary object of the tests is to determine whether local strain range, mean strain and mean stress control crack initiation in notched specimens in accordance with the same quantitative rules as they do for unnotched specimens. If this correlation could be firmly established, practical predictions of crack initiation could be made from analysis and unnotched fatigue data.

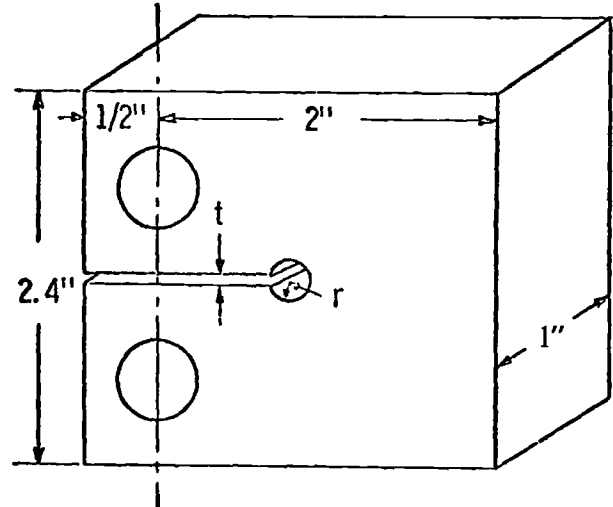


FIG. 129-2-31 — Compact tension specimen modified for crack initiation tests.

He suggests as a first step to investigate two steels, T-1 and Type 304 stainless, with a low and a high strain hardening exponent, respectively. Load cycle $R = 0$. One series with controlled load, the other with controlled amplitude. Load levels, one estimated to crack in 1000 cycles, the other to crack at about 20,000 cycles. Two "ESCF", $k_t = 1.5$ and 10.

The author states his proposal accentuates the crack initiation studies because this subject is not being given enough attention, while work is already in progress on crack propagation. He suggests that the specimen width be investigated in order to define which of the two conditions, wide or thin, is more conservative for crack initiation.

Langer also reviews the results of LCF tests described in R. 19, R. 23 and R. 17 and comes to the conclusion that the derived several fatigue strength reduction factors cannot be compared because of widely different test procedures. However, he suggests that for practical strain-controlled conditions such as occur when the source of cyclic loading is differential thermal expansion, the tests described in R. 17 give the most realistic picture. See also Section F. 6.

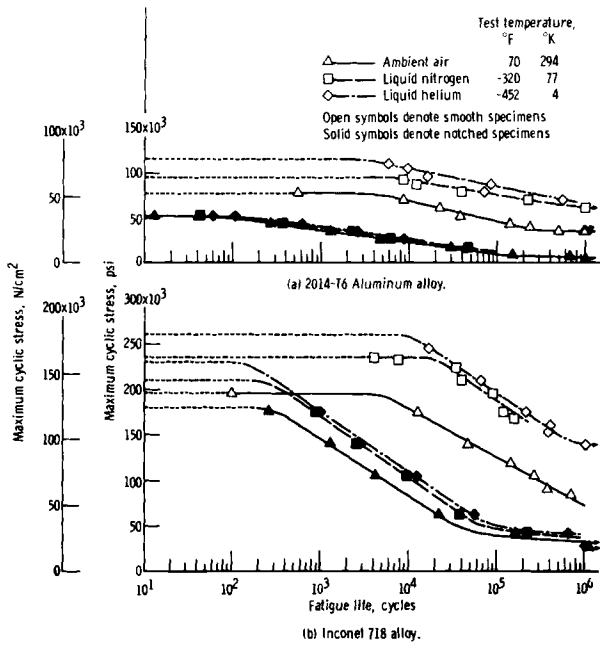


FIG. 130-4ab-37 – Comparison of fatigue curves for smooth and notched specimens at three temperatures. $R = 0.14$.

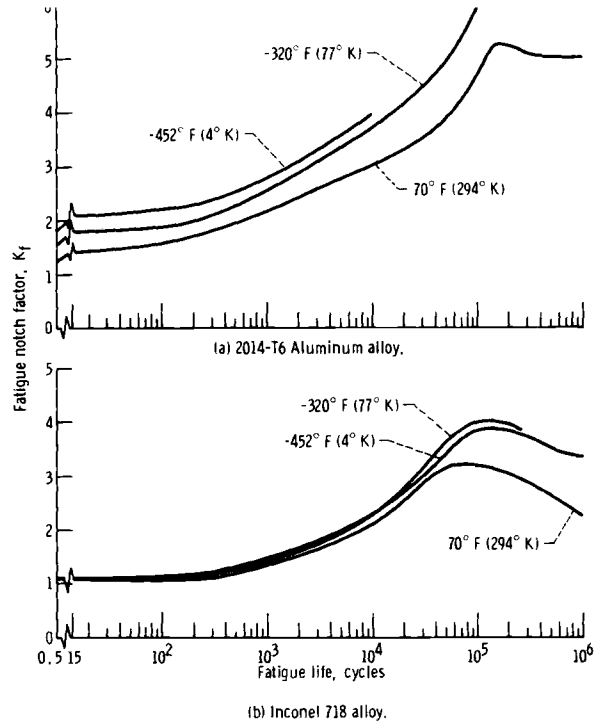


FIG. 131-6-37 – Variation of fatigue notch factor with testing temperature and fatigue life. $R = 0.14$.

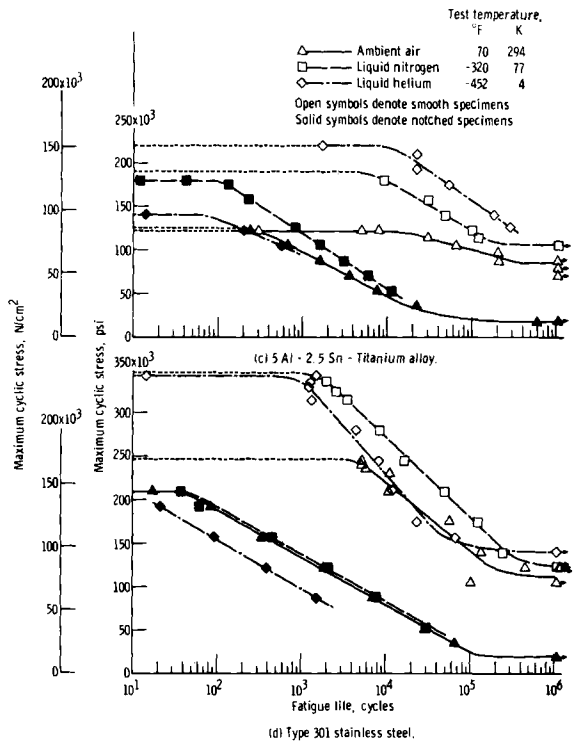


FIG. 130-4cd-37 – Figure 130 continued.

Material	Radius, R, in.	Calculated elastic-stress concentration factor, K_e	Measured fatigue notch factor, K_f
7075 T6 aluminum	0.008	3	2.9
7075 T6 aluminum	.025	2	1.7
4340 steel (annealed)	.008	3	2.9
4340 steel (annealed)	.025	2	2.0

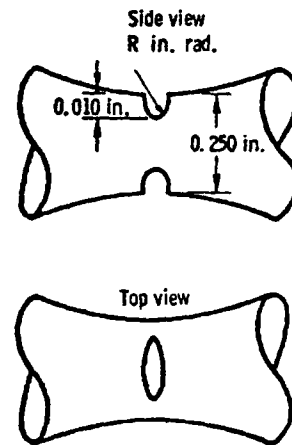


FIG. 132-3-33 – Test section of notched fatigue specimen.

**SECTION K
REFERENCES**

1. BARON, H. G. and BRINE, F. E., "A Note on Low-Endurance Fatigue at Regions of Stress Concentration". Ref. 58. pp 113-121
2. BELL, W. J. and BENHAM, P. P., "The Effect of Mean Stress on The Fatigue of Plain and Notched Stainless Steel Sheet in the Range from 10 to 10⁷ Cycles". ASTM. STP #338, 1963. pp 25-46
3. BERLING, J. T. and SLOT, T., "Effect of Temperature and Strain Rate on Low-Cycle Fatigue Resistance of AISI 304, 316 and 348 Stainless Steels", *Fatigue at High Temperature, ASTM, STP 459*, 1969. pp. 3-30
4. BLATHERWICK, A. A., and OLSON, B. K., "Stress Redistribution in Notched Specimens During Fatigue Cycling", *Experimental Mechanics*, Vol. 8, Aug. 1968, pp. 356-361
5. COLES, A., et al, "The High-Strain Fatigue Properties of Low-Alloy Creep-Resisting Steels" Ref. 58. pp 270-294
6. CREWS, J. H., Jr. and HARDRATH, H. F., "A Study of Cyclic Plastic Stresses at a Notch Root". *Experimental Mechanics*, June 1966 pp 313-320
- Also CREWS, J. H., Jr., "Local Plastic Stresses In Sheet Aluminum Alloy Specimens With Stress-Concent. Factor of 2 Under Constant Amplitude Loading" NASA TN D-3125, Dec. 1965 22 pg.
7. CREWS, JOHN H. JR., "Elastoplastic Stress-Strain Behavior at Notch Roots in Sheet Specimens Under Constant-Amplitude Loading", NASA TN D-5253, June 1969 33 pp
8. DAWSON, R. A. T., et al, "Factors To Be Considered in The Design and Operation of Turbines to Prevent Failure by Thermal Fatigue", Ref. 58. pp 40-54
9. DAWSON, R. A. T., et al, "High-Strain Fatigue of Austenitic Steels". Ref. 58. pp 239-269.
10. FORREST, P. G., "The Use of Strain Cycling Tests For Assessing Thermal Fatigue Resistance" *Applied Materials Research*, Oct. 1963 pp 239-246
11. FELTNER, C. E., and LANDGRAF, R. W., "Selecting Materials to Resist Low-Cycle Fatigue". Paper presented at the ASME Design Engineering Conference, New York, N. Y. May 5-8, 1969. Paper ASME 69-DE-59.
12. GRIFFITH, G. E., "Experimental Investigation of the Effects of Plastic Flow in a Tension Panel With a Circular Hole". NACA TN 1705, 1948
13. GROSS, M. R., "Low Cycle Fatigue of Materials for Submarine Construction". *Naval Engineering Journal*, Oct. 1963. pp 783-797
14. HARDRATH, H. F., and OHMAN, L., "A Study of Elastic and Plastic Stress Concentration Factors Due to Notches and Fillets in Flat Plates". NASA Report 1117, 1953.
15. HARDRATH, H. F., and ILLG, W., "Fatigue Tests at Stresses Producing Failure in 2 to 10,000 Cycles. 24S-T3 and 75S-T6 Aluminum-Alloy Sheet Specimens With a Theoretical Stress-Concentration Factor of 4.0". NASA TN 3132 Jan. 1954. 14 pp
16. HAYDL, H. M., "Stress and Strain Concentration in The Plastic Range With Application to Low-Cycle Fatigue". Presented at the Fall Meeting of the Society for Experimental Stress Analysis, San Francisco, Cal. Oct. 28-Nov. 1, 1968
17. HICKERSON, J. P. and PENSE, A. W., and STOUT, R. D., "The Influence of Notches on The Fatigue Resistance of Pressure Vessel Steels" *Welding Journal*, Welding Research Supplement, February 1968 pp 63S-71S
18. IBRAHIM, S. M. and MC CALLION, H. and DUDLEY, B. R., "Elastic-Plastic Deformation Around A Circular Hole In A Plate Under Cyclic Loading". Institute of Mechanical Engineers - Proceedings, 1965-1966 Vol. 180 Pt. 3I 10 pp
19. IIDA, K., "Fatigue Strength Reduction Factor In Plastic Strain Cycling". Internat. Institute of Welding, Document XIII-427-66
20. ILLG, W., "Fatigue Tests on Notched and Un-notched Sheet Specimens of 2024-T3 and 7075-T6 Aluminum Alloys and SAE 4130 Steel With Special Consideration of The Life Range From 2 to 10,000 Cycles". NASA TN-3866 Dec. 1956 39 pp
21. ISBERG, L. J., and WOZNEY, G. P., "Mechanical and Thermal Low Cycle Fatigue Tests of Grooved Cylinders". General Electric Co., Large Steam Turbine Dept., Schenectady, N. Y. Report. November 25, 1964.
22. KOOISTRA, L. F., and LANGE, E. A., and PICKETT, A. G., "Full Size Pressure Vessel Testing and Its Application to Design". Transactions ASME. Journal of Engineering for Power. Oct. 1964, No. 4 pp 419-428
23. KREMPL, E., "Low Cycle Fatigue Strength Reduction In Notched Flat Plates". Trans. ASME. Paper 67-MET-13 11 pp
24. KREMPL, E., "The Influence of Prior Plastic

- Strain Cycles on the Stress-Strain and Tensile Properties of Three Piping Materials at Room Temperature". Report issued by General Electric Co. Atomic Power Dept. GEAP 5474, Appendix B, San Jose, Cal. - Sept. 1968
25. KREMPL, E., "Determination of Smooth Bar Data" (6. 3. 1) Report issued by General Electric Co. Atomic Power Dept. GEAP 5082, San Jose, Cal. - Jan. 1966
 26. KREMPL, E., "The Influence of Stress-Strain Concentration and Mean Stress on The Low-Cycle Fatigue Behavior of Three Structural Steels at Room Temperature". Report issued by the General Electric Co. Atomic Power Dept. GEAP 5726, San Jose, Cal. - Sept. 1968
 27. KREMPL, E., "Notched High-Strain Fatigue Behavior of Three Low-Strength Structural Steels". Submitted for presentation at the ASME Pressure Vessel Meeting, Delft, Holland, Sept. 1969. Also, report issued by the General Electric Co. Atomic Power Department GEAP-5714.
 28. KREMPL, E., "Memorandum - Fatigue Strength Reduction Factors". General Electric Co. Memorandum, Nov. 1968 - Personal Communication.
 29. KREMPL, E., "Remarks concerning the Westinghouse Report WAPD-T-2093 by A. L. Snow, B. F. Langer, W. G. Gibbons (See 4-29)". General Electric Co. Memorandum, July 1968 - Personal Communication.
 30. LANDGRAF, R. W., and MORROW, JO DEAN, and ENDO, T., "Determination of The Cyclic Stress-Strain Curve". *Journal of Materials*, Vol. 4, No. 1, March 1969 pp 176-188
 31. LANGER, B. F., "Proposed Research on Low-Cycle Fatigue of Notched Members". Westinghouse Electric Co. Research Memo 67-IDO-Codes-M1. Oct. 31, 1967 11 pp
 32. MANSON, S. S., "Thermal Stresses and Low-Cycle Fatigue". Book. McGraw-Hill 1966 435 pp pp 180-182
 33. MANSON, S. S., and HIRSCHBERG, M. H., "Low-Cycle Fatigue of Notched Specimens by Consideration of Crack Initiation and Propagation". NASA TN D-3146, June 1967. 27 pp. Replaces NASA TMX-52126 and paper presented at the "International Conference on Fracture", Sendai, Japan Sept. 1965
 34. MANSON, S. S., and HIRSCHBERG, M. H., "Fatigue Behavior in Strain Cycling in The Low and Intermediate-Cycle Range". In book: "Fatigue. An Interdisciplinary Approach", Syracuse Univ. Press, N. Y. 1964 pp 133-178
 35. MANSON, S. S., "Fatigue: A Complex Subject. Some Simple Approximations". *Experimental Mechanics*, Vol. 5 #7, July 1965 pp 193-226
 36. MOWBRAY, D. F. and SLOT, T., "Note on Stress and Strain Distribution In A Notched Plate Specimen During Cyclic Loading". Transactions, ASME, Vol. 91, Series D, *Journal of Basic Engineering*, Sept. 1969, pp 379-382
 37. NACHTIGALL, A. J., and KLIMA, S. J. and FRECHE, J. C., "Fatigue Behavior of Rocket Engine Materials at -452°F", *Journal of Materials*, Vol. 3, #2, June 1968 pp 425-443
 38. NEUBER, H., "Theory of Stress Concentration for Shear-Strained Prismatical Bodies With Arbitrary Nonlinear Stress-Strain Law". Transactions, ASME, *Journal of Applied Mechanics*, Dec. 1961 pp 544-550
 39. NEUBER, H., "Stress Concentration in Strength Calculations". *Konstruktion*, 1968 #7, in German. pp 245-251
 40. PETERSON, R. E., "Fatigue of Metals in Engineering and Design". ASTM. Edgar Marburg Lecture, 1962. Also, *Materials Research Standards*, Vol. 3, No. 21, Feb. 1963. pp 122-139
 41. PETERSON, R. E., "Design Relations for The Low-Cycle Notch Effect and A Chart of Conditions for Crack Propagation". In book, "Mechanics of The Solid State". Edited by F. P. J. Rimrott and J. Schwaighoffer. Univ. of Toronto Press 1968. pp 146-153
 42. PICKETT, A. G., and GRIGORY, S. C., "Prediction of the Low-Cycle Fatigue Life of Pressure Vessels". ASME Transactions, Paper 67-MET-3 *Journal of Basic Engineering*, Dec. 1967 pp 858-870
 43. PIAN, T. H., and D'AMATO, R., "Low-Cycle Fatigue of Notched and Unnotched Specimens of 2024 Aluminum Alloy Under Axial Loading" WADC TN-5827. Also, ASTIA AD 142307, Feb. 1958.
 44. SARNEY, G. W., "Stress-Strain Concentration Factors in Plastic Flow". Report DF-65-LS-41. June 2, 1965, General Electric Co., Large Steam-Turbine Dept., Schenectady, N. Y.
 45. SNOW, A. L., and LANGER, B. F., and GIBBONS, W. G., "Low-Cycle Fatigue Strength of Notched Ni-Cr-Fe Alloy 600 and Low Alloy Steel". *Journal of Materials*, JML SA, Vol. 5, No. 3, Sept. 1970 pp 719-737
 46. STOWELL, E. Z., "Stress and Strain Concentration At A Circular Hole In An Infinite Plate". NACA TN-2073. Feb. 1950.
 47. STOWELL, E. Z., "The Calculation of Fatigue Life In The Presence of Stress Concentrations". *Nuclear Engineering and Design*, 1968 pp 313-316
 48. TAGART, S. W., "Plastic Fatigue Analysis of Pressure Components". Transactions, ASME. Paper 68-PVP-3 17 pp
 49. TOPPER, T. H., and WETZEL, R. M., and MORROW, JO DEAN, "Neuber's Rule Applied to

- Fatigue of Notched Specimens". *Journal of Materials*, Vol. 4, No. 1, March 1969 pp 200-209
50. TUBA, I. S., "An Analytic Method For Elastic-Plastic Solutions". *International Journal of Solids and Structures*, 1967 Vol. 3 pp 543-564
 51. WELLINGER, K., and GASSMAN, H., and LUTHE, J., "Attending Plastic Deformation and Strain Concentration Factor". *V. D. I. Berichte* No. 129, 1968. 6 pages. In German.
 52. WELLINGER, K., and LUFT, G., "Tensile Tests Under Pulsating Load on Notched Specimens in The Low-Cycle Fatigue Range". Periodical: *Mitteilungen Der V. G. B.*, June 1968. In German. pp 210-215
English Translation: *British Iron and Steel Institute* Translation Service BISI 6695.
 53. WELLINGER, K., and LIEBRICH, M., "Notch Sensitivity of Steels In The Low-Cycle Fatigue Region". *Konstruktion* Vol. 20, No. 3, 1968. In German. pp 81-89
 54. WETZEL, R. M., "Smooth Specimen Simulation of Fatigue Behavior of Notches". *Journal of Materials*, Vol. 3, No. 3, Sept. 1968 pp 646-657
 55. WUNDT, B. M., "Bibliography on Low-Cycle Fatigue 1957-1968. Part 1". Compiled for the Metal Properties Council, Oct. 1968. Published by ASTM STP 449.
 56. YOUNGER, D. G., "Cyclic Plasticity and Fatigue At Stress Concentrations". Presented at 1968 SESA Spring Meeting. Albany, N. Y. May 1968.
 57. ZWICKY, E. E., JR., "Cyclic Plastic Strain Concentration Factors". *Transactions ASME*. Paper 67-WA/PVP-6 8 pp
 58. BOOK, "Thermal and High-Strain Fatigue". International Conference, Institute of Metals and Iron and Steel Institute, London, June 1967. Published by The Metals and Metallurgy Trust Monograph and Report Series, No. 32, 1967. pp 435
 59. PRICE, A. T., and ELDER, W. J., "High Strain Fatigue and Crack Propagation in Type 316 Steel". *Journal of The Iron and Steel Institute*, June 1958. pp 594-598
 60. BOWLES, C. Q., "Strain Distribution and Deformation at the Crack Tip in Low-Cycle Fatigue". Army Materials and Mechanics Research Center. AMMRC. CR 70-23, June 1970. 62 pp
 61. CREWS, J. H. JR., "Crack Initiation at Stress Concentrations as Influenced by Prior Local Plasticity". Achievement of High Fatigue Resistance in Metals and Alloys. ASTM STP 467, 1970 pp 37-52
 62. MORROW, JO DEAN, and WETZEL, R. M., and TOPPER, T. M., "Laboratory Simulation of Structural Fatigue Behavior Effects of Environment and Complex Load History on Fatigue Life. ASTM. STP 462. 1970 pp 74-91
 63. MOWBRAY, D. F., and McCONNELLEE, J. E., "Application of Finite Element Elastic-Plastic Stress Analysis To Notched Fatigue Specimen Behavior." Presented at the First International Conference on Structural Mechanics in Reactor Technology. Berlin Germany. 20-24 Sept. 1971.
 64. OSMAN, H. A., "Stress and Strain Distribution in Notched Members Under Cycling Loading". Proc. 3rd Conference on Dimensioning. Budapest, Hungary, 1968. pp 177-184. (In English)
 65. SMITH, K. N., and TOPPER, T. H., "Basics of Structural Fatigue". Society of Automotive Engineers Inc. Paper 700555. April 14, 1970. 12 pp
 66. TOPPER, T. H., and BYRE GOWDA, C. V., "Local Stress-Strain Approach to Fatigue Analysis and Design". Trans. ASME. Paper 70-DE-24. 11 pp
 67. UDOGUCHI, T., and WADA, T., "Notch Effect on Low-Cycle Fatigue Strength of Metals". Bulletin of Japan Soc. Mech. Engrs. (JSME) 1969 Vol. 12, No. 52. pp 673-682
- Also First International Conference on Pressure Vessel Technology. Delft, the Netherlands. Sept. 29-Oct. 2, 1969. Sponsored by ASME. Part II. Materials and Fabrication. pp 1191-1202. Discussion pp 211-213
68. OSMAN, H. A., "Evaluation of Local Plastic Strain History of Fatigue" 1970. 107 pp. University Microfilms, Ann Arbor, Michigan. U.S.A.
 69. HIDA, K., "Crack Initiation Life and Microfractographic Analysis in Strain Cycling Fatigue". *Welding Research Abroad*. January 1972 pp 2-11
 70. LEIS, B. N., GOWDA, C. V. B., TOPPER, T. H. "Cycle Inelastic Deformation and The Fatigue Notch Factor". Presented at the ASTM Symposium on Cyclic Stress-Strain Behavior, Analysis and Failure Prediction. Bal Harbour, Florida, 7 and 8 December 1971.
 71. MOWBRAY, D. F., McCONNELLEE, J. E. "Applications of the Cyclic-Stress-Strain Curve in Determining Notch Fatigue Deformation and Life". Presented at the ASTM Symposium on Cyclic Stress-Strain Behavior. Bal Harbour, Florida. 7 and 8 Dec. 1971.
 72. MORRO, J., MARTIN, J. F., DOWLING, N. E., "Local Stress-Strain Approach to the Fatigue of Notched Members". Presented at the ASTM Symposium on Cyclic Stress-Strain Behavior. Bal Harbour, Florida. 7 and 8 Dec. 1971.
 73. PAPIRNO, R., "Plastic Stress-Strain History at Notch Roots in Tensile Strips Under Monotonic Loading". *Experimental Mechanics* October 1971 pp 446-452. Also Army Materials and Mechanics Research Center, Watertown, Mass. Report. AMMRC TR 70-72, Feb. 1970.

74. GONYEA, D. C., "A Method for Low-Cycle Fatigue Design Including Biaxial Stress and Notch Effects." To be presented at ASTM-ASME-ASM Symposium on Fatigue at Elevated Temperatures". The University of Connecticut, Storrs, Conn. June 1972.
75. DOWDA, C. V. B., TOPPER, T. H., "Cycle Deformation Behaviour of Notched Mild Steel Plates in Plane Stress". To be published by SESA. Paper No. 1705.
76. LEIS, B. N., GOWDA, C. V. B., TOPPER, T. H. "Some Studies on the Influence of Localized and Gross Plasticity on the Monotonic and Cyclic Concentration Factors." Presented at 1971 Annual Meeting of the A.S.T.M. Atlantic City, N.J.

